**UNIVERSITY OF THE WITWATERSRAND
JOHANNESBURG**

**FACULTY OF ENGINEERING AND THE
BUILT ENVIRONMENT**

PASSIVE VIBRATION ISOLATION SYSTEMS INTEGRATED WITH A DYNAMIC VIBRATION ABSORBER

By

Katlego Thakadu

A thesis submitted to the Department of Civil and Environmental Engineering in conformity with the requirements for the degree of ***Master of Science (Engineering)***

DECLARATION

I declare that this thesis** is my own, unaided work. It is being submitted for the Degree of Master of Science in Engineering at the University of the Witwatersrand, Johannesburg. It has not been submitted before for any degree or examination at any other University.

(Signature of candidate)

8th day of November 2022 at Sandton

* dissertation or research report as applicable

** or Master of Science as applicable.

ABSTRACT

Isolating vibration using an isolator and/or vibration absorber are the two commonly used measures of vibration control in practice. The presented investigation explores multiple passive vibration isolator configurations, integrated with a dynamic vibration absorber, to improve the performance of vibration isolating.

In the first section, A Passive vibration Isolator Integrated with a Skyhook and Groundhook Vibrational Absorber is investigated. The dynamic behaviour of the proposed isolators with the lumped mass, fixed to an inertial reference, is investigated using force, and displacement transmissibility equations. The force and displacement transmissibility equations are derived by modelling the dynamic system as a two-degree-of-freedom system. Derivations for both configurations of the isolator, integrated with a skyhook and groundhook are presented, including numerical simulations and parameter sensitivity analyses. The analysis conducted, indicates that both configurations, is indeed a passive linear isolator, which can support a static load whilst achieving significant vibrational isolation, employing a relatively low damping element. Additionally, the practical applications of the proposed configurations are plausible with the currently available material, which makes the research viable within the field of engineering.

In the second section, A Passive vibration Isolator Integrated a Dynamic Vibration Absorber with Negative Stiffness Spring is investigated. The dynamic behaviour of the isolator supporting a lumped mass, is investigated using force and displacement transmissibility equations of the isolator. The force and displacement transmissibility are derived by modelling the dynamic system as a two-degree-of-freedom system. A unique constraint on the negative stiffness ratio, α, for the isolator's stable operation, is developed. The optimal design of such an isolator was demonstrated with a design example. Extensive numerical simulation and parameter studies on the isolator were performed, which revealed attractive dynamic characteristics of the isolator. It is a passive linear isolator, without any non-linear elements, spring or damper.

However, it can bear a large static load and, at the same time, achieve a greatly increased vibration isolation. These two effects are considered mutually exclusive in linear isolator and can be overcome in some extent by properly configured nonlinear isolators only. Moreover, numerical simulation and parameters study shows that the negative stiffness ratio and the mass ratio required can be very small, which makes the implementation of such an isolator in practice convenient. All these make the isolator attractive for engineering application.

The third section of this research is on the optimal design of a two-stage isolator, a isolator integrated with another isolator. Performance of a passive two-stage vibration isolator and its design was rigorously evaluated and recorded in this study. It is revealed that the vibration isolating performance of a linear passive two-stage vibration isolator depends on the configurational parameters of the isolator. The transmissibility, a non-dimensional parameter used to quantify the effectiveness of an isolation system, of the passive two-

stage vibration isolator was derived. A numerical optimization on the transmissibility of the isolator was developed and performed using the Minimax algorithm. It is demonstrated that an optimally designed linear passive two-stage vibration isolator produces significantly better isolating than a single-stage linear isolator at all frequencies, high and low. The proposed linear passive two-stage isolator is not only effective against high-frequency isolation, which used to be the primary use of a passive two-stage isolator but shows outstanding isolation performance at all frequencies.

The proposed linear passive two-stage vibration isolator outperforms many complicated nonlinear isolators, including both single-stage or two-stage isolators. Parameter selection, dynamic performance driven optimal design and potential application of the proposed isolator were also investigated and presented.

DEDICATIONS

I dedicate this thesis to my loved ones and friends that have been my support and motivational system during the course of my research.

I also dedicate this thesis to my supervisor, Dr Kuinian Li, who has given me the freedom to explore this topic and much needed guidance and mentorship that has nurtured my understanding and developed my interest in the topic of Vibration Isolation.

And lastly, but not least; I would like to dedicate this thesis to my daughter, Kgalalelo, may it be a source of encouragement and motivation to seek out and develop innovative solutions rather than conforming to what is available.

ACKNOWLEDGEMENTS

I would like to express my deepest gratitude to my supervisor, Dr Kuinian Li for inspiring my interest and initiating such an interesting and though provoking research project. His guidance, keen interest and enthusiasm has made the development of this research thesis a very pleasant and encouraging experience.

I would also like to thank, Professor John Ndiritu who has given me great support throughout my undergraduate and postgraduate studies, I humbly thank you for your patience throughout my development.

And lastly, I would like to thank my parents and sister, for all their support and words of encouragement have provided me with the strength to move forward.

TABLE OF CONTENTS

LIST OF FIGURES

ABBRVIATIONS AND NOMANCLATURE

M mass of a machine excited by dynamic force or a piece of equipment isolated from base excitation

m mass of the dynamic vibration absorber which is integrated into a traditional vibration isolator.

μ $=\frac{m}{M}$ mass ratio

k negative stiffness of the negative stiffness spring of the DVA

k_1 stiffness of the supporting spring of the isolator

k_2 stiffness of the spring of the DVA

c_2 damping coefficient of the damper in the DVA

ξ $=\frac{c_2}{2\sqrt{k_2 m}}$ damping ratio

α $=\frac{k}{k_2}$ negative stiffness ratio

ω_1 $=\sqrt{\frac{k_1}{M}}$

ω_2 $=\sqrt{\frac{k_2}{m}}$

v $=\frac{\omega_2}{\omega_1}$ frequency ratio

ω loading/excitation frequency

λ $=\frac{\omega}{\omega_1}$ loading frequency ratio

T transmissibility

T_{fI} force transmissibility of the suggested isolator in configuration I

T_{fII} force transmissibility of the suggested isolator in configuration II

T_{dI} displacement transmissibility of the suggested isolator in configuration I

T_{dII} displacement transmissibility of the suggested isolator in configuration II

T_{fI0} force transmissibility of the suggested isolator in configuration I when α=0

T_{fII0} force transmissibility of the suggested isolator in configuration II when α=0

CHAPTER ONE - INTRODUCTION

1.1 Background

Dynamic loads are time-based loads imposed on a system, which result in the transition of potential energy to kinetic energy. Dynamic loads vary in loading sequence and depend on the source of loading. The typical loading sequences encountered are sinusoidal, cyclical, and random, which result in a variety of responses of the primary mass. In comparison, for a static load, the system will deform, elastically or plastically, depending on the severity of loading, and remain relatively stationary, whilst loaded, thus indicating, that the system is in static equilibrium. For a dynamic load, the system is in constant motion and therefore, is not in static equilibrium. An inertia force is induced; thus, Newton's Second Law of motion is applicable. The two basic elements requirements for dynamic response, due to vibration, to occur are the elastic and inertia elements, and the non-basic element, is the damping element. Thus, the equation of motion of a single degree of mass (SDoF) object in motion is:

$$m\ddot{x} = -c\dot{x} - kx + f(t) \tag{1-1}$$

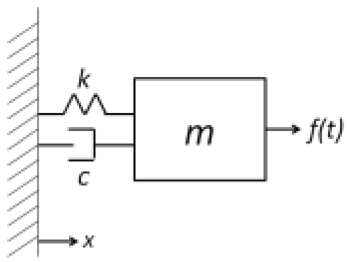

Figure 1 *- Single-degree of freedom vibration dissipation system*

Where:
m = the mass of an object
k = stiffness
c = damping co-efficient

All damping systems are based on and derived from this basic principle. A vibration control system is typically, based on a vibration absorber, consisting of an auxiliary mass, secondary stiffness element, and a damping device, typically termed as a dash port. Different configurations of these three elements will produce different outputs, and the purpose of this thesis is to explore these configurations, when attached to a traditional vibration isolator, and develop the most optimum solution analytically, for practical implementation.

Every civil engineering structure whether it be a building, or a bridge, has what is commonly referred to be a natural frequency or a band of natural frequencies, depending on its configuration and size. These are the frequencies that the structure oscillates under harmonically, when in free vibration, for both non-restricted and non-induced conditions. These natural frequencies are critical variables for structural dynamic design, as all dynamic loads apply a loading frequency or a band of loading frequencies, depending on the sequence and source of loading, on to a structure, which will result in the structure oscillating, at both the natural and loading frequencies. This is acceptable for high frequencies, that are not perceivable to the structure's occupants. Loading from external sources, may however, pose potentially catastrophic results at low frequencies, which are within the frequency band of the first natural frequency, which can induce a phenomenon known as resonance.

Resonance will occur if, the frequencies in the loading frequency band is equal to the first natural frequency of the structure, which is the lowest frequency in the natural frequency band. Under resonance, the deflections due to the dynamic and static loading are exponentially increased, to values that far exceed the allowable deflections in any building codes of practice, leading to significant damage of the structure and potential damage of adjacent structures as well. Due to this phenomenon, a study of dynamic vibration absorbers was developed, to allow for the construction of structures, in areas volatile to dynamic (seismic) loading, by equipping the structure with an energy dissipating device [1], that converts the excess energy imposed by the dynamic load into a heat energy, while efficiently and safely reducing the amplitude of the vibrations imposed on to the structure.

The theory of material damping was conceptualised after the discovery that every structure, typically has a natural damping compatibility which is largely dependent of the construction materials used in the construction of the structure [2]. The damping compatibility is measure used the parameter, ξ, which is used to denote the damping ratio of the structure, expressed as:

$$\xi = \frac{c/2m}{\sqrt{k/m}} = \frac{c}{2\sqrt{km}} = \frac{c}{c_c} \tag{1-2}$$

Where c is the damping co-efficient, m is the primary mass of structure and k is the stiffness of a structure. Extensive research has indicated that predominantly steel structures have been discovered to have a maximum damping ratio of 3% [2] while concrete has the highest damping ratio, estimated to a maximum value of 5% which is partially dependent on the composition of the concrete and member size as vibrations travel faster through steel than in concrete hence in steel vibrations are more perceivable than in concrete where the vibrations are dampened due to the composite nature of the concrete.

The primary aim in vibration control, in the structural engineering industry, is the dissipation of excess energy, which can cause structural vibrations, that may lead to failure if resonance occurs. This is achieved by increasing the damping ratio of the structure, or the stiffness of the structure. while making use of the minimum number of resources as possible, to establish equilibrium with the structural elements readily available and to ensure optimality. Various dampers have been proposed, of which some are not feasible in practice, such as those that make use of nonlinear elements [3], but it should be noted that this thesis is only concerned with linear passive vibration absorbers as in practical cases, when a significant dynamic load is imposed on a civil engineering structure, power loss commonly occur, rendering active vibration absorbers useless.

As efficient as traditional tuned mass passive dampers are in practical implications, they are subject to a very fatal flaw [4], which must be accounted for in the post design of a vibration absorber, as most passive dampers are modelled from the optimised closed form solution of minimising the dynamic response, of undamped primary systems with a Tuned Mass Damper (TMD) proposed by Den Hartog [11], the absorbers are designed to activate when the loading frequency approaches the first natural frequency of the structure, hence they are tuned to that specific frequency. This in turn, results in the absorbers becoming prone to a defect of detuning, whereby the absorber gradually becomes off-phase with natural frequency which renders the absorber ineffective, in dissipating the vibration energy under resonance events. This, for structural integrity must be prevented at all costs to ensure efficiency and safety of the structure for occupation and safe evacuation, during seismic events.

1.2 Aims and Objectives

The aim of this research is to explore the performance of passive linear vibration absorbers performance when integrated with a variety of Dynamic Vibration Absorbers (DVAs) in order to increase the efficiency of energy dissipation without compromising on the practical applicability of the proposed solutions. Extensive theoretical and numerical simulations have been undertaken to evaluate the performance of the proposed isolators.

To achieve this aim, key objectives were identified prior to the commencement of the study, to establish a sound and consistent purpose of the study, which are:

I. To develop and present a comprehensive and practical passive vibration isolator for a variety of applications that can effectively and efficiently dissipate excess vibrations, meet the static load requirements while maintaining robustness to detuning over the span of their intended use.

II. To examine the proposed vibration isolators performance to traditional systems that are widespread in the field to ascertain the merits and demerits of integration DVAs to existing systems.

III. To develop a mathematical model that can accurately depict the performance of the proposed vibration isolators under a variety of boundary conditions to evaluate the efficiency and practicality of application within a specific field.

IV. To identify key areas where further research is required in order to further improve the performance of the proposed vibration isolators in practical applications.

1.3 Thesis Outline

This study is an extension of an initial study conducted, by Dr. Kuinian Li and myself, to evaluate the performance of DVAs incorporated with linear items that can improve the efficiency of a traditional vibration absorber while increasing the system's robustness to the phenomenon of detuning. The first step of the research involved the analytical derivation of the equations of motion, of the proposed vibration isolator, and the subsequent optimisation of the parameters using the procedures proposed by Den Hartog [11].

Post optimisation, the transfer functions of the proposed dynamic isolators, integrated with a dynamic vibration absorber, were plotted against a traditional vibration isolator, to draw a comparison of the efficiency of the proposed isolators. Based on the successful modelling of the improved efficiency of the vibration isolator, in transferring the vibrations on to the damping mass, a numerical solution was derived to verify the obtained results from the analytical analysis using the Minimax/Runge-Kutta (RK4) optimisation technique.

The final step of the absorber-computerised simulation. Was the testing against detuning using the Simulink platform on the MATLAB computer application, to map the absorbers response and evaluate the rate of energy dissipation in the system, when exposed to a white noise frequency band, to the determine the sensitivity of the absorber to detuning. Upon successful numerical analysis, of the proposed absorbers, the next step would have been the physical model construction and testing of the absorber.

Chapter 2 presents a novel passive vibration isolator, that incorporated both a virtual skyhook and ground hook system without the need for an inertial reference. The proposed systems are extensively evaluated against a traditional vibration isolator using derived force and displacement transmissibility equations. The force and displacement transmissibility equations are derived from a two-degree of freedom system equations of motion. An extensive sensitivity analysis was conducted to evaluate the performance of the proposed isolator under a variety of boundary and tuning conditions in order to evaluate the vibration dissipation efficiency of the proposed system as well as to observe the robustness of the system to detuning. Numerical simulation of the proposed system was carried out using the Runge-Kutta (RK4) method and further numerical modelling was conducted under the MATLAB Simulink platform to evaluate the performance of the proposed system under sinusoidal, random, and white noise loading in order to evaluate the wholistic performance of the proposed vibration isolator.

Chapter 3 presents a novel passive vibration isolator that incorporates a DVA with a negative stiffness element. The proposed systems are extensively evaluated against a traditional vibration isolator using derived force and displacement transmissibility equations. The force and displacement transmissibility equations are derived from a two-degree of freedom system equations of motion. An extensive sensitivity analysis was conducted to evaluate the performance of the proposed isolator under a variety of boundary and tuning conditions in order to evaluate the vibration dissipation efficiency of the proposed system as well as to observe the robustness of the system to detuning. A stability equation is derived in order to establish the safe and stable operating parameters of the proposed vibration isolator. Numerical simulation of the proposed system was carried out using the Minimax optimisation method and further numerical modelling was conducted under the MATLAB Simulink platform to evaluate the performance of the proposed system under sinusoidal, random, and white noise loading in order to evaluate the wholistic performance of the proposed vibration isolator.

Chapter 4 presents a novel passive two-stage vibration isolator. The proposed systems are extensively evaluated against a traditional single-stage vibration isolator using derived force and displacement transmissibility equations. The force and displacement transmissibility equations are derived from a two-degree of freedom system equations of motion. An extensive sensitivity analysis was conducted to evaluate the performance of the proposed isolator under a variety of boundary and tuning conditions in order to evaluate the vibration dissipation efficiency of the proposed system as well as to observe the robustness of the system to detuning. Numerical simulation of the proposed system was carried out using the Minimax optimisation method and further numerical modelling was conducted under the MATLAB Simulink platform to evaluate the performance of the proposed system under sinusoidal, random, and white noise loading in order to evaluate the wholistic performance of the proposed vibration isolator.

Chapter 5 presents a comprehensive conclusion to the study and evaluates key areas that require further research and development in order to enhance the performance of the proposed vibration isolators and develop practical procedures for real-time applications.

1.4 Publications by the author

Thakadu, K., Li, K. A Passive Vibration Isolator Integrated a Dynamic Vibration Absorber with Negative Stiffness Spring. J. Vib. Eng. Technol. (2021). https://doi.org/10.1007/s42417-021-00364-0

Thakadu – 50% (conducted the research, interpreted the data and edited the manuscript);

Li 50% (supervisor, original idea, funded the research and reviewed the manuscript).

1.5 Research Limitations and Restrictions

Practical application testing was initially intended to be incorporated into the thesis, but due to the restrictions encountered through the course of the Covid-19 pandemic, the investigation was conducted through extensive numerical modelling and simulation, to determine the dynamic performance under varying boundary and loading conditions.

All graphs presented in the research were generated using the MATLAB software package, using the conceptualised two-degree-of-freedom equations, derived from the proposed configuration of elements, of the proposed isolators. The force and transmissibility equations were derived from the two-degree-of-freedom equations of each proposed configuration, and plotted using a band of loading frequencies, with varying mass ratio, damping ratio and relevant stability parameters, to determine the dynamic behaviour of the proposed isolators, under varying boundary conditions.

The numerical simulations were conducted with the Simulink platforms using predetermined primary system constants. The primary system, for a traditional single stage isolator, was modelled initially to establish a benchmark performance, required to be able to draw comparisons with the proposed systems. The corresponding system parameters of each of the proposed systems were determined, using the primary system boundary parameters, using the equations derived in each section of analysis, and used as constants in the Simulink model, to determine the comparison graphs, of the primary mass and damping mass oscillations, to determine, the dynamic behaviour of the proposed systems, and determine the degree of vibration isolation, as compared to the primary system, under the same loading.

Three loading scenarios were investigated, as these represent an extensive band of dynamic loading encountered in practice. Sinusoidal loading, which is representative of machine loading on structures. Random loading, which is representative of unpredictable loading patterns, such as oceanic loading and White-Noise loading, which is representative of seismic loading, such as earthquakes, were imposed on the primary and proposed systems and comparative graphs generated and discussed, to present the observed performance and evaluation according to the research aims and objectives, stated in section 1.2.

1.6 Literature Review

1.6.1 Introduction

Vibration attenuation has long since been a key field area of research, in the search for solutions for stability in systems, exposed to excessive vibrations, thus, there exists a plethora of vibration isolation concepts, for both active and passive systems, which cater for a wide range of applications within the automotive, aeronautical, nuclear, marine, and infrastructure engineering industries, to name a few [1]. The concepts suggested by subject matter experts, majorly make use of distinct components to be able to achieve the required vibration attenuation requirements, to maintain system stability. These components are namely, the stiffness and damping components, which reduce the energy the primary system is exposed, through the transfer to potential energy to kinetic energy, to dissipate the external energy imposed to the system through vibrations. The success criteria for determining the effectiveness of the proposed vibration isolation system differs, according to the scope of applicability, whereas some systems are designed to ensure comfort and to reduce measured vibration exposure, as per BS 6841:1987, which apply to mainly service industries, such as automotive and aeronautical industries, to reduce the perceived, system vibrations, to give users peace of mind and reinforce the feeling of safety in the design of the system[7]. However, for industries such as in marine and infrastructure engineering [1], the primary objective is to increase the system's lifespan through the reduction of fatigue inducing vibrations, exposed to the primary system, thus improving the factor of safety of the system, to ensure temporary stability even in the most detrimental situations, to facilitate safe evacuation of the vessel/structure by the inhabitants.

For the purposes of the research presented in this thesis, linear passive vibration isolation systems are studied and evaluated, as they produce far more reliable results in the most catastrophic situations that the primary system can be exposed to, as they do not require an external power supply to dissipate vibrations. In the event of a catastrophe, power supply can be disrupted thus rendering active systems obsolete. The aim of this thesis is to propose and study, the effect of optimisation of existing vibration isolation, system through the optimal configuration of core damping elements such as stiffness and damping, in the form of a vibration absorber, as well as the addition of elements that show significant vibration isolation such as negative stiffness elements, in order to provide comprehensive and practical systems that can be implemented in practice, using existing knowledge, skills and resources. The concept of vibration is briefly discussed initially in this literature review to provide context in the proceeding sections of this thesis.

Vibration is typically defined, in the context of this thesis, as any repetitive response of a mechanical system to periodic, random, and oscillatory loading. The term frequency is used to numerically define the rate of loading of the system, measured in Hertz (Hz). The term amplitude refers to the measured exposure to loading over a time, in which the loading on the system is plotted to graphically depict the sequence and magnitude of loading for a period to determine the rate of loading as well as the maximum peak loading that the primary system is exposed to.

Vibrations may be classified per the nature of the source of loading. Vibrations classification can be summarised into two main categories, free/natural and forced vibrations [6]. Free/Natural vibrations are typically introduced to the system through natural excitation sources, such as wind or vibrations from surrounding components/structures transmitted through the air, from sound waves, resulting in excitation of the base structure at its 'natural' frequency. The natural frequency of a system is the result of the stiffness and damping properties of the primary system, without any additional damping or isolation systems in place, it is the frequency that the system will vibrate in should it be excited by a unit displacement or vibrations transmitted by an adjacent system similar to the phenomena induced by the use of a tuning fork.

Forced vibrations refer to loading imposed onto a system, by either a machine, or external loading due to environmental factors, such as impact loading due to blasting, oceanic loading in marine environments, and seismic loading from shifting tectonic plates. Forced vibrations are typically classified according to the response predictability, if the response of a system under forced vibration can be approximately predicted then the vibration source is termed to be deterministic, alternatively, vibration responses that cannot be accurately or approximately predicted are termed to be random. The practice of vibration isolation/damping is the engineering solution, introduced to suppress excessive and perceivable vibrations. Vibration isolation serves multiple functions besides the suppression of vibrations, effective vibration isolation reduces the effect of fatigue on a system's components by reducing transverse loading due to vibration thus improving the efficiency of the system and optimising the performance. In civil engineering practice, vibration isolation also provides a critical function, of limiting the primary system's response to a resonant event, this is the phenomena whereas the imposed loading vibrates at frequency approximate or equal to the (first) natural frequency of the structure, this amplifies the amplitude of the displacement of the primary mass, leading to catastrophic failure of structures. In order to further expand on this phenomenon, we consider a single-degree-of-freedom (SDoF) system, defined in Eq. (1-1), which has a sinusoidal loading imposed on it, thus the equation of motion may be expressed as:

$$m\ddot{x} + c\dot{x} + kx = f(t) = P_0 sin\Omega t \tag{1-3}$$

The system, under a deterministic vibration source, can be assumed to have a steady state solution that can approximate the response of the system to loading as a function of time termed t. The steady state solution may be expressed as:

$$x(t) = \left(\frac{P_0}{k}\right) H(r) \sin(\Omega t - \phi) \tag{1-4}$$

Whereas Ω is the loading frequency from the sinusoidal loading source, $\omega = \sqrt{\frac{k_1}{m}}$ is the natural frequency of the system and ϕ is the phase angle expressed as:

$$\phi = \tan^{-1} \frac{2\xi r}{1-r^2} \tag{1-5}$$

Where $\xi = \frac{c}{2m\omega_1}$ is the damping ratio of the system. The principle of amplification can be expressed using the principle of the dynamic coefficient, expressed as:

$$H(r) = \frac{1}{\sqrt{(1-r^2)^2 + 4\xi^2 r^2}} \tag{1-6}$$

Whereas $r = \frac{\Omega}{\omega}$. The amplitude of the system comprises of two components, a constant section dependent on the load applied by the source and the stiffness of the system, whereas the second component is the dynamic coefficient, which is primarily dependent on the value of r, as it is the dominant variable in the equation, as it has the greatest impact on the magnitude of the dynamic coefficient. From Eq. (1-6) we observe that in order to reduce the magnitude of the dynamic coefficient $\omega > \Omega$, as $\Omega \to \omega$ the value of $H(r) \to \infty$, this phenomenon is described as resonance whereas the system's first natural frequency, which is the lowest, is equal to the loading frequency thus vastly increasing the system's amplitude of deflection to beyond serviceability and ultimate limit states and resulting in catastrophic failure such an example is that of the Tacoma Narrows Bridge in Pierce County in Washington, USA [5].

Vibration attenuation can be implemented, either to isolate/reduce vibrations, through reduction of shock and vibration at its source, through the addition of vibration isolation/absorption devices. Multiple techniques can be employed to limit excessive vibrations, such as the addition vibrational isolators, absorbers and stiffening the structure [1]. Ideally, reduction may be done through the modification of the design, to improve efficiency and reduce vibrations. This technique improves the lifespan of the mechanical system whilst meeting the serviceability criteria for perceivable vibrations, as mechanical vibrations, are a by-product of misalignment of axis of rotation of the motor and the centroid of the system, which reduces the lifespan of the motor, as bearings and seals are exposed to eccentric loading, thus shortening the lifespan. However, this technique has a limited range of application, as it can only service vibrations induced by machines, for structural engineering applications, such as in the event of an earthquake or oceanic loading, this technique become impractical.

Another technique that may be employed is the reduction of vibration at its response. This technique primarily emphasises the redesign of the main system, of which the loading is applied to, to minimise the magnitude of its response to the vibrational loading. This may be achieved through increasing stiffness of the primary system, to increase the difference of the loading frequency from the natural frequency, of the primary system, thus reducing the effect of the dynamic coefficient on the amplitude of the primary mass displacement, due to the loading. This technique is prone to limitation within the range of its application, as this approach requires the modification of either the primary mass or stiffness of the primary system to change the natural frequency of the primary system, this has a major cost implication for large scale systems such as skyscrapers or bridges, additionally, for mechanical systems such as in automotive and aeronautical applications, spatial limitations may affect the ability to modify the parameters.

The technique of adding a vibration absorber/isolator is employed to dissipate/attenuate excessive vibrations, to reduce the amplitude of displacement of the primary mass and, critically, avoid a resonance event [1]. Vibration attenuation using an isolator and vibration damping using damper, are the two most employed measures for vibration control. Vibration isolation is a technique for reducing or suppressing unwanted vibrations in structures and machines, in which the load transmission path is interrupted, to reduce the impact of the loading on the primary system. Dynamic vibration absorbers are secondary systems, comprising of an auxiliary mass, that is a fraction of the primary system's mass, whereas the ratio between the auxiliary and primary mass is termed as the mass ratio, defined as μ. The objective of the secondary system is to dissipate excess vibrations, through the conversion of potential energy to kinetic energy, whereas the inertia of the damping mass is used to negate the kinetic movement of the system, thus dissipating the excess energy within the system. The dynamic vibration absorber system commonly comprises of the auxiliary mass, supported by either a secondary stiffness, dashpot or even a combination of both [1]. This thesis is based on the study and development of systems comprising of both, the vibrational isolator, and the dynamic vibration absorber, hence the literature is primarily based on these vibrational control systems.

1.6.2 Dynamic Vibration Absorbers

Vibration dampers are widely used in vibration control. The most widely used should be tuned mass damper which consists of a damper mass, a spring, and a dashpot. Since its simplicity and no power input requirements, passive vibration control devices have been a favoured option. The popular passive tuned mass dampers can be in various physical forms, including solids mass and liquids mass (TLD) [25] and various springs and dampers have been developed to improve the traditional tuned mass damper [26].

The most used and extensively studied passive dynamic vibration absorber (DVA), is the Tuned Vibration Absorber (TVA), or Tuned Mass Damper (TMD). Passive DVAs are available in various physical forms, including solids mass and liquids mass (TLD) [32] and various springs and dampers have been developed to improve the traditional DVA [33]. By introducing/adding a negative stiffness spring element, dynamic vibration absorber with negative stiffness element were developed and studied [34].

Extensive research has been conducted on dynamic vibration absorbers with negative stiffness (NSDVA), including parameter study and optimization, that were performed by [35], [36] and [37]. Even though the NSDVA shows attractive vibration absorbing effect and several negative stiffness devices/structures have been developed, the implementation of negative stiffness, especially when the absolute value of the negative stiffness is significant, is still not convenient in practice.

A design example of a dynamic vibration absorber is presented and studied analytically in detail by [14]. The equations of motion are obtained and through Laplace transforms are converted to dynamic vibration parameters that are applied to the fixed-point theory. The optimum parameters of the vibration absorber are derived using the fixed-point theory and consideration of the stability of the system with respect to the negative stiffness element. A numerical analysis using a fourth order Runge-Kutta procedure is carried out to assess the accuracy and precision of the analytical results from the optimised parameters. The proposed design is then compared with other proposed dynamic vibration absorbers based on the same concepts including the traditional Tuned Mass Damper (TMD) proposed by [11] and the variant design by [13] under harmonic and random excitation in order to show the improved performance of the new design. The structural model of the proposed system is shown in figure 2 below.

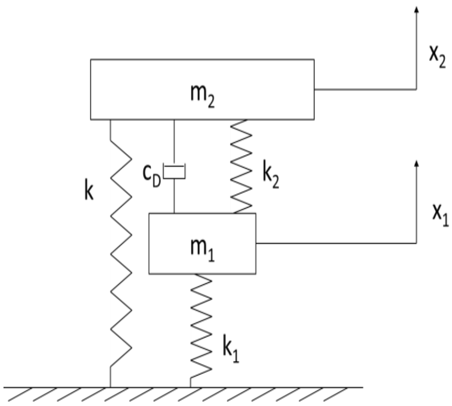

Figure 2 *- Model of the negative stiffness based DVA system [7]*

The equations of motion are:

$$m_1\ddot{x}_1 + k_1x_1 + k_2(x_1 - x_2) + c_D(\dot{x}_1 - \dot{x}_2) = Fcos(\omega t) \qquad (1-7a)$$

$$m_2\ddot{x}_2 + kx_2 + k_2(x_2 - x_1) + c_D(\dot{x}_2 - \dot{x}_1) = 0 \qquad (1-7b)$$

Where:

$$\alpha = \frac{k}{k_2}$$

$$v = \frac{\sqrt{\frac{k_2}{m_2}}}{\sqrt{\frac{k_1}{m_1}}}$$

$$\xi = \frac{c}{2m_2\sqrt{\frac{k_2}{m_2}}}$$

The optimum tuning conditions and optimum damping can be deduced as

$$v_{opt} = \sqrt{\frac{1}{a + (1+\mu)^2}} \quad (1-8)$$

$$\xi_{opt} = \sqrt{\frac{\mu(3 + 3a + 3\mu + 2a\mu)}{8(1+\mu)^2 + 4(2+\mu)[a^2 + 2a(1+\mu)]}} \quad (1-9)$$

$$\alpha_{opt} = -1 - \mu(2+\mu) + (1+\mu)\sqrt{\mu(2+\mu)} \quad (1-10)$$

A variant design of a dynamic vibration absorber is presented and studied analytically in by [13]. In this design, the equations of motion are obtained and converted to dynamic vibration parameters, using a Laplace transform, that are applied to the fixed-point theory, to derive the transmissibility equation. The optimum parameters of the vibration absorber are then derived, using the optimisation methods proposed by [11]. The proposed design is then compared with the traditional Tuned Mass Damper (TMD) under harmonic excitation to show the improved performance of the variant design. The structural model of the proposed system is shown in Figure 3 below.

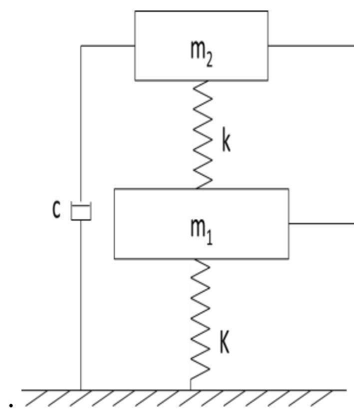

Figure 3 *– Variant of the Tuned Mass DVA [15}*

The equations of motion are:

$$M\ddot{x}_1 + Kx_1 + k(x_1 - x_2) = Fcos(\omega t) \quad (1-11a)$$

$$m\ddot{x}_2 + k(x_2 - x_1) + c\dot{x}_2 = 0 \quad (1-11b)$$

Where:

$$v = \frac{\sqrt{\frac{k}{m}}}{\sqrt{\frac{K}{M}}}$$

$$\xi = \frac{c}{2m\sqrt{\frac{k}{m}}}$$

The optimum tuning conditions and optimum damping are presented as:

$$v_{opt} = \sqrt{\frac{1}{1-\mu}} \qquad (1-12)$$

$$\xi_{opt} = \sqrt{\frac{3\mu}{8(1-0.5\mu)}} \qquad (1-13)$$

Figure 4 represents the traditional TMD proposed and analytically tuned by [11] where the optimum conditions are derived to depend on the ratio of the damping mass to the primary mass. The design parameters shown below are derived from the fixed-point theory represent an approximate solution:

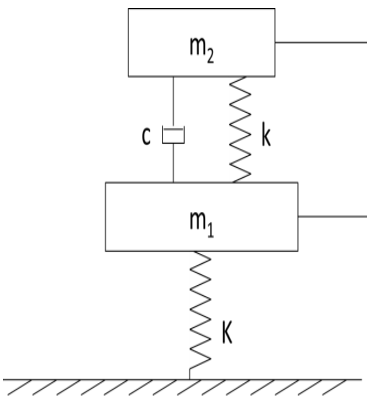

Figure 4 *– Tuned Mass DVA proposed by Den Hartog (1956) [6]*

The equations of motion are:

$$M\ddot{x}_1 + Kx_1 + k(x_1 - x_2) + c(\dot{x}_1 - \dot{x}_2) = Fcos(\omega t) \qquad (1-14a)$$

$$m\ddot{x}_2 + k(x_2 - x_1) + c(\dot{x}_2 - \dot{x}_1) = 0 \qquad (1-14b)$$

Where:

$$v = \frac{\sqrt{\frac{k}{m}}}{\sqrt{\frac{K}{M}}}$$

$$\xi = \frac{c}{2m\sqrt{\frac{k}{m}}}$$

The optimum tuning conditions and optimum damping are presented as:

$$v_{opt} = \frac{1}{1+\mu} \tag{1-15}$$

$$\xi_{opt} = \sqrt{\frac{3\mu}{8(1+\mu)}} \tag{1-16}$$

A design of a dynamic vibration absorber is presented and studied analytically in detail by [15]. The equations of motion are obtained and converted to dynamic vibration parameters that are applied to the fixed-point theory. The optimum parameters of the vibration absorber are partially derived using the optimisation methods proposed by [11], except for the damping ratio, the remaining parameters are derived from sensitivity analyses of the DVA parameters. The stability of the system with respect to the negative stiffness ratio is presented through a condition of the maintenance overall stiffness of the system. The proposed design is then compared with the traditional Tuned Mass Damper (TMD) proposed by [11] under harmonic excitation in order to show the improved performance of the new design. The structural model of the proposed system is shown in figure 5 below.

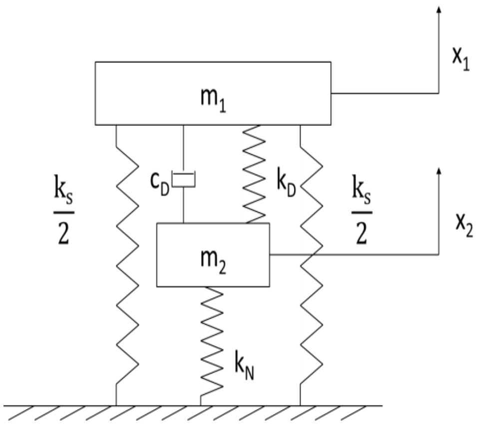

Figure 5 *– Proposed K-damper Model [8]*

Equations of motion:

$$m\ddot{x} + c_D(\dot{x}-\dot{y}) + k_S x + k_P(x-y) = f \tag{1-17a}$$

$$m_D\ddot{y} - c_D(\dot{x}-\dot{y}) - k_P(x-y) + f_{ND}(u) = 0 \tag{1-17b}$$

Operating condition of the DVA:

$$k_S + \frac{k_P k_N}{k_P + k_N} = k \qquad (1-18)$$

(Where k_N =Negative Stiffness, k_P =Positive Stiffness and k_D =Damping Stiffness, $k =$ total static stiffness, c_D =Damping co-efficient, ζ_D =Damping ratio)

Where:

$$\kappa = -\frac{k_N}{k_D} = -\frac{k_N}{(k_P + k_{N)}}$$

$$k_N = -\kappa\mu\rho^2 k$$

$$k_P = (1+\kappa)\mu\rho^2 k$$

$$k_S = 1 + \kappa(1+\kappa)\mu\rho^2 k$$

$$c_D = \frac{2\zeta_D}{\sqrt{(k_P + k_N)m_D}}$$

The optimum tuning conditions are presented as:

$$\rho_{OPT} = \sqrt{\frac{1}{(1+\mu+\kappa\mu)(1+\mu) - \kappa^2\mu}} \qquad (1-19)$$

$$\kappa_{MAX} = (1+\mu)\frac{1+\sqrt{1+\frac{4}{\mu}}}{2} \qquad (1-20)$$

Vibration absorption devices are effective in dissipating excess energy imposed on the primary system and a variety of configurations exist that may be employed depending on the boundary conditions of the primary system, environmental factors as well as availability of materials all based on the work conducted by [11]. However, Dynamic Vibration Absorbers (DVAs) are inherently prone to the phenomenon of detuning whereas the DVA becomes off-phase with the first natural frequency of the system thus reducing its efficiency in dissipating the excess energy introduced to the system and compromising the factor of safety against a resonance event. Many authors such as [15] have proposed alternative systems from the traditional TMD that are not prone to detuning an offer vibration absorption at a larger spectrum of loading frequencies, some, however, remain novel devices due to the complexity of implementation in practice thus limiting the options that can be employed in practical applications.

1.6.3 Vibration Isolators

Vibration isolation is a commonly used technique in the reduction or suppressing of excessive vibrations in structures and machines. A vibration isolator is employed to isolate the source of vibration from the structure. The traditional model of an isolator is that of a single degree of freedom system whereas the system can be configured to accommodate two cases of loading on the main system. In the first case, the source of vibration is the payload itself, and in this case the intention is to prevent the vibration to be transmitted to its host structure (the base). In the second case, the disturbance to the payload (which is to be protected now) is caused by vibration of the host structure and the goal is to minimize the transmitted vibration. There are mainly two distinct cases for vibrational loading, the first case is referred to as the force transmissibility problem. whereas the source of vibration is the payload itself, and in this case the intention is to prevent the vibration to be transmitted to its host structure (the base). The second is referred to as the displacement transmissibility problem, whereas the disturbance to the payload (which is to be protected from excessive vibrations) is caused by vibration of the host structure and the goal is to minimize the transmitted vibration transmitted to the payload. The non-dimensional parameter which is used to quantify the effectiveness of an isolation system is transmissibility. For a linear vibration isolator which is a single-degree-of-freedom system, the force transmissibility and displacement transmissibility of the isolator are the same [38]:

The first case is referred to as the force transmissibility problem whilst the second as the displacement transmissibility problem. The non-dimensional parameter which is used to quantify the effectiveness of an isolation system is the transmissibility.

The transmissibility of a traditional linear isolator, previously conducted research has indicated that the vibration can only be attenuated at frequencies above the square root of two times the fundamental natural frequency of the system, i.e. $T < 1$ only happens as $\lambda > \sqrt{2}$ or $\omega > \sqrt{2}\omega_1$. Therefore, in order to enable an isolator to start isolating vibration at lower frequency, it is desired the fundamental natural frequency of the system, ω_1, become close to zero. That means, for a given mass m_1 , the stiffness of the isolator k_1 is desired to be zero. However, in practice, there is a limitation on minimum value of k_1 as it is required to support the static load imposed on the system. Ideally, instead of an isolator with constant stiffness, the isolator should have a high-static-stiffness to bear the load without much static displacement, and a low-dynamic-stiffness – which will provide the low fundamental natural frequency required for improved vibration isolating performance. It is impossible for a linear isolator to meet these two requirements. This High-Static-Low-Dynamic-Stiffness (HSLDS) characteristic can be achieved with a nonlinear isolator using nonlinear spring [16, 17, 18].

Nonlinear isolator using nonlinear damping was also developed and studied [19]. It is highlighted that, even though a lot of research on vibration isolators using nonlinear spring and/or nonlinear dappling having been done, it is still not convenient to realize a spring or damping with the nonlinearity required in practice [20]. Introducing negative stiffness element to improve traditional vibration isolator was also studied [21, 22]. It should be noticed that the direct intruding of negative stiffness element to traditional isolator usually produce isolators could not bear heavy static load and introducing stability problem to the dynamic system as well. Adding up an inerter to the traditional spring-damper isolator, inerter-spring-damper isolator was developed and studied [23]. It is highlighted that, out that the introducing of large nonlinearity could improve the isolation, but the relative motion is increased [24].

A virtual skyhook vibration isolation system was introduced [27,28] by hooking a dashpot to the “sky”, an inertial reference. Both traditional vibration isolator and skyhook vibration isolator are a single-degree-of-freedom system. The only difference is for a traditional vibration isolator the dashpot is connected to the base (ground) while for a skyhook vibration isolator the dashpot is connected to the “sky”, the inertial reference. Inerter is introduced and set in parallel with dashpot and hook to the “sky” to improve suspension of vehicle [28].

The virtual skyhook system presented in [28] demonstrated enhanced vibration isolation and reduction of transmissibility at high frequencies whilst removing the requirement of an inertial reference frame which has limited the application of the skyhook principle within practice. The result is a broadband isolation system that not only reduces the peak resonance of the primary system but also preserves lightly damped transmissibility above the resonance frequency [28]. The system provides improved vibration attenuation at lower mass ratios which provides a trade-off for the requirement of a secondary suspension system. The experimental analysis undertaken shows a that the practical application of the concept to be feasible and implementable in a variety of applications for a passive vibration isolation system. Skyhook vibration isolator gets the benefit of limiting vibration amplitude at resonance without increasing transmissibility at higher frequencies. Unfortunately, such a “sky” does not exist or is costly to “build” in reality, which leads to the introducing of virtual skyhook dampers and active or semi-active skyhook dampers [29] and their application in suspension of vehicles [30,31].

Innovative research in damping material is explored by [35]. The article contains an extensive theoretical framework that is tailored to emphasise an equivalent SDoF oscillator’s performance as compared to an equivalent traditional SDoF system that is already implemented in practice for passive vibration isolation. The authors explored a simplified approach to derive equivalent equations of motion, based on logical assumptions that by magnitude, do not have a significant impact on the transmissibility responses obtained, if and only if, the base assumptions are still valid and applicable for the engineering implementation under consideration. The analysis contained in the article also addresses a drawback identified with systems that incorporate a negative stiffness element which is the static and dynamic stability of the oscillator through a limitation identified as the neutral stability point.

This limit is safeguarded using an engineering factor of safety ε as a prohibition to prevent any possibility of violation of the stability limit. The article also explores parameter optimisation, by simplification and relation of parameters, three parameters were identified to be key in the optimal performance of the considered oscillator, namely, ε, α and ζ_n which are optimised through a sensitivity analysis within a predefined range that does not compromise the system stability. The authors further explore the use of acoustic metamaterials as damping elements through a theoretical approach on substation of ‘atoms’ in the metamaterials with the stiffness elements components of the considered oscillator and generate impact response of the improvement on the energy dissipation of the system using an acoustic metamaterial damping element as compared to traditional elements used in practice and outline the magnitude of improvement on the damping ratio of the system as a result.

For a linear isolator, vibration can only be attenuated at frequencies above the square root of two times the fundamental natural frequency of the system, *i.e.*, $T < 1$ only when $\lambda > \sqrt{2}$ or $\omega > \sqrt{2}\omega_1$. Therefore, the objective of this study is to develop an isolator that can isolate vibration at lower frequency, it is desired that the natural frequency of the system, ω_1, be close to zero. That means, for a given mass m_1 , the stiffness of the isolator k_1 is ideally zero.

However, in practice, there is a limitation on the minimum value of k_1 to ensure that the structural static load can be supported properly. Ideally, instead of an isolator with constant stiffness, the isolator should have a high-static-stiffness to bear the load without much static displacement, and a low-dynamic-stiffness – which will provide the low natural frequency required for improved vibration isolation performance. Previously published research suggested that it is impossible for a linear isolator to meet these two requirements. This High-Static-Low-Dynamic-Stiffness (HSLDS) characteristic can be achieved with a nonlinear isolator using nonlinear spring [39], [40] and [41]. A nonlinear isolator using nonlinear damping was also developed and studied [42]. Introducing negative stiffness element to improve traditional vibration isolator was also studied [43,44]. It should be noted that the direct intruding of a negative stiffness element to traditional isolator usually produces isolators that cannot not bear heavy static load and additionally, introduces stability problem to the dynamical system. By adding an inerter to the traditional spring-damper isolator, inerter-spring-damper isolator was developed and studied [41]. It should be noted that introduction of a large nonlinearity could improve the isolation, however, the relative motion will also be increased [46]. Lever mechanism was introduced [47,48] into traditional vibration isolator to improve the isolating performance.

Multi-degree-of-freedom vibration systems are also widely used in engineering practice [49], even for vibration isolation [50]. A two-stage vibration isolator, sometimes referred to as double-mounting, is a two-degree-of-freedom dynamical system. However, a two-stage vibration isolator, formed by connecting two single-stage isolators in series cannot improve the isolating performance of a single-stage isolator (a single-degree-of-freedom system) significantly. To improve the vibration isolating performance of a traditional isolator, using X-shape supporting structure, a 6DOF vibration isolator [51] was developed.

With the same intention of increasing the range over which vibrations are isolated without sacrificing the static load bearing capacity, a passive vibration isolator integrated a dynamic vibration absorber with a negative stiffness spring is developed, modelled, and optimized. The study conducted reveals that this isolator is a linear isolator and can meet both the requirements of “high-static stiffness” and “low-or-even-zero dynamic stiffness”, which are considered irreconcilable and unachievable with a linear isolator.

This High-Static-Low-Dynamic-Stiffness (HSLDS) characteristic can be achieved to some extent with a nonlinear isolator using nonlinear springs [54,55]. Nonlinear vibration isolation systems based on the quasi-zero-stiffness (QZS) have been investigated [56, 57]. A nonlinear isolator using nonlinear damping was also developed and studied [58]. It is highlighted that, even though a lot of research on vibration isolators using nonlinear spring and/or nonlinear damping having been done, it is still not convenient to realize a spring or damping with the nonlinearity required in practice [59]. Introducing negative stiffness element to improve traditional vibration isolator was also studied [60,61]. It should be noted that, the direct intruding of negative stiffness element to traditional isolator usually produce isolators that could not bear heavy static load and introduces a stability problem to the dynamic system as well. Introducing inerter to the traditional single-stage isolator has also been investigated whereas an inerter-spring-damper isolator was developed and studied [62]. Introducing a large nonlinearity could improve the isolation, however, the relative motion of the system is also subsequently increased.

CHAPTER TWO – A PASSIVE VIBRATION ISOLATOR INTEGRATED WITH A SKYHOOK OR A GROUNDHOOK ANCHOR

2.1 Introduction

Vibration isolating using isolator and vibration damping using damper are the two measures used for vibration control. Vibration isolation is a commonly used technique for reducing or suppressing unwanted vibrations in structures and machines. A vibration isolator is employed to isolate the source of vibration from the object to be protected. Figure 6 presents the single-degree-of-freedom model of a traditional isolator. In the first case, the source of vibration is the payload itself, and in this case the intention is to prevent the vibrations to be transmitted to its host structure (the base). In the other case, the disturbance to the payload (which is to be protected now) is caused by vibration of the host structure and the goal is to minimize the vibration transmitted.

The first case is referred to as the force transmissibility problem whilst the second as the displacement transmissibility problem. The non-dimensional parameter which is used to quantify the effectiveness of an isolation system is the transmissibility. For a traditional linear vibration isolator, the force transmissibility and displacement transmissibility of the isolator are the same [16] as:

$$T = \left|\frac{F_t}{F_e}\right| = \left|\frac{X_t}{X_e}\right| = \sqrt{\frac{1+4\zeta^2\lambda^2}{(1-\lambda^2)^2+4\zeta^2\lambda^2}} \qquad (2\text{-}1)$$

Where $\lambda = \frac{\omega}{\omega_1}$ is called frequency ratio or non-dimensional excitation frequency while $\omega_1 = \sqrt{\frac{k_1}{m_1}}$; $\zeta = \frac{c}{2m_1\omega_1}$. ω_1 is the fundamental natural frequency of the system and ζ is damping ratio. The transmissibility of a traditional linear isolator, as shown in Figure 6, is shown in Figure 7.

It can be seen that vibration can only be attenuated at frequencies above the square root of two times the fundamental natural frequency of the system, i.e. $T < 1$ only happens as $\lambda > \sqrt{2}$ or $\omega > \sqrt{2}\omega_1$. Therefore, to make a isolator start isolating vibration at lower frequency, it is desired the fundamental natural frequency of the system, ω_1, close to zero. That means, for a given mass m_1 , the stiffness of the isolator k_1 is wished to be zero. However, in practice, there is a limitation on minimum value of k_1 to make sure the static load can be bearded properly.

The purpose of this chapter is to introduce a system that effectively counters the limitations identified for previously proposed traditional vibrational isolator which do not require an impractical value of ω_1 and can support the static load requirements of the system through the primary stiffness k_1 thus making it viable for practical application. An extensive study is conducted on the behaviour of the transmissibility on two systems derived from the principles of the skyhook damper discussed in Chapter 1. A novel vibrational isolator integrated with a skyhook and another with a groundhook damper, based on the inertial reference used are depicted, studied and numerically simulated in the subsequent sections in order to evaluate the vibration isolation performance against of a traditional vibrational isolator that is readily available in practice.

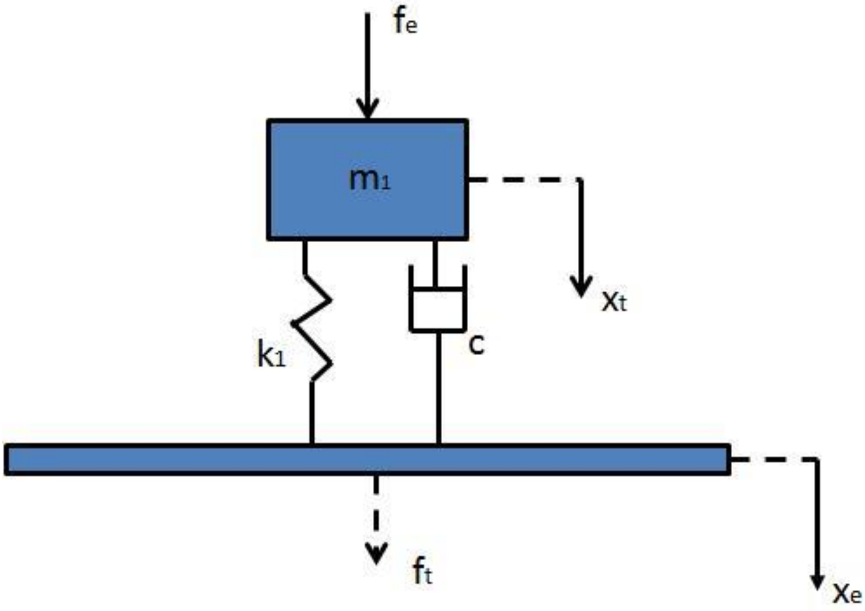

Figure 6 *– Model of a traditional vibration isolator*

Figure 7 definitively depicts that for a traditional vibration isolator to achieve good isolating performance, high damping elements must be employed.

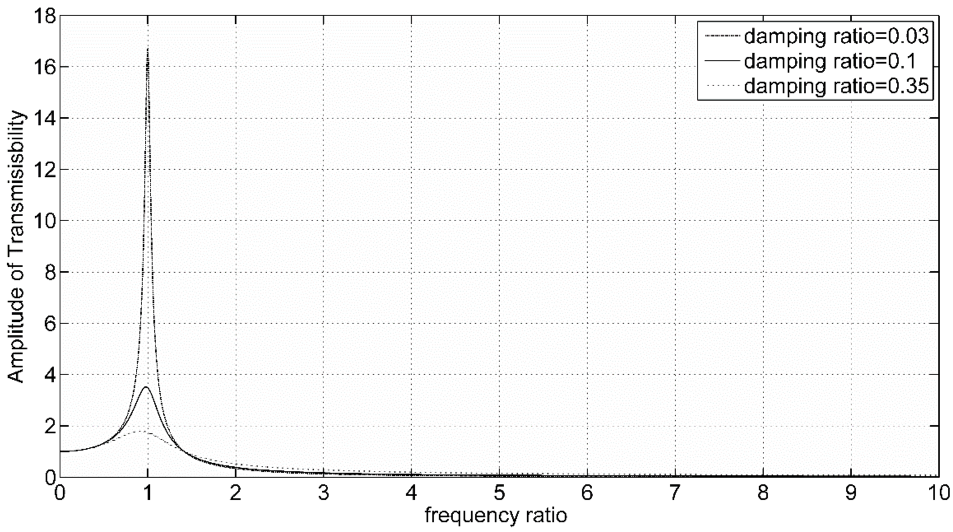

Figure 7 *- Transmissibility of a traditional vibration isolator at different damping ratio*

Vibration dampers are also widely used in vibration control. The most widely used should be tuned mass damper which consists of a damper mass, a spring and a dashpot. Since its simplicity and no power input requirements, passive vibration control devices have been a favoured option. The popular passive tuned mass dampers can be in various physical forms, including solids mass and liquids mass (TLD) [25] and various different springs and dampers have been developed to improve the traditional tuned mass damper [26].

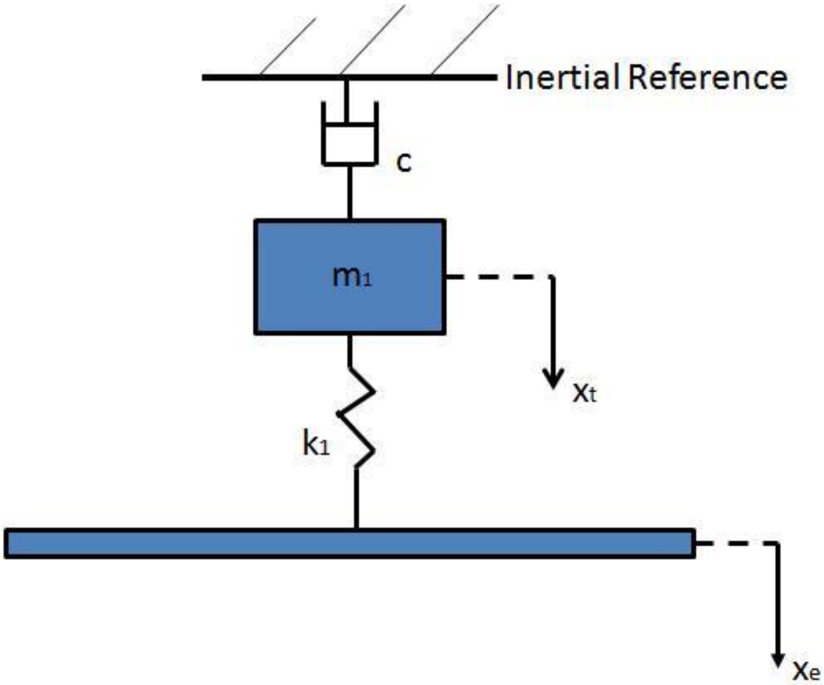

Figure 8 *- Model of a virtual skyhook vibration isolator*

A virtual skyhook vibration isolation system was introduced [27] by hooking a dashpot to the "sky", an inertial reference, as shown in Figure 8. Both traditional vibration isolator and skyhook vibration isolator are a single-degree-of-freedom system. The only difference is for a traditional vibration isolator the dashpot is connected to the base (ground) while for a skyhook vibration isolator the dashpot is connected to the "sky", the inertial reference. Inerter is introduced and set in parallel with dashpot and hook to the "sky" to improve suspension of vehicle [28]. Skyhook vibration isolator gets the benefit of limiting vibration amplitude at resonance without increasing transmissibility at higher frequencies. Unfortunately, such a "sky" does not exist or is costly to "build" in reality, which leads to the introducing of virtual skyhook dampers and active or semi-active skyhook dampers [29] and their application in suspension of vehicles [30,31].

2.2 A vibration isolator integrated with a Skyhook/Groundhook damper

.
The suggested passive vibration isolator integrated a skyhook damper is depicted by Figure 8 and the isolator integrated a groundhook damper is presented in Figure 10.

Mass M can either represent a machine excited by dynamic force or a piece of equipment isolated from base excitation. For a traditional passive isolation system as show in Figure 6, a viscous damper is set in parallel with spring k_1 and they work together to isolate vibration. Highly damped system usually is needed to achieve high isolation efficiency. However, the vibration isolator suggested, as shown in Figure 9 or Figure 10, besides the damper c_1 in parallel with k_1, a damper (not just a dashpot) which consists of three elements: an auxiliary mass m, a spring k_2 and a damper(dashpot) c, connected in series, is added in parallel. Mass m, spring k_2 and damper c connected in series forms the damper to be integrated in the traditional vibration isolator. If the dashpot c is hooked up to M, not "sky" or "virtual sky", a passive vibration isolator integrated with a skyhook damper, as shown in Figure 9, is produced. It highlighted that the term “sky” here refers to M,which is real and existing. If the dashpot c of the damper is connected down to the base, an isolator integrated a groundhook damper, as shown in Figure 10, is obtained. It should be pointed out that the passive vibration isolator suggested, either the isolator integrated a skyhook damper, or the isolator integrated a groundhook damper, is a two-degree-of-freedom dynamical system while most vibration isolators existing is a single-degree-of-freedom system, though various different spring and damping elements may employed or even an inerter is added in.

2.2.1 Force Transmissibility

The passive vibration isolator integrated a skyhook damper, as shown in Figure 9, is modelled as a two-degree-of- freedom system. For this system, with $x_e = 0$, the equations of motion, when M under harmonic force excitation, are given by:

$$\begin{cases} M\ddot{x}_1 + \mathrm{c}_1\dot{x}_1 + c(\dot{x}_1 - \dot{x}_2) + k_1 x_1 = F_e\cos(\omega t) & (2-2) \\ m\ddot{x}_2 + k_2 x_2 + c(\dot{x}_2 - \dot{x}_1) = 0 & (2-3) \\ F_t = k_1 x_1 + k x_2 + c_1\dot{x}_1 & (2-4) \end{cases}$$

Performing Fourier transform on Eq. (2-3), the following relationship will be obtained:

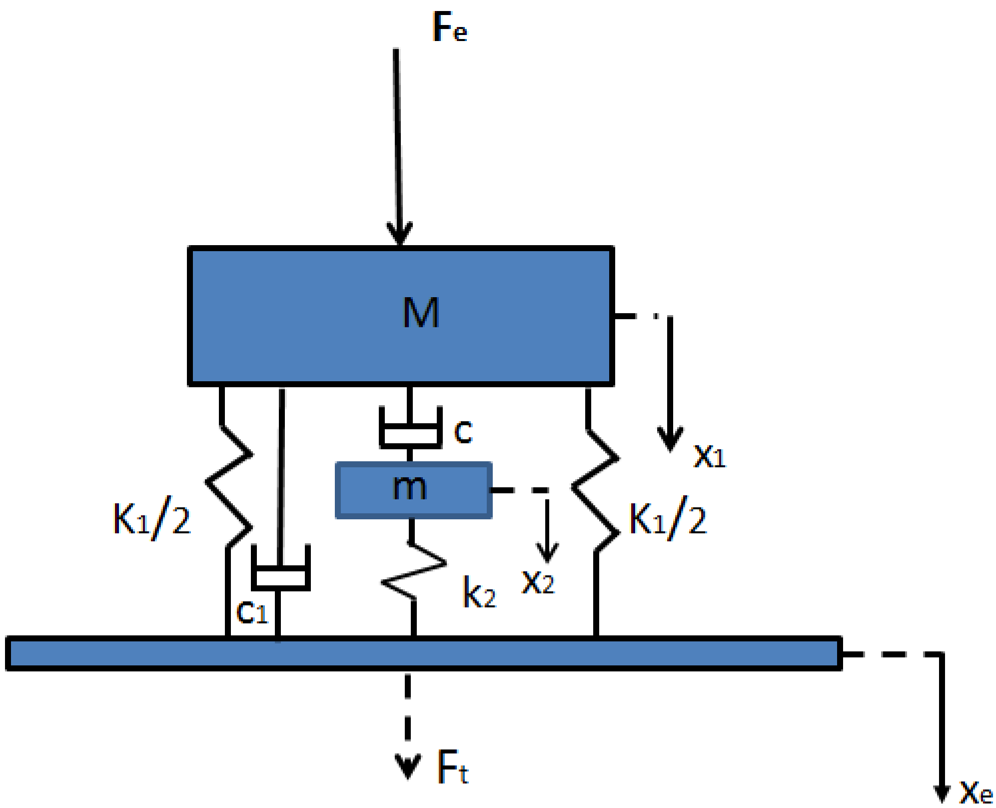

Figure 9 *- Two-degree-of-freedom model of the vibration isolator integrated a skyhook damper*

$$X_2 = \frac{j\omega c}{-m\omega^2 + j\omega c + k_2} X_1 \tag{2-5}$$

Implementing transform on Eq (2-2) and then making use of the relationship given by Eq. (2-5), one will get:

$$X_1 = \frac{k_2 - m\omega^2 + j\omega c}{[k_1 - M\omega^2 + j\omega(c + c_1)][k_2 - m\omega^2 + j\omega c] + \omega^2 c^2} F_e \tag{2-6}$$

Eq. (2-4) results in:

$$F_t = (j\omega c_1 + k_1)X_1 + \frac{j\omega c k_2}{-m\omega^2 + j\omega c + k_2} X_1 \tag{2-7}$$

Therefore, the force transmissibility of the isolator integrated a skyhook damper can be obtained as:

$$T_{fs} = \frac{F_t}{F_e} = \frac{(j\omega c_1 + k_1)(-m\omega^2 + j\omega c + \mathrm{k}_2) + \mathrm{j\omega c k}_2}{[-M\omega^2 + j\omega(c + c_1) + k_1](-m\omega^2 + j\omega c + k_2) + \omega^2 c^2} \tag{2-8}$$

Introducing:

$$\mu = \frac{m}{M}; \omega_1 = \sqrt{\frac{k_1}{M}};\ \omega_2 = \sqrt{\frac{k_2}{m}}; v = \frac{\omega_2}{\omega_1}; \alpha = \frac{c_1}{c}; \xi = \frac{\mathrm{c}}{2\sqrt{k_2 m}}$$

(2-9)

Here μ is defined as mass ratio and α is damping ratio, the ratio of c_1 to c . Now the force transmissibility of the isolator, Eq. (2-8), can be reduced to:

$$T_{fs} = \frac{-\lambda^2(1 + 4\xi^2\alpha\mu v^2) + v^2 + 2j\xi v\lambda(1 + \alpha\mu v^2 + \mu v^2 - \alpha\mu\lambda^2)}{\lambda^4 - (v^2 + 4\alpha\mu\xi^2 v^2 + 1)\lambda^2 + v^2 + 2j\xi v\lambda[1 + \mu v^2(1 + \alpha) - (1 + \mu(1 + \alpha))\lambda^2]}$$

(2-10)

Where $\lambda = \frac{\omega}{\omega_1}$ is defined as frequency ratio and ω is the frequency of excitation force/loading and $\omega_1 = \sqrt{\frac{k_1}{M}}$.

Taking the similar procedures, the force transmissibility of the isolator integrated a groundhook damper which is modelled as a two-degree-of-freedom system, as shown in Figure 10, can be obtained as:

$$T_{fg} = \frac{-\lambda^2(4\xi^2\alpha\mu v^2 + 1) + v^2 + 2j\xi v\lambda(1 + \alpha\mu v^2 + \mu v^2 - \alpha\mu\lambda^2)}{\lambda^4 - (v^2 + 4\mu\alpha\xi^2 v^2 + \mu v^2 + 1)\lambda^2 + v^2 + 2j\xi v\lambda[(1 + \mu v^2 + \alpha\mu v^2 - (1 + \alpha\mu)\lambda^2]} \tag{2-11}$$

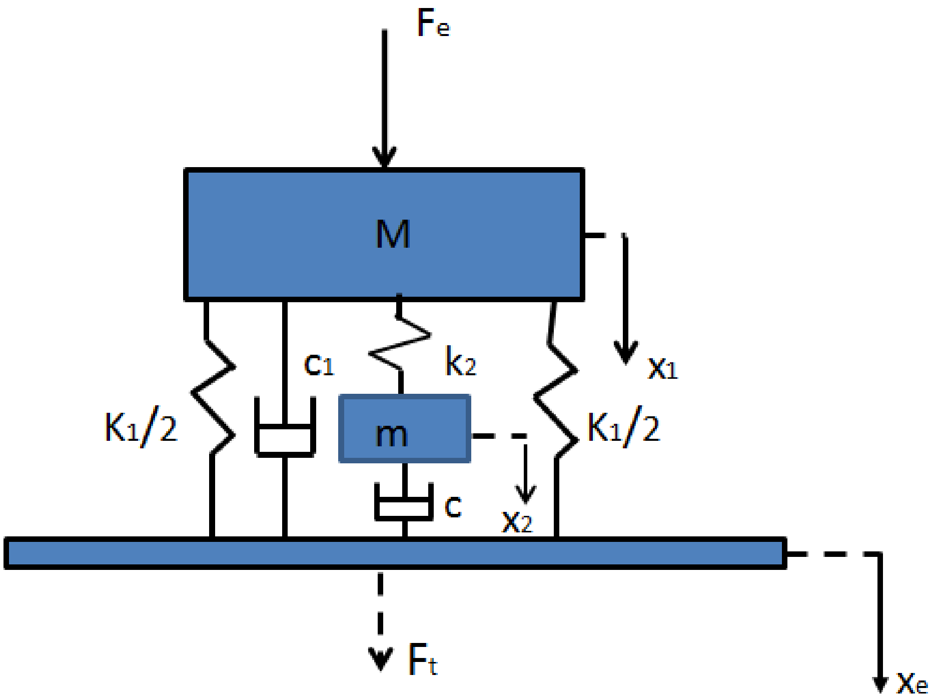

Figure 10 *- Two-degree-of-freedom model of the vibration isolator integrated a groundhook damper*

2.2.2 Displacement Transmissibility

For the system shown in Figure 10, with $F_e = 0$, the equations of motion for displacement excitation of the base (the source of vibration) x_e, are:

$$\begin{cases} M\ddot{x}_1 + k_1(x_1 - x_e) + k_2(x_1 - x_2) + c_1(\dot{x}_1 - \dot{x}_e) = 0 & (2-12) \\ m\ddot{x}_2 + k_2(x_2 - x_1) + c(\dot{x}_2 - \dot{x}_e) = 0 & (2-13) \end{cases}$$

Eq. (2-12) and Eq. (2-13) can be rewritten as:

$$\begin{cases} \ddot{x}_1 + \frac{c_1}{M}\dot{x}_1 + \frac{k_1+k_2}{M}x_1 - \frac{c_1}{M}\dot{x}_e = \frac{k_1}{M}x_e + \frac{k_2}{M}x_2 & (2-14) \\ \ddot{x}_2 + \frac{c}{m}\dot{x}_2 + \frac{k_2}{m}x_2 - \frac{c}{m}\dot{x}_e = \frac{k_2}{m}x_1 & (2-15) \end{cases}$$

Applying the definitions of parameters in Eq. (2-9) and Performing Fourier transform on Eq. (2-14) and Eq. (2-15), one gets:

$$\begin{cases} (-\omega^2 + 2j\xi\mu\alpha\omega_2\omega + \omega_1^2 + \mu\omega_2^2)X_1 - \mu\omega_2^2X_2 = (\omega_1^2 + 2j\xi\mu\alpha\omega_2\omega)X_e & (2-16) \\ (-\omega^2 + 2j\xi\omega_2\omega + \omega_2^2)X_2 - 2j\xi\omega_2\omega X_e = \omega_2^2X_1 & (2-17) \end{cases}$$

Solving Eq. (2-16) and Eq. (2-17), the displacement transmissibility of the vibration isolator integrated a groundhook damper can be obtained as:

$$T_{dg} = \frac{X_1}{X_e} = \frac{A+j\xi B}{C+j\xi D} \tag{2-18}$$

Where:

$$A = -\lambda^2(1 + 4\xi^2\mu\alpha v^2) + v^2 \tag{2-19}$$

$$B = 2v\lambda(1 + \mu\alpha v^2 + \mu v^2 - \mu\alpha\lambda^2) \tag{2-20}$$

$$C = \lambda^4 - (1 + \mu v^2 + v^2 + 4\alpha\mu\xi^2 v^2)\lambda^2 + v^2 \tag{2-21}$$

$$D = 2v\lambda[1 + \mu v^2 + \alpha\mu v^2 - (1 + \alpha\mu)\lambda^2] \tag{2-22}$$

Inserting equations (2-19), (2-20), (2-21) and (2-22) into Eq.(2-18) and comparing the resulted displacement transmissibility of the isolator integrated a groundhook damper, T_{dg}, with the force transmissibility of the isolator, T_{fg} presented in Eq(2-11), it is easy to find that: $T_{dg} = T_{fg}$, therefore, this isolator is a linear isolator.

The displacement transmissibility function of the isolator integrated a skyhook damper T_{ds} can be developed in similar procedures and it will meet $T_{ds} = T_{fs}$. Therefore, the isolator integrated a skyhook damper is also a linear isolator.

2.3 Numerical simulations and discussion

2.3.1 Performance of the vibration isolator

Intensive numerical study on the passive vibration isolator integrated a skyhook/groundhook damper was performed. Figure 10 presents the amplitude of force transmissibility $|T_{fg}|$ and $|T_{fs}|$ against frequency ratio λ respectively at mass ration $\mu = 0.25$; $\alpha = \frac{c_1}{c} = 0$ (which means no damper c_1); damping ratio $\boldsymbol{\xi}$ = 0.03 and $v = 15$. According to the definition of these parameters given in Eq. (2-9), such parameter values are not difficult to achieve in practice. Mass ratio $\mu = 0.25$ may be considered big. However, it may just require more space in practice. Especially for the isolator integrated a skyhook damper, big damper mass m only requires a bigger space to fit in, not necessarily leads to higher costs or other difficulties. $v = \frac{\omega_2}{\omega_1} = 15$ can be achieved by increase k_2 accordingly in practice.

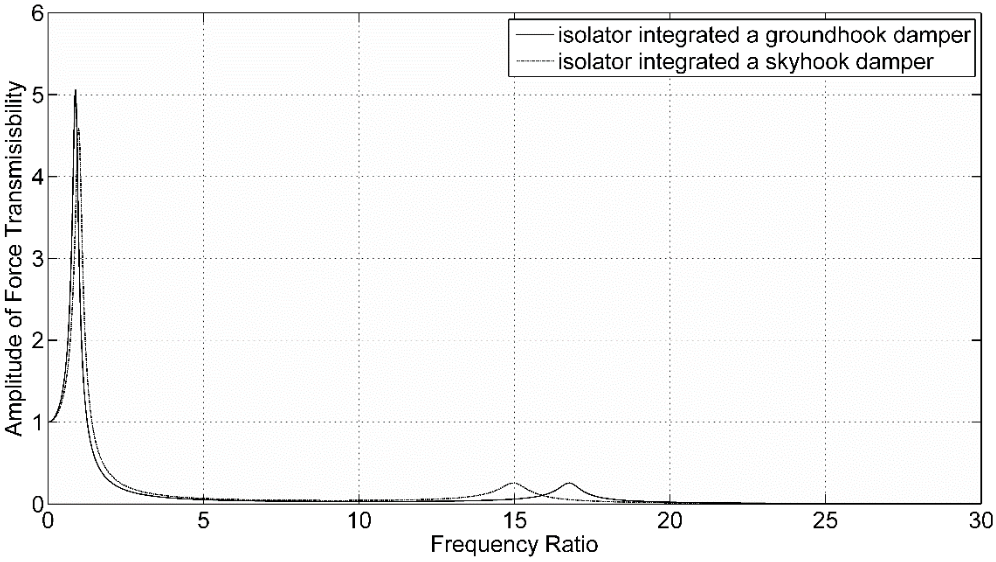

Figure 11 *- Force transmissibility of the isolator integrated a groundhook damper or a skyhook damper at mass ratio μ=0.25; α=0; damping ratio ξ=0.03 and ν=15*

Figure 11 clearly shows that both the transmissibility of the isolator integrated a skyhook damper, and the transmissibility of the isolator integrated a groundhook damper have two peaks, not like the transmissibility graph of a traditional vibration isolator only has one peak at λ=1, as shown in Figure 7. This fundamental difference resulted from the fact that the isolator integrated a skyhook damper or a groundhook damper is a two-degree-of-freedom system while the traditional isolator is a single-degree-of-freedom system. The first peak of transmissibility of the isolator integrated a groundhook damper is 5.062 (at λ=0.885). And for the isolator integrated a skyhook damper, the first peak of transmissibility is 4.585 (at λ=0.985). It should be noted that the first peak occurs at λ< 1, which is an advantage of the new isolator suggested over the traditional vibration isolator, for it means the extending of the range of attenuation towards lower frequency. For the isolator with groundhook damper, transmissibility $T_{fg} \leq 1$ from λ≥ 1.265. T_{fg} drops quickly to 0.27 at λ=2 and keeps very low until the second peak at λ=16.8. For the isolator integrated a skyhook damper, transmissibility $T_{fs} \leq 1$ from λ≥ 1.41. T_{fs} drops quickly to 0.36 at λ=2 and keeps very low until the second peak at λ=15.

The position of the second peak of transmissibility of the isolator suggested depends on the value of parameter v. For the isolator integrated skyhook damper, the second peak occurs at λ= v =15 while for the isolator integrated groundhook damper, the second peak occurs at λ=16.8, a little bit higher than v =15. Based on this fact, in the design of the isolator suggested, it can be designed to ensure $\lambda = \frac{\omega}{\omega_1} < v$ by designing the value of v. It also needs to remember that the performance of the isolator suggested as shown in Figure 28 is achieved without damper $c_1(\alpha = 0)$ and damping ratio ξ=0.03. Moreover, in design of the new isolator, k_1 can be designed according to the static load bearing requirement, there is no need to make k_1 dynamically small or even zero.

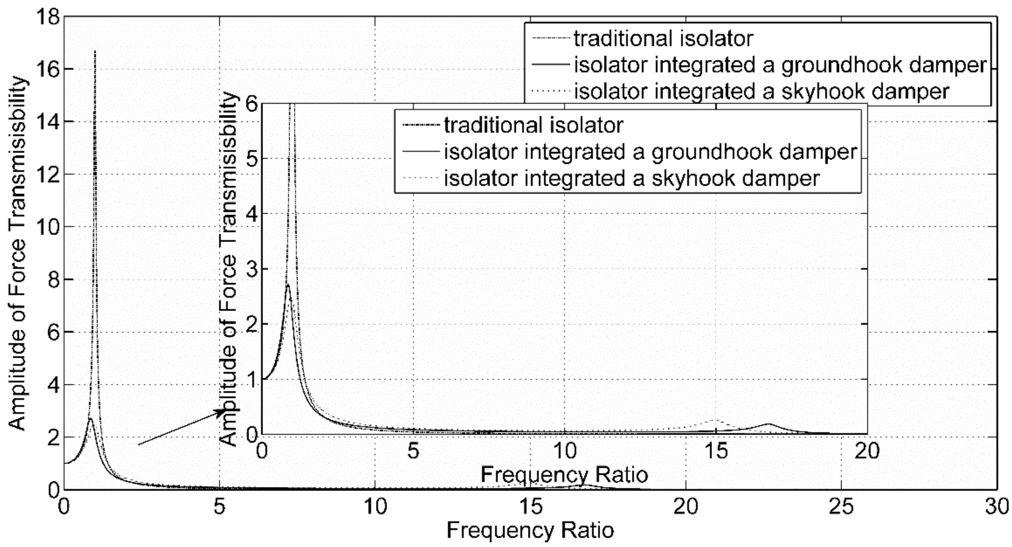

Figure 12 *- Transmissibility of the isolator suggested at mass ratio μ=0.25; α=1; damping ratio* ***ξ****=0.03 and v=15 in contrast with the transmissibility of a traditional isolator at same damping ratio of ζ=0.03*

Figure 12 presents the transmissibility of the isolator integrated a skyhook damper or a groundhook damper at mass ratio $\mu = 0.25$; $\alpha = 1$; damping ratio ξ=0.03 and $v = 15$ in contrast with the transmissibility of a traditional isolator at same damping ratio of $\zeta = 0.03$. It is observed that the peak value of the transmissibility of the isolator integrated a skyhook damper or a groundhook damper is only about 15% of the peak value of the traditional vibration isolator with same damping ratio. Moreover, after the peak until $\lambda \leq 14$, the transmissibility of the isolator suggested has no significant difference with the transmissibility of a traditional isolator. The second peak of transmissibility of the isolator integrated a skyhook damper or a groudhook damper is low ($<$0.3) and occurs at high frequency ($\lambda >$ 14).

2.3.2 Numerical Optimisation and Analysis

Numerical parameter study shows that the mass ratio μ of the new isolator suggested plays an important rule on the performance of the isolator. When $\alpha = 0$, i.e., there is no damper c_1, if $\mu < 0.07$, the adding up of a skyhook damper or a groundhook damper cannot improve the vibration isolation performance, for the peak of the transmissibility of the new isolator, approximates same height as that of a traditional isolator as shown in Figure 13. If μ goes further smaller, the peak of the new isolator could become higher than that of the traditional isolator. If $\alpha = 1$, only when $\mu \geq 0.035$ the adding up of the skyhook damper or groundhook damper starts to benefit vibration isolation. A higher mass ratio μ will further reduce the height of the peak of transmissibility. Figure 14 is the result when mass ratio is increased to $\mu = 0.4$.

Parameter v affects the performance of vibration isolating significantly. When $v < 1$, the adding up of skyhook damper or groundhook damper can only make the vibration isolating performance worse as the peak of the transmissibility is higher than that of a traditional isolator, though the graphs will not be presented here to save space

.

As shown in Figure 15, when $v = 1$, the isolator integrated a skyhook damper yields very high peak of transmissibility, much higher than that of a traditional isolator. In this case, the second peak which occurs at λ=$v = 1$ added up to the first peak which occurs at λ=1, which makes only one peak appearing on the transmissibility as that of a single-degree-of-freedom isolator. However, the isolator integrated a groundhook damper now becomes a traditional vibration isolator with a tuned mass damper which is tuned to the fundamental frequency of the traditional vibration isolator ($v = \frac{\omega_2}{\omega_1} = 1$), which turned the single peak of the transmissibility of a traditional isolator into two peaks. The first peak occurs at λ=0.78< 1 and the second peak at λ=1.28>$v = 1$, which shows the same characteristics of the isolator suggested as that revealed in *3.1*

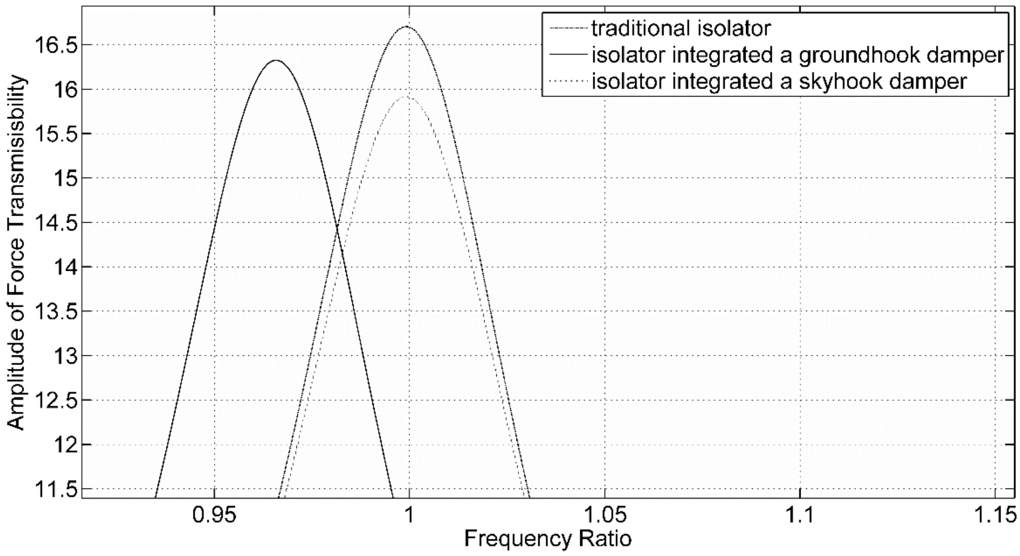

Figure 13 *- Transmissibility of the isolator suggested at mass ratio μ=0.07; α=0; damping ratio ξ=0.03 and v=15 against the transmissibility of a traditional isolator at same damping ratio of ζ=0.03.*

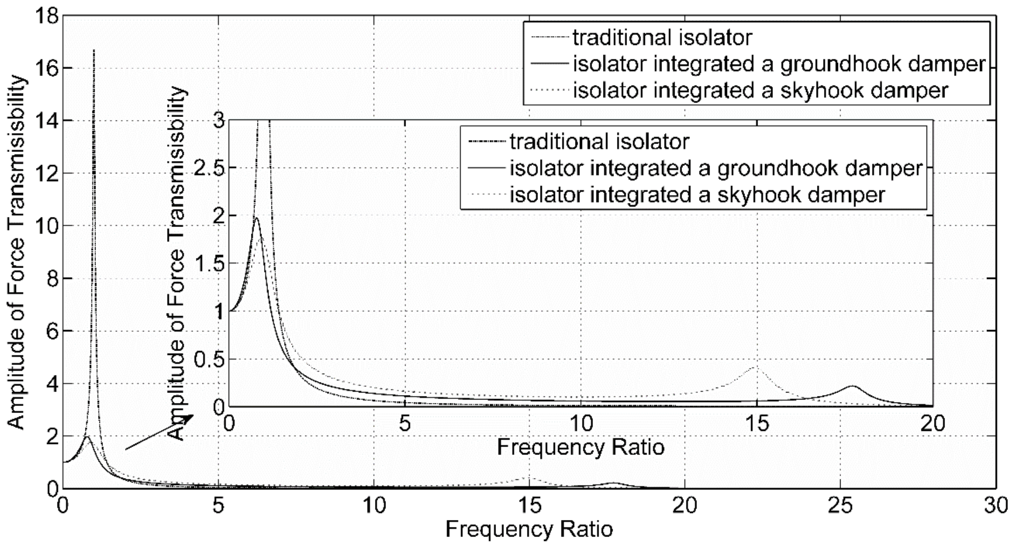

Figure 14 *- Transmissibility of the isolator suggested at mass ratio μ=0.4; α=1; damping ratio ξ=0.03 and v=15 against the transmissibility of a traditional isolator at same damping ratio of ζ=0.03*

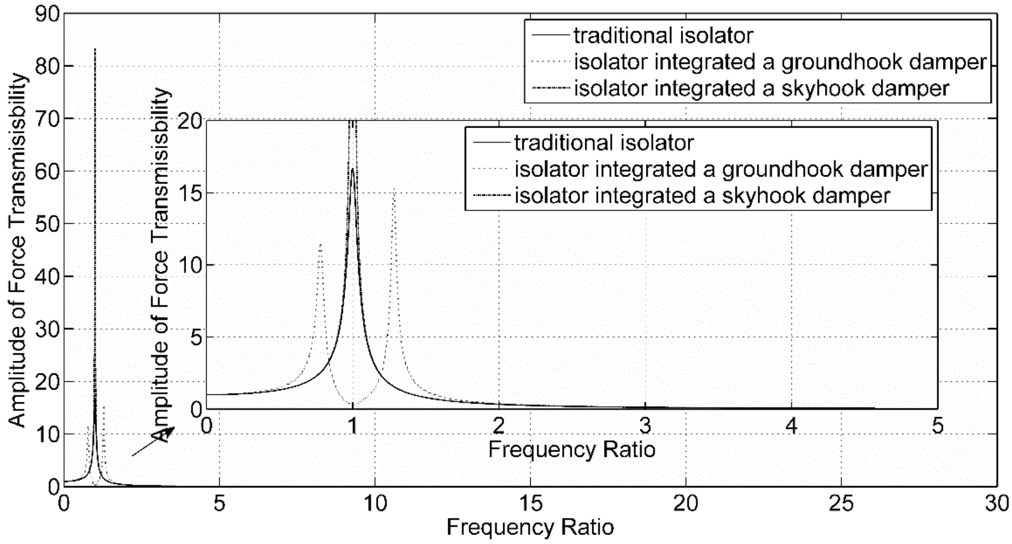

Figure 15 *- Transmissibility of the isolator suggested at mass ratio μ=0.25; α=1; damping ratio ξ=0.03 and v=1 against the transmissibility of a traditional isolator at same damping ratio of ζ=0.03*

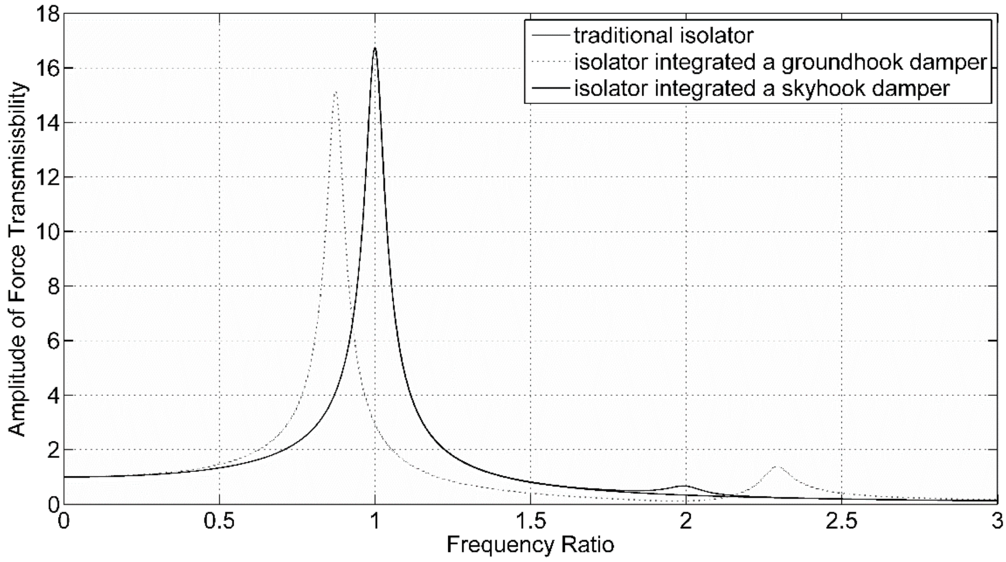

Figure 16 *- Transmissibility of the isolator suggested at mass ratio μ=0.25; α=1; damping ratio ξ=0.03 and v=2 against the transmissibility of a traditional isolator at same damping ratio of ζ=0.03*

When $v = 2$, as shown in Figure 6, the transmissibility of the isolator integrated a skyhook damper has no significant difference from that of a traditional isolator except that at λ=2 the transmissibility of the isolator integrated a skyhook damper gets the second peak. The peak of the transmissibility of the isolator integrated a groundhook damper is only a little bit lower than that of a traditional isolator, but not significant. All these results indicate that in the design of the new vibration isolator suggested term $v > 2$ should be met.

When $v \geq 3$, the isolator integrated a skyhook damper or groundhook damper produces significantly lower peak of transmissibility than the peak of transmissibility of a traditional isolator. The higher the value of v is, the more reducing in the height of the peak of transmissibility produces. It can also be seen that with higher value of v, the transmissibility at higher frequencies becomes slightly higher compared with that of a traditional vibration isolator. Figure 17 shows results at $v = 20$. It can be seen that the peak value becomes smaller and transmissibility at higher frequencies goes up a little bit.

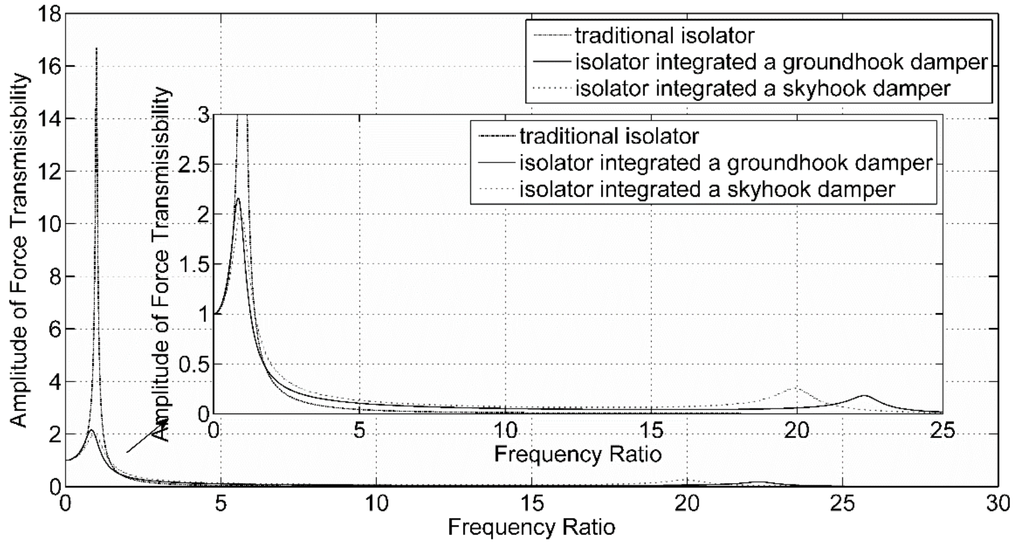

Figure 17 *- Transmissibility of the isolator suggested at mass ratio μ=0.25; α=1; damping ratio ξ=0.03 and v=20 against the transmissibility of a traditional isolator at same damping ratio of ζ=0.03*

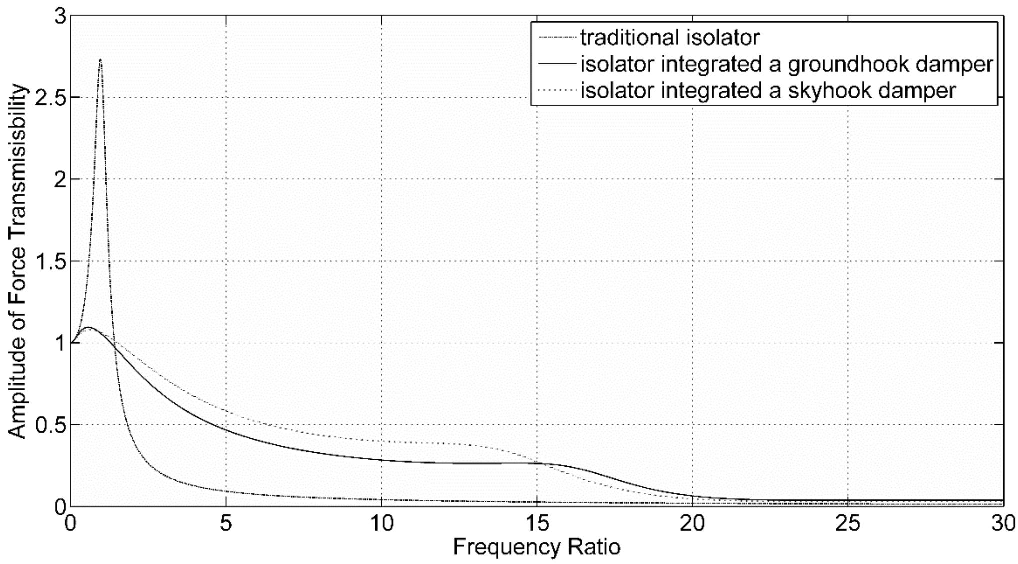

Figure 18 *- Transmissibility of the isolator suggested at mass ratio μ=0.25; α=1; damping ratio ξ=0.2 and v=15 against the transmissibility of a traditional isolator at same damping ratio of ζ=0.2*

Damping always benefits vibration isolation. Higher values of α increase the efficiency in isolating vibration. Higher values of ξ reduces the peak value of the transmissibility of the isolator but adversely, also increase transmissibility at higher frequencies, as shown in Figure 18.

Numerical simulation

Numerical simulation was performed to check results obtained above. 4[th] order Runge-Kutta method (RK4) was employed in numerical simulation. The parameters of the isolator to be simulated numerically are: $M = 10kg$; $k_1 = 1000N/m$. Taking mass ratio $\mu =$

$\frac{m}{M}$=*0.25*, then the mass of the damper to be embodied in is: $m = \mu M = 0.25 \times 10 = 2.5kg$. Taking $v = \frac{\omega_2}{\omega_1} = 15$, therefore, the stiffness of the damper is:

$$k_2 = m\omega_2^2 = m \times v^2 \times \omega_1^2 = m \times v^2 \times \frac{k_1}{M} = 2.5 \times 15^2 \times \frac{1000}{10} = 56250N/m.$$

Taking $\xi = 0.03$, then, $c = 2\xi\sqrt{k_2 m} = 2 \times 0.03 \times \sqrt{56250 \times 2.5} = 22.5$. Taking $\alpha = \frac{c_1}{c} = 0$, then, $c_1 = 0$. Assuming that the harmonic load acting on M is $F_e = 100\cos\omega t$ (N). For the isolator integrated a skyhook damper, the force transmitted to the base is : $F_T = k_1x_1 + kx_2 + c_1\dot{x}_1$ while for the isolator integrated a groundhook damper, the force transmitted to the base is: $F_T = k_1x_1 + c\dot{x}_2 + c_1\dot{x}_1$. After x_1 , x_2, $\dot{x}_1$ and $\dot{x}_2$ being determined numerically, F_T and further the transmissibility of the isolator $T = \frac{F_T}{F_e}$ can be determined. First let the loading frequency $\omega = \omega_1 = 10$, i.e., $\lambda = 1$, numerical simulations were performed on the isolator integrated a skyhook damper and isolator integrated a groundhook damper respectively. Figure 19 presents the transmissibility of the isolator integrated a skyhook damper or a groundhook damper respectively at mass ratio $\mu = 0.25$; $\alpha = 0$; damping ratio ξ=0.03 and $v = 15$. From Figure 15, it can be read out that the force transmissibility of the isolator integrated a skyhook at $\lambda = 1$ is $T_{fs} = 4.5604$ and the transmissibility of the isolator integrated a groundhook damper at $\lambda = 1$ is $T_{fg} = 3.0387$.

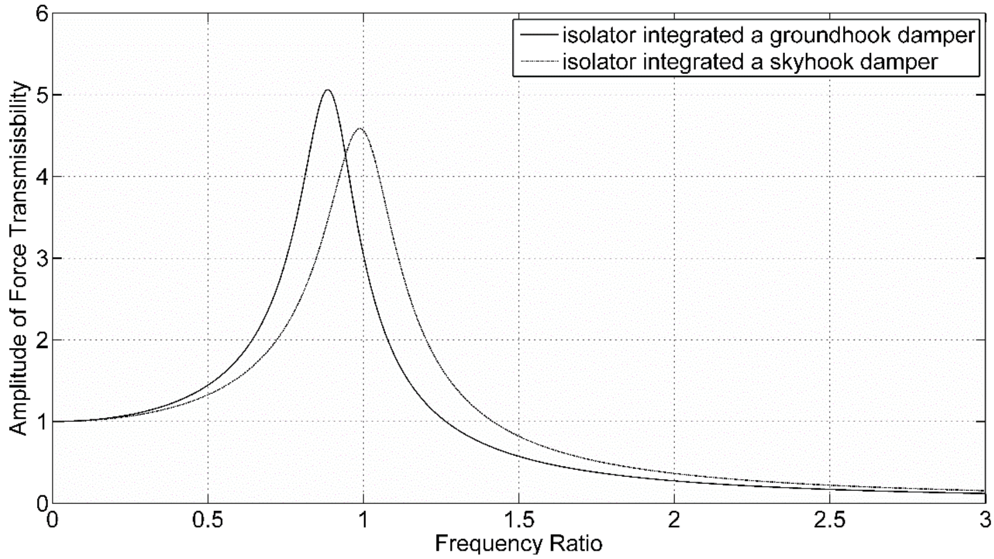

Figure 19 *- Transmissibility of the isolator suggested at mass ratio μ=0.25; α=0; damping ratio ξ=0.03 and v=15*

In Figure 19, we observe that the amplitude of force transmissibility of both the isolator integrated with a skyhook and groundhook, begins to approach unity at a frequency ratio of 2.5, beyond this point, no subsequent peaks are observed hence, for clarity, the figure is plotted to a maximum frequency ratio of 3.

Figure 20 presents the simulated force transmitted to the base, F_T, for the isolator integrated a skyhook damper. It can be found that the peak value of F_T is 456.04N. The peak value of F_e is 100N.Therefore, the transmissibility at $\lambda = 1$ is $T_{fs} = \frac{456.04}{100} = 4.5604$, which is exactly the same as the transmissibility at $\lambda = 1$ determined from Figure 15. Figure 21 presents the simulated force transmitted to the base, F_T, for the isolator integrated a groundhook damper. It can be found that the peak value of $\mathrm{F_T}$ is 303.87N. The peak value of $\mathrm{F_e}$ is 100N. Therefore, the transmissibility at $\lambda = 1$ is $T_{fs} = \frac{303.87}{100} = 3.0387$, which is equal to the transmissibility at $\lambda = 1$ determined from Figure 36.

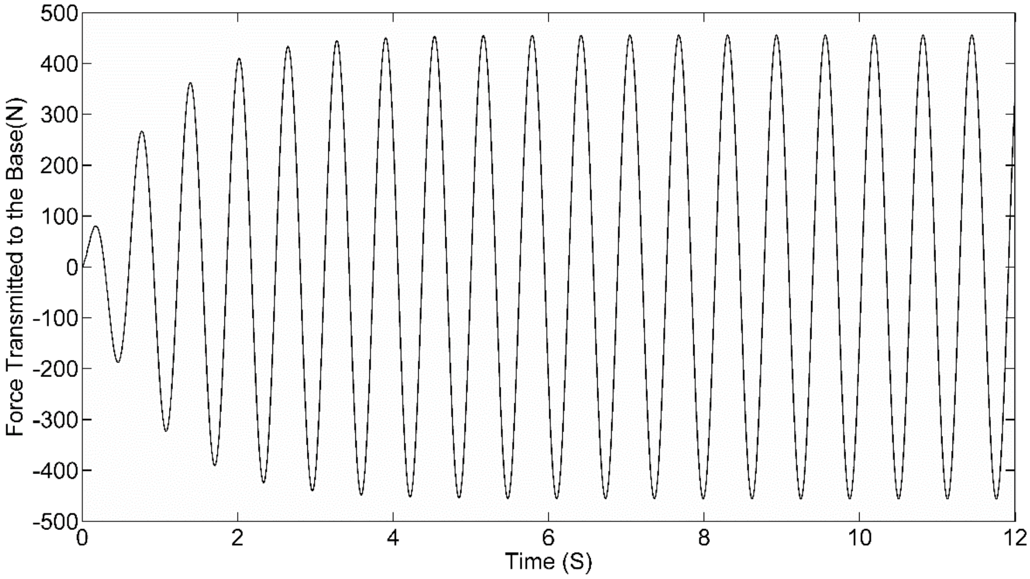

Figure 20 *- The simulated force transmitted to the base of the isolator integrated a skyhook damper*

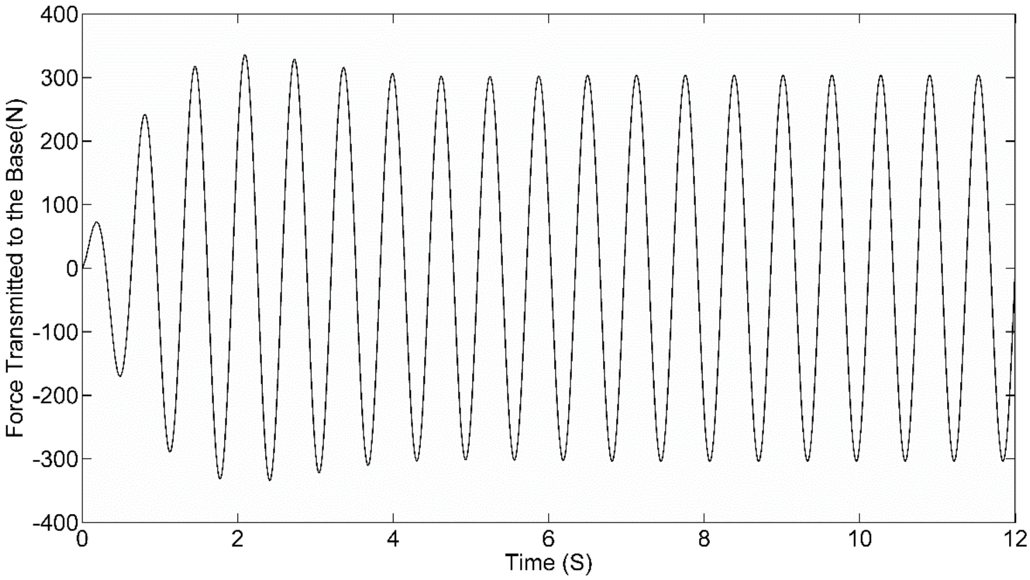

Figure 21 *- The simulated force transmitted to the base of the isolator integrated a groundhook damper*

Extensive simulation on the force transmitted to the base at various values of λ and with different values of parameters of the isolator, such as different μ, different v and so on, were performed. The transmissibility from the ratio of the peak force transmitted to the base (after the system getting steady) to the peak of the loading force always gives the same transmissibility value obtained from the transmissibility function at the corresponding λ, though the simulation results will not be presented here to save space.

2.4 Simulation under sinusoidal, random and white-noise loading

Computer simulations were performed to check results obtained above. The MATLAB Simulink platform was employed in numerical simulation. The parameters of the isolator to be simulated numerically are: $M = 10kg;\ k_1 = 1000N/m$. Taking mass ratio $\mu = \frac{m}{M}$=0.25, then the mass of the damper to be embodied in is: $m = \mu M = 0.25 \times 10 = 2.5kg$. Taking $v = \frac{\omega_2}{\omega_1} = 15$, therefore, the stiffness of the damper is:

$$k_2 = m\omega_2^2 = m \times v^2 \times \omega_1^2 = m \times v^2 \times \frac{k_1}{M} = 2.5 \times 15^2 \times \frac{1000}{10} = 56250N/m.$$

Taking $\xi = 0.03$, then, $c = 2\xi\sqrt{k_2 m} = 2 \times 0.03 \times \sqrt{56250 \times 2.5} = 22.5$. Taking $\alpha = \frac{c_1}{c} = 0$, then, $c_1 = 0$. Simulations were performed on the isolator integrated a skyhook damper.

The results obtained from the Simulink analysis were compared against a traditional isolator system in order to draw a concise comparison of the effect of the inclusion of the additional damping mass and the system's configuration as to ascertain the level of improvement of the proposed configuration. Three key performance areas were identified in order to provide a comprehensive comparison of advantages of the proposed system as compared to the traditional single stage isolator. For the purpose and integrity of the analysis, key parameters of the primary system were kept constant whereas the proposed system's parameters were optimised according to the optimisation techniques derived and discussed in the preceding sections, namely, these parameters are:

$M = 10kg;\ k_1 = 1000N/m$

Taking $\xi = 0.03$, then, $c = 2\xi\sqrt{k_1 M} = 2 \times 0.03 \times \sqrt{1000 \times 10} = 6$

For the purposes of seismic analysis, the uniform random and white-noise loading were analysed as seismic loading inputs whereas the loading on the primary system was modelled as:

$$M\ddot{x} + c\dot{x} + k_1 x = -M\ddot{x}_g$$

The gravitation acceleration due to gravity was assumed to be constant at a value of:

$$g = 9.8\ m/s^2$$

For the traditional isolator, the force transmitted to the base is : $F_T = k_1 x_1 + c\dot{x}_1$.

2.4.1 Sinusoidal Loading

Suppose that a harmonic load is acting on M is $F_e = 100\sin\omega t$ (N).

Where the loading frequency $\omega = \omega_1 = 10$

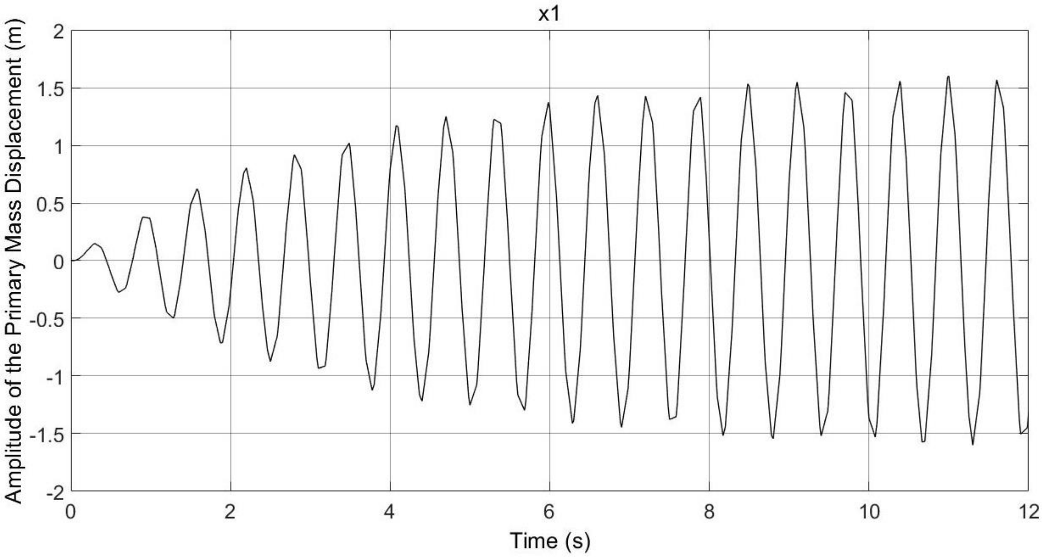

Figure 22 *- Simulated Primary Mass Displacement of the Traditional Single Stage Isolator under Sinusoidal Loading*

Figure 22 shows the simulated displacement response of the traditional isolator shown in Figure 6. The displacement of the primary mass shows a gradual increase in amplitude as the system initialises, the displacement shows a stable period in oscillations due to the imposed sinusoidal loading, the plot indicates that the system requires an increased time lapse in order to stabilise into a steady state condition with the imposed loading, the system is observed to stabilise at a time lapse of 8.476 seconds. A peak amplitude of 1.533 metres is observed within the simulated timeframe of the analysis.

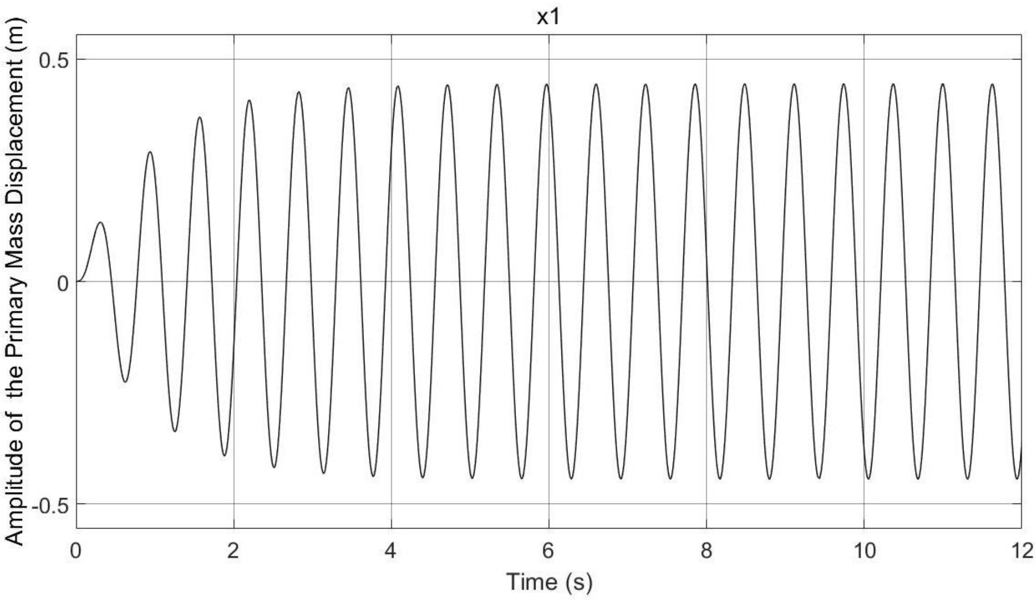

Figure 23 *- Simulated Primary Mass Displacement of the System Integrated with a Skyhook damper under Sinusoidal Loading*

Figure 23 shows the performance of the vibrational isolator integrated with a skyhook damper as shown in Figure 9. The system with the vibrational isolator integrated with a skyhook damper displays significant decrease in the maximum peak displacement of the primary mass as opposed to the traditional isolator shown in Figure 22 whereas in Figure 23 we observe a maximum displacement of 0.4363 metres which is a 71.53% reduction in primary mass displacement. Furthermore, the system stabilises at a shorter timeframe than the traditional isolator at a time lapse of 3.440 seconds. The response system with the vibrational isolator integrated with a skyhook damper shows a smoother sequence of displacement of the primary mass as compared with the response of the system with a traditional vibrational isolator which is essential in limiting adverse effects such as fatigue on the primary system's components.

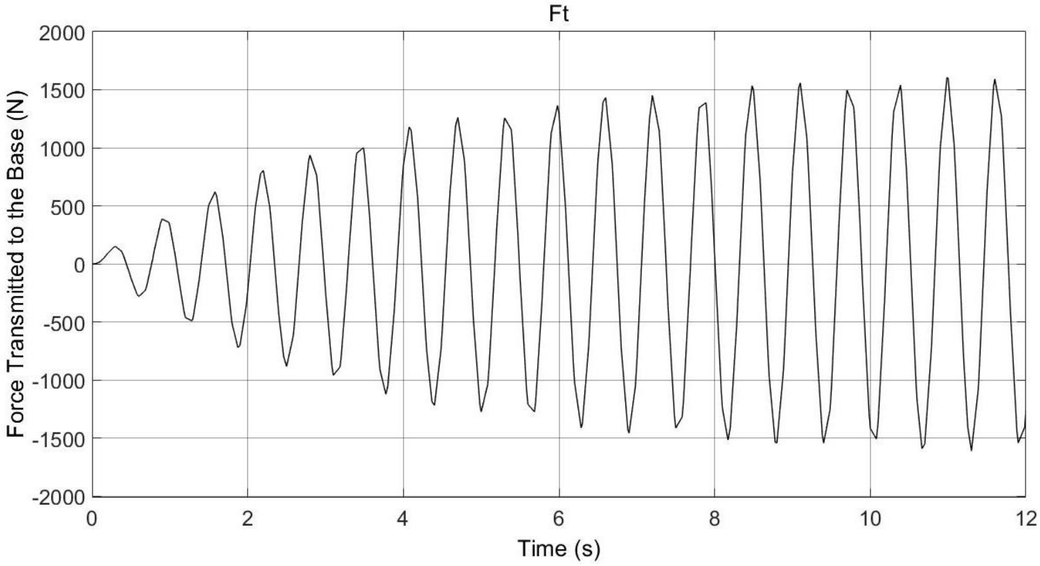

Figure 24 *- The simulated force transmitted to the base of the traditional single stage isolator under Sinusoidal Loading*

Figure 24 shows the simulated loads transferred to the base of a system with a traditional isolator shown in Figure 6. The loads transferred to the base of the primary system shows a gradual increase in amplitude as the system initialises and stabilises at a time lapse of 8.746 seconds achieving a maximum load transfer of 1547N.

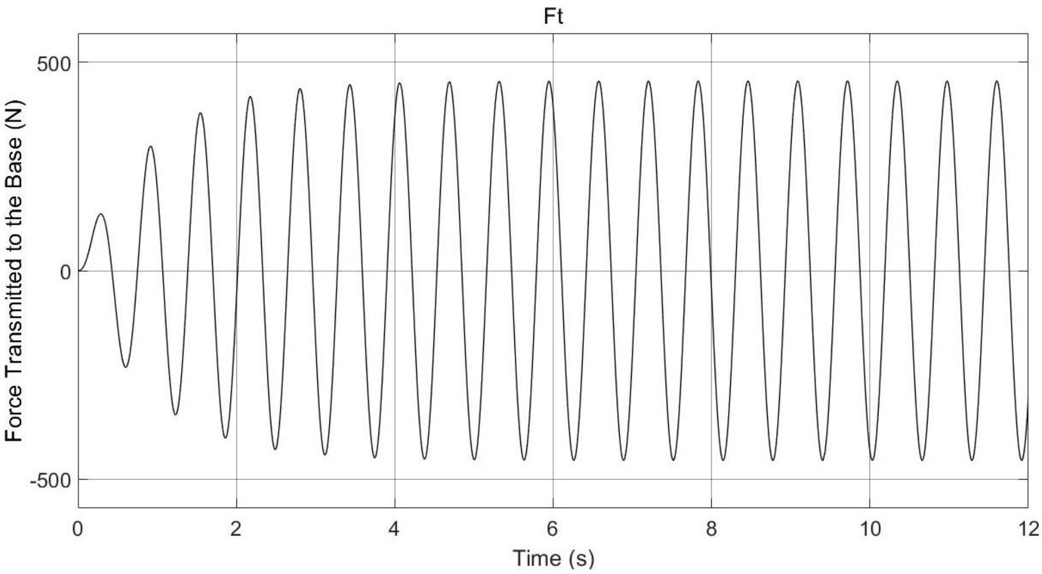

Figure 25 *- The simulated force transmitted to the base of the isolator integrated a skyhook damper under Sinusoidal Loading*

Figure 25 shows the simulated loads transferred to the base of a system with a vibrational isolator integrated with a skyhook damper. The system with the vibrational isolator integrated with a skyhook damper displays a significant decrease in the maximum peak loads transferred to the base of the primary mass as opposed to the traditional isolator shown in Figure 24 whereas in Figure 25 we observe a maximum load transferred to the base of the primary system of 447.71N which is a 71.06% reduction in load transferred to the base of the primary system with a traditional isolator.

2.4.2 Random Loading

Suppose that a uniform random load is acting on M

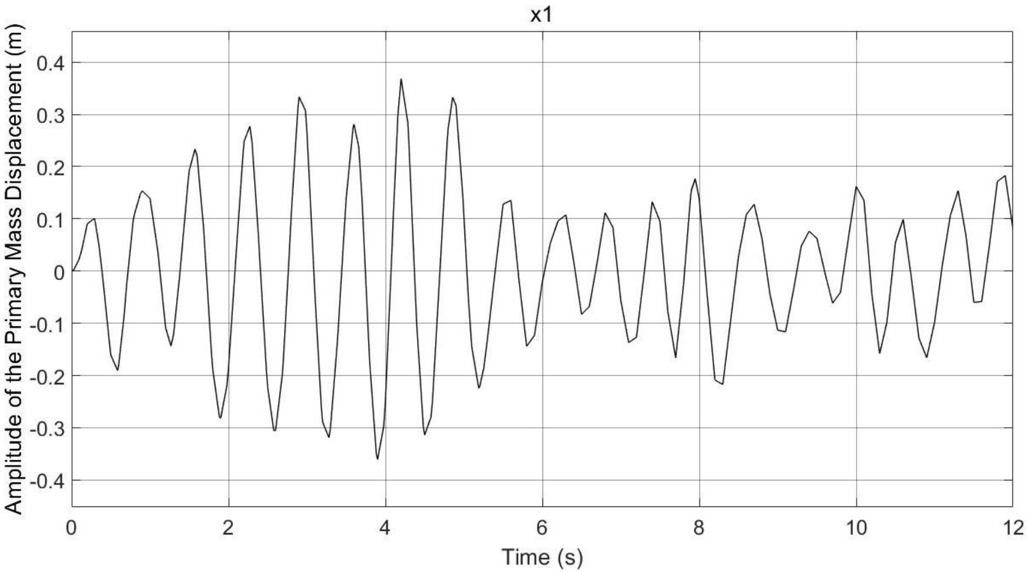

Figure 26 *- Simulated Primary Mass Displacement of the Traditional Single Stage Isolator under Random Loading*

Figure 26 shows the simulated displacement response of the traditional isolator under random loading. The displacement of the primary mass shows a varied response throughout the time lapse, the peak displacement recorded occurs at a time lapse of 4.203 seconds at a peak value of 0.370 metres.

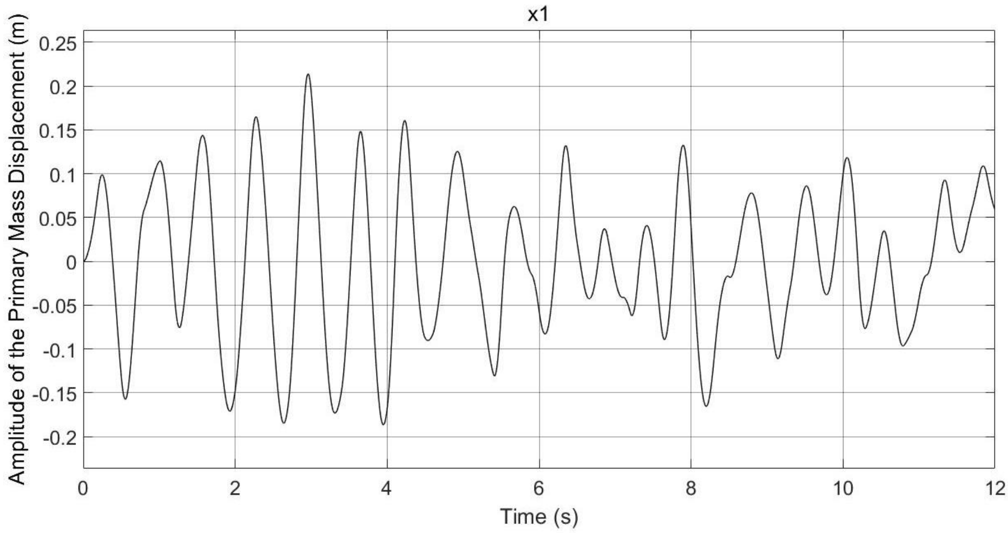

Figure 27 *- Simulated Primary Mass Displacement of the Isolator integrated with a skyhook damper under Random Loading*

Figure 27 shows the displacement response of a system with a vibrational isolator integrated with a skyhook damper under random loading. A similar sequence of loading is shown in Figure 27 as in Figure 26. However, the peak displacement recorded is 0.214 metres at a time lapse of 2.964 seconds, which is a 42.18% reduction as compared to the peak displacement recorded in Figure 26.

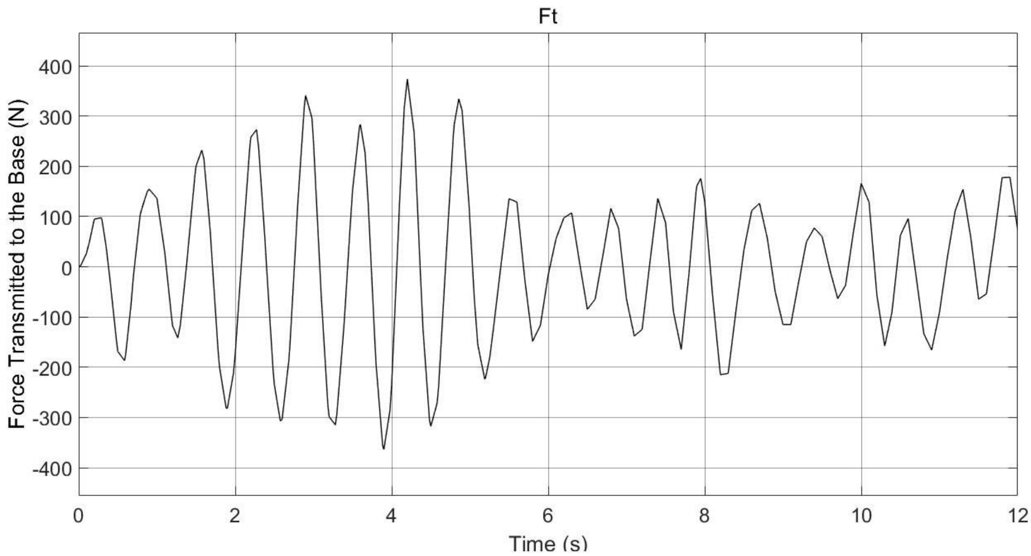

Figure 28 *- Simulated Loads Transferred to the Base of the Primary System with a Traditional Single Stage Isolator under Random Loading*

Figure 28 shows the simulated loads transferred to the base of a system with a traditional isolator under random loading. The loads transferred to the base of the primary mass shows a varied response as time lapses with a peak load transfer of 374.394N at a time lapse of 4.203 seconds.

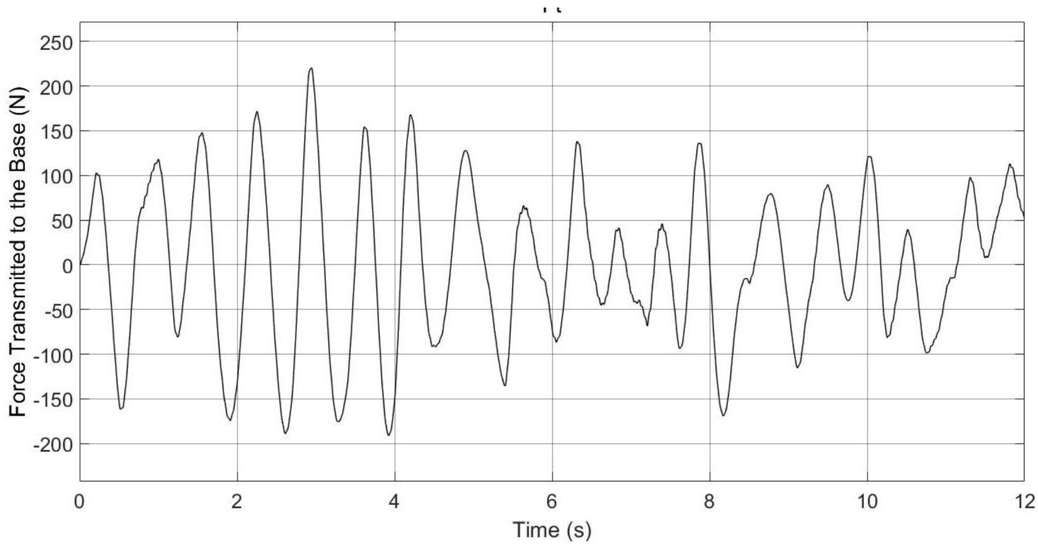

Figure 29 *- Simulated Loads Transferred to the Base of the Primary System with a Isolator Integrated with a Skyhook damper under Random Loading*

Figure 29 shows the simulated loads transferred to the base of a system with a vibrational isolator integrated with a skyhook damper. The system with the vibrational isolator integrated with a skyhook damper displays a significant decrease in the maximum peak loads transferred to the base of the primary mass as opposed to the traditional isolator shown in Figure 28 whereas in Figure 29 we observe a maximum load transferred to the base of the primary system of 219.266N which is a 41.43% reduction in load transferred to the base of the primary system with a traditional isolator.

2.4.3 White-Noise Loading

Suppose that an earthquake (white-noise band) load is acting on M

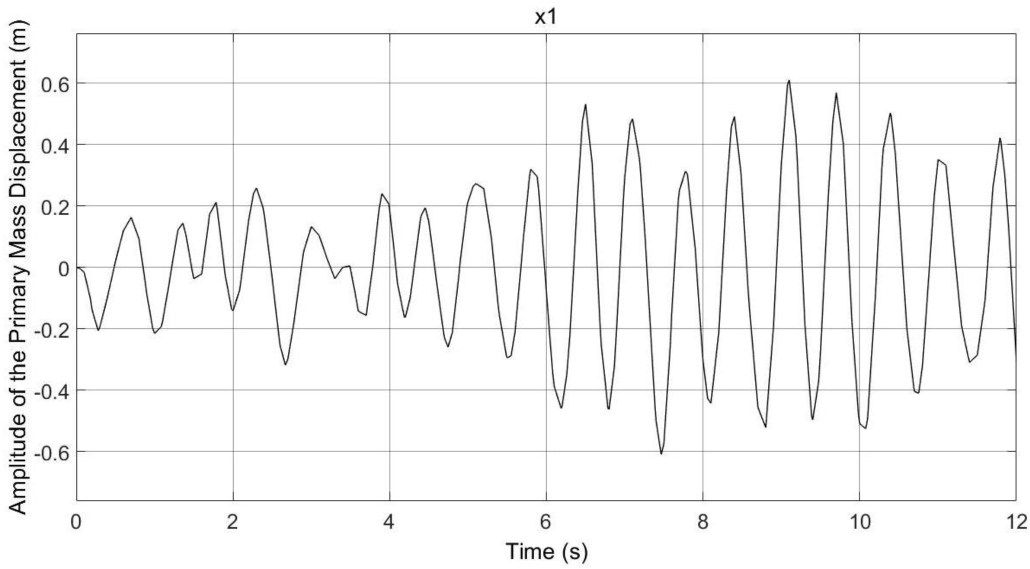

Figure 30 *- Simulated Primary Mass Displacement of the Primary System with the Traditional Single Stage Isolator under White Noise Frequency Band Loading*

Figure 30 shows the simulated displacement response of the traditional isolator under white-noise loading. The displacement of the primary mass shows a varied response throughout the time lapse, the peak displacement recorded occurs at a time lapse of 7.464 seconds at a peak value of 0.603 metres.

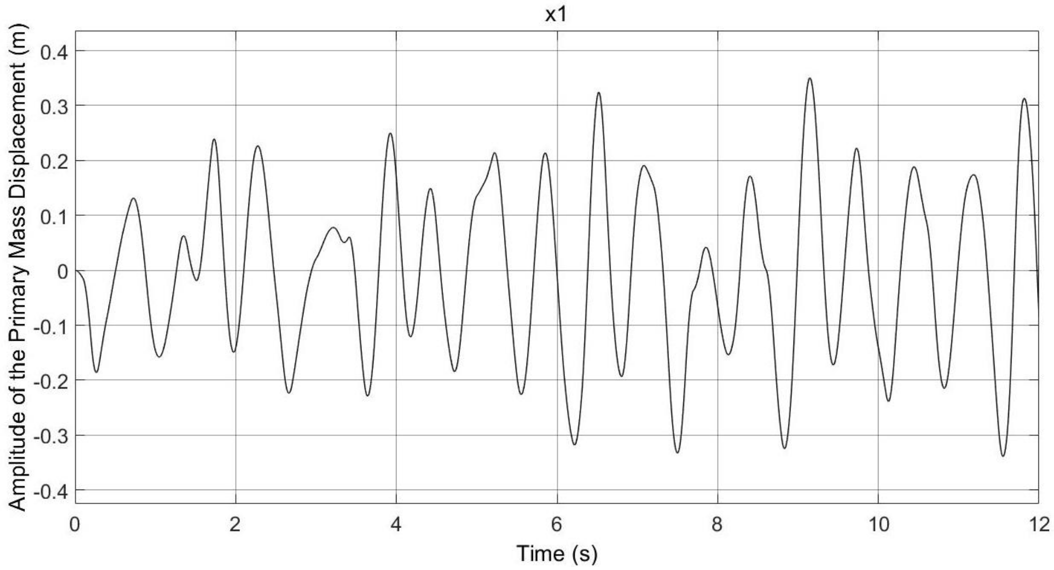

Figure 31 *- Simulated Primary Mass Displacement of the Primary System with the Isolator Integrated with a Skyhook damper under White Noise Frequency Band Loading*

Figure 31 shows the displacement response of a system with a vibrational isolator integrated with a skyhook damper under random loading. A similar sequence of loading is shown in Figure 31 as in Figure 30. However, the peak displacement recorded is 0.351 metres at a time lapse of 9.1486 seconds, which is a 41.79% reduction as compared to the peak displacement recorded in Figure 30.

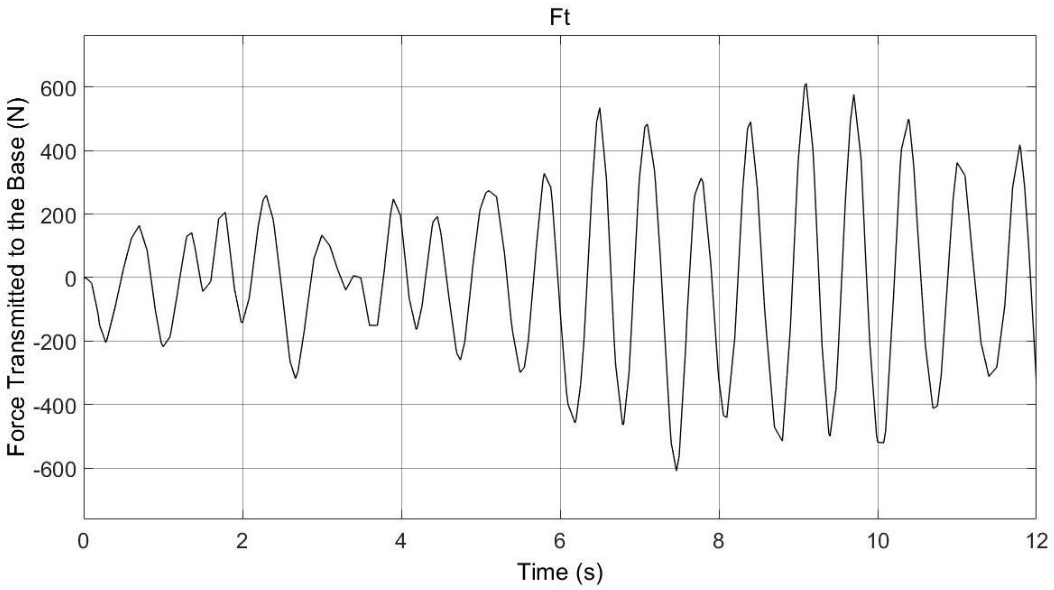

Figure 32 *- Simulated Loads Transmitted to the Base of the Primary System with a Traditional Single Stage Isolator under a White Noise Frequency Band Loading*

Figure 32 shows the simulated loads transferred to the base of a system with a traditional isolator under white-noise loading. The loads transferred to the base of the primary mass shows a varied response as time lapses with a peak load transfer of 604.931N at a time lapse of 7.472 seconds.

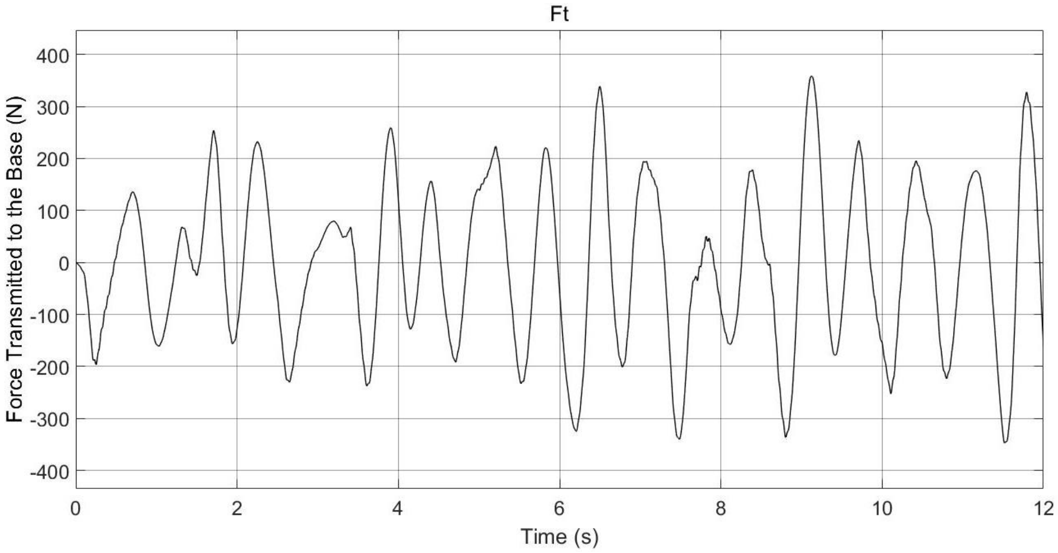

Figure 33 *- Simulated Loads Transmitted to the Base of the Primary System with the Isolator Integrated with a Skyhook damper under a White Noise Frequency Band Loading*

Figure 33 shows the simulated loads transferred to the base of a system with a vibrational isolator integrated with a skyhook damper. The system with the vibrational isolator integrated with a skyhook damper displays a significant decrease in the maximum peak loads transferred to the base of the primary mass as opposed to the traditional isolator shown in Figure 32 whereas in Figure 33, we observe a maximum load transferred to the base of the primary system of 359.276N which is a 40.61% reduction in load transferred to the base of the primary system with a traditional isolator.

2.5 Conclusion

A passive vibration isolator integrated a skyhook damper or a groundhook damper is presented and studied. The force and displacement transmissibility, a common measure of an isolator, of the isolator were derived, based on the two-degree-of-freedom model of the isolator. It is proven that the isolator suggested is a linear isolator, since the force transmissibility of the isolator is exactly the same as its displacement transmissibility.

Numerical studies revealed that, without employing high damping elements ($c_1 = 0\ and\ \xi = 0.03$), the isolator integrated a skyhook damper or a groundhook damper can achieve very good vibration isolating performance whereas significantly lower initial peak values of transmissibility were obtained whereas the transmissibility varied gradually until the second peak which is controlled by the value of parameter v.

The inherent conflict requirements on a linear isolator: high static stiffness to bear high static load or limit static displacement and low or even zero dynamic stiffness to reduce the fundamental natural frequency so that the frequency range over which attenuation ($\mathrm{T} < 1$) occur can be increased, is eliminated. Thus allowing the stiffness of the new isolator, k_1 , can be designed according to the requirement of static load bearing capacity only.

Parameter optimization under different type of loading needs to be further investigated. Prototype developing and experimental investigation need to be performed. A design guideline needs to be developed for its application practice.

Simulations conducted displayed enhanced vibration isolation for the vibration isolator integrated with a skyhook damper. A minimum reduction of 40% of peak values of primary mass displacement and loads transferred to the base as compared to the recorded responses for a system traditional isolator were observed under the same base conditions. The proposed isolator further displayed greater resilience under random and white noise loading which for structural engineering purposes, may be considered to approximate the loading from an earthquake event, thus the proposed isolator can provide enhanced seismic loading isolation. The theoretical analysis conducted on evaluating the transmissibility response of the proposed isolator is corroborated by the numerical analysis and simulations conducted thus making both the proposed vibration isolator integrated with a skyhook and groundhook damper a viable system that can be further developed to be used in practice.

However, the information contained in this chapter is primarily theoretical. Practical testing is thus still required using simulations, initially, using configurations displayed in [28] and subsequently moving to larger scale testing in order to initially verify the theoretical results as well as to formulate design and construction standards that will be used in practice.

CHAPTER THREE – A PASSIVE VIBRATION ISOLATOR INTEGRATED WITH A DYNAMIC VIBRATION ABSORBER WITH A NEGATIVE SPRING

3.1 Introduction

The traditional model of an isolator is that of a single degree of freedom system whereas the system can be configured to accommodate two case of loading on the main system as discussed in Chapter 1 and 2. In the first case, the source of vibration is the payload itself, and in this case the intention is to prevent the vibration to be transmitted to its host structure (the base). In the second case, the disturbance to the payload (which is to be protected now) is caused by vibration of the host structure and the goal is to minimize the transmitted vibration. There are mainly two distinct cases for vibrational loading, the first case is referred to as the force transmissibility problem. whereas the source of vibration is the payload itself, and in this case the intention is to prevent the vibration to be transmitted to its host structure (the base). The second is referred to as the displacement transmissibility problem, whereas the disturbance to the payload (which is to be protected from excessive vibrations) is caused by vibration of the host structure and the goal is to minimize the transmitted vibration transmitted to the payload. The non-dimensional parameter which is used to quantify the effectiveness of an isolation system is transmissibility. For a linear vibration isolator which is a single-degree-of-freedom system, the force transmissibility and displacement transmissibility of the isolator are the same [39].

For a linear isolator, vibration can only be attenuated at frequencies above the square root of two times the fundamental natural frequency of the system, *i.e.*, $T < 1$ only when $\lambda > \sqrt{2}$ or $\omega > \sqrt{2}\omega_1$. This requirement is inherently restrictive to the application of effective vibration isolation, as it limits the value of the fundamental natural frequency of the primary system. This imposes a restriction on the primary stiffness of the system which is essential in meeting the static load requirements thus making practical application impossible. In this chapter, a novel linear passive vibrational isolator which integrates a negative stiffness element is proposed and extensively studied. The proposed isolator is presented in two configurations of which contain the same elements, but the position of the negative stiffness element is varied to determine the configuration that produces enhanced performance against dynamic loading.

A numerical optimisation using a minimax approach is undertaken to determine the optimal parameter selection for enhanced performance of both configurations of the proposed vibrational isolator. The addition of a negative stiffness element introduces additional requirements, with regard to the stability of the proposed isolator as studied in [35] thus extensive stability limits are also discussed in equations derived using Routh-Hurwith stability criterion in order to establish operational and functional limits for the enhanced vibration isolation and stability of the proposed vibration isolator. Extensive sensitivity analysis of governing parameters in undertaken to evaluate the transmissibility response under varied boundary conditions and determine optimal parameter values for the numerical simulations undertaken using the Simulink platform on the MATLAB suite of applications. The numerical simulations are used as a practical evaluation of the performance of the proposed linear isolator against a traditional vibrational isolator depicted in Figure 6 in Chapter 2.

3.2 A vibration isolator integrated with dynamic vibration absorber with a negative spring

3.2.1 Proposed vibration isolator

The suggested passive vibration isolator integrated a dynamic vibration absorber with a negative stiffness spring are depicted in Figure 34 (configuration I) and Figure 35 (configuration II). Mass M can either represent a machine excited by dynamic force or a piece of equipment isolated from base excitation. For a traditional passive isolation system, which is a single-degree-of-freedom system, viscous damper is set in parallel with spring k_1 and they work together to isolate vibration. For such an isolator, high damping is usually required to achieve high isolation efficiency [47].

However, in the vibration isolator suggested, as shown in Figure 34 and Figure 35, the damper(dashpot) parallel with k_1 is eliminated to show the role and effect of the dynamic vibration absorber with a negative stiffness spring integrated into the isolation system. Mass m, spring k_2, damper c_2 and the negative stiffness , k, spring combine into the dynamic vibration absorber (DVA) with a negative stiffness spring, which is integrated with k_1 and result in the new vibration isolation system suggested. Linear spring k_1, k_2, and negative stiffness k, which are all constants, can be determined according to the requirement on static load bearing capacity. One of the aims of the study is to determine if the integration in of the DVA with a negative stiffness spring, instead of changing/reducing the system's stiffness, will assist in meeting the requirement of low or even zero dynamic stiffness of the isolation system

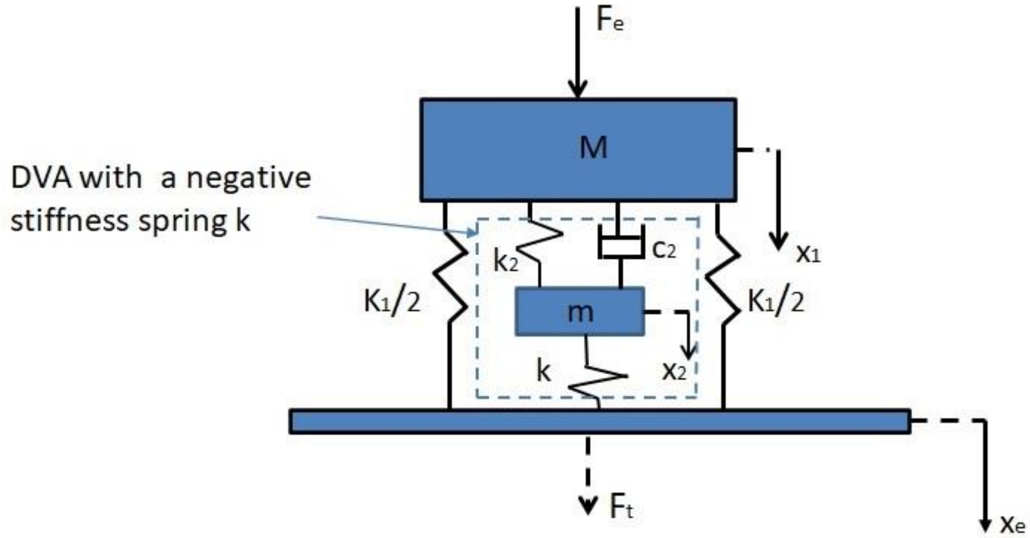

Figure 34 *- Vibration isolator integrated a DVA with negative stiffness spring k --Configuration I: k between m and base*

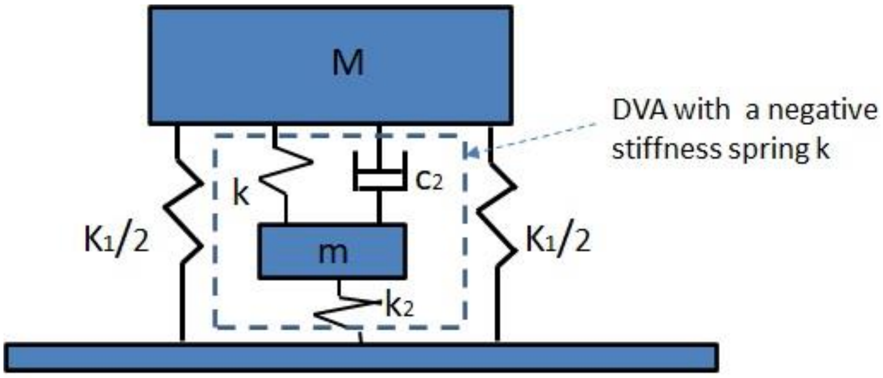

Figure 35 *- Vibration isolator integrated a DVA with negative stiffness spring k --Configuration II: k between m and M*

3.2.2 Force Transmissibility

The passive vibration isolator integrated a DVA with a negative stiffness spring as shown in Figure 34 is a two-degree-of-freedom system.

For this system, with $x_e = 0$, the equations of motion, when M under harmonic force excitation, are given by:

$$\begin{cases} M\ddot{x}_1 + k_1 x_1 + k_2(x_1 - x_2) + c_2(\dot{x}_1 - \dot{x}_2) = F_e\cos(\omega t) & (3-2) \\ m\ddot{x}_2 + kx_2 + k_2(x_2 - x_1) + c_2(\dot{x}_2 - \dot{x}_1) = 0 & (3-3) \\ F_t = k_1 x_1 + kx_2 & (3-4) \end{cases}$$

Performing Fourier transform on Eq. (3-3), the following relationship will be obtained:

$$X_2 = \frac{k_2 + j\omega c_2}{-m\omega^2 + j\omega c_2 + (k_2 + k)} X_1 \qquad (3\text{-}5)$$

Implementing transform on Eq. (2-2) and then making use of the relationship given by Eq. (2-5), one will get:

$$X_1 = \frac{k_2 + k - m\omega^2 + j\omega c_2}{[(k_1 + k_2) - M\omega^2 + j\omega c_2][(k_2 + k) - m\omega^2 + j\omega c_2] - (k_2 + j\omega c_2)^2} F_e \qquad (3\text{-}6)$$

Therefore, the force transmissibility of the isolator can be obtained as:

$$T_{fI} = \frac{F_t}{F_e} = \frac{k_1 X_1 + kX_2}{F_e} = \frac{\left[k_1 + k\frac{k_2 + j\omega c_2}{-m\omega^2 + j\omega c_2 + (k_2 + k)}\right] X_1}{F_e} \qquad (3\text{-}7)$$

Inserting Eq. (3-6) into Eq. (3-7) yields:

$T_{fI} =$

$$\frac{-\frac{m}{M}\omega^2\frac{k_1}{M}+\frac{k_2+k}{M}\cdot\frac{k_1}{M}+\frac{k_2}{M}\cdot\frac{k}{M}+j\omega\frac{c_2}{M}\cdot(\frac{k_1+k}{M})}{\frac{m}{M}\omega^4-\left(\frac{k_2}{M}+\frac{k}{M}+\frac{m}{M}\frac{k_2}{M}+\frac{m}{M}\frac{k_1}{M}\right)\omega^2+\left(\frac{k_2}{M}\frac{k_1}{M}+\frac{k}{M}\frac{k_1}{M}+\frac{k_2}{M}\frac{k}{M}\right)+j\omega\frac{c_2}{M}\left[\frac{k_1+k}{M}-\frac{(M+m)}{M}\omega^2\right]}$$

(3-8)

Introducing:

$$\mu=\frac{m}{M};\omega_1=\sqrt{\frac{k_1}{M}};\ \omega_2=\sqrt{\frac{k_2}{m}};v=\frac{\omega_2}{\omega_1};\alpha=\frac{k}{k_2};\zeta=\frac{c_2}{2\sqrt{k_2m}} \quad (3\text{-}9)$$

Here μ is defined as mass ratio and α is negative stiffness ratio, defined as the ratio of negative stiffness k to k_2 , instead of the isolator's mount stiffness $k_{1.}$ Now the force transmissibility of the isolator, Eq. (3-8), can be reduced to:

$$T_{fI}=\frac{-\lambda^2+(1+\alpha)v^2+\alpha\mu v^4+2j\xi v\lambda(1+\alpha\mu v^2)}{\lambda^4-(v^2+\alpha v^2+\mu v^2+1)\lambda^2+(v^2+\alpha v^2+\alpha\mu v^4)+2j\xi v\lambda[1+\alpha\mu v^2-(1+\mu)\lambda^2]}$$

(3-10)

Where $\lambda=\frac{\omega}{\omega_1}$ is defined as frequency ratio and ω is the frequency of excitation force/loading and $\omega_1=\sqrt{\frac{k_1}{M}}$.

By applying the same procedures as above, the transmissibility of the isolator in configuration II as shown in Figure 30 can be obtained as:

$$T_{fII}=\frac{-\lambda^2+(1+\alpha)v^2+\alpha\mu v^4+2j\xi v\lambda(1+\mu v^2)}{\lambda^4-(v^2+\alpha v^2+\alpha\mu v^2+1)\lambda^2+(v^2+\alpha v^2+\alpha\mu v^4)+2j\xi v\lambda[1+\mu v^2-(1+\mu)\lambda^2]}$$

(3-11)

Figure 36 present the amplitude of force transmissibility $|T_{fI}|$ and $|T_{fII}|$ against frequency ratio λ respectively at mass ratio $\mu=0.03$; negative stiffness ratio $\alpha=-0.25$; damping ratio $\boldsymbol{\xi}$ = 0.15 and $v=10$.

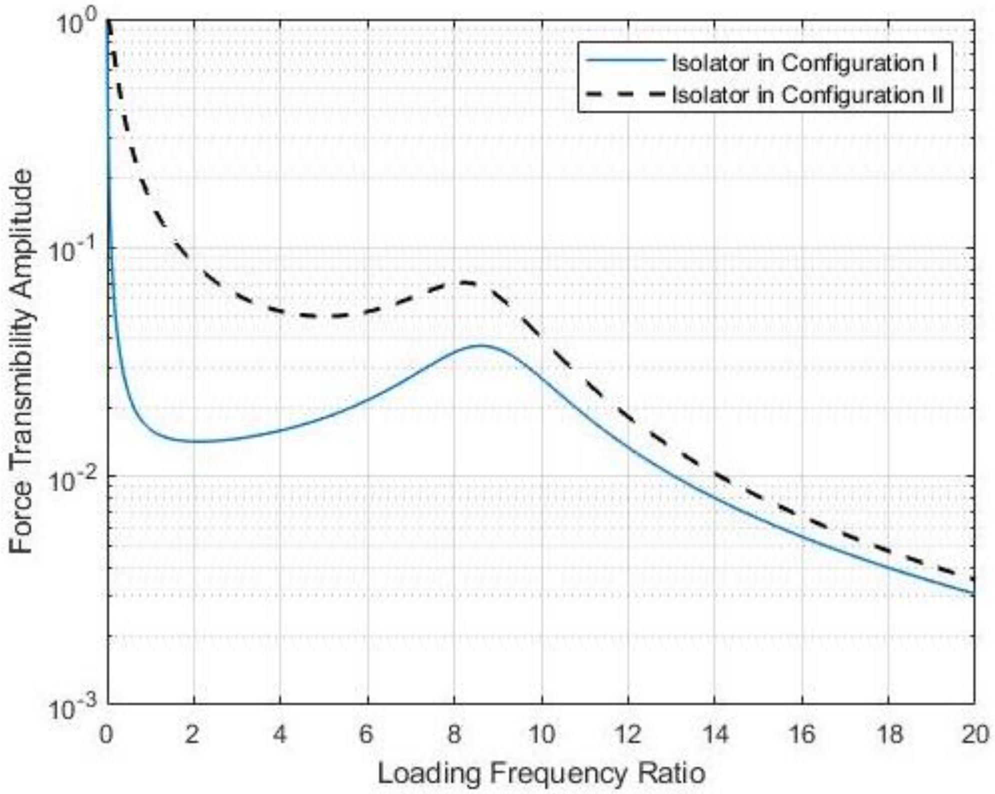

Figure 36 *- Force transmissibility |TfI | and |TfII | of the isolator in configuration I and configuration II at mass ratio μ=0.03; negative stiffness ratio α=-0.25; damping ratio ξ= 0.15 and v=10.*

From the definition of these parameters given in Eq. (3-9), such values are not difficult to achieve in practice. For example, $\alpha = -0.25$ is not a high negative stiffness and there are many ways can achieve in practice which also applies to $\mu = 0.03$ and $v = 10$. Practical adaptations of negative stiffness configurations have studied and assembled by [35] and [66, 67], depending on the scope of application, one of these proposed configurations can be incorporated into the system and tuned to the required negative stiffness, as not to destabilise the system.

Figure 36 shows promising and exciting results for the suggested isolator, as for both configuration I or configuration II, vibrations are attenuated at all any frequencies rather than only attenuated at frequencies above the square root of two times the fundamental natural frequency of the system. In short, for the new isolator, $|T_{fI}| < 1$ when $\lambda > 0$ and $|T_{fI}| = 1$ only at λ=0 or $\omega = 0$. and $|T_{fII}| < 1$ when $\lambda > 0$ and $|T_{fII}| = 1$ only at λ = 0 or $\omega = 0$. Therefore, the requirement of lower or zero ω_1, or for a given mass M, the system's static stiffness is zero , which eliminates the conflicting requirement of limiting the value of k_1 in order to support the static load. For the passive suggested isolator, zero dynamic stiffness is achieved without sacrificing the static stiffness or static load bearing capacity. And the static stiffness of the system can be determined independently according to the static load bearing capacity needed.

Figure 36 also clearly shows that the force transmissibility of the isolator drops sharply from 1, when $\lambda = 0$, especially $|T_{fI}|$. Actually, $|T_{fI}| < 0.1$ when $\lambda > 0.095$ and $|T_{fII}| < 0.1$ when $\lambda > 1.675$

It is important to also determine if the observed results all these merits resulting from the attaching of a DVA or tuned mass damper. Therefore, the effect of eliminating the negative stiffness spring k must be investigated. The suggested isolator is thus reduced to an isolator with a traditional three elements tuned mass damper or DVA attached. By letting $k = 0$ or $\alpha = 0$, the force transmissibility of this isolator can be obtained from Eq. (3-10) as:

$$T_{fI0=} = \frac{-\lambda^2+v^2++2j\xi v\lambda}{\lambda^4-(v^2+\mu v^2+1)\lambda^2+v^2+2j\xi v\lambda[1-(1+\mu)\lambda^2]} \qquad (3\text{-}12)$$

Similarly, for configuration II when $k = 0$

$$T_{fII0=} = \frac{-\lambda^2+v^2++2j\xi v\lambda(1+\mu v^2)}{\lambda^4-(v^2+\mu v^2+1)\lambda^2+v^2+2j\xi v\lambda[1+\mu v^2-(1+\mu)\lambda^2]} \qquad (3\text{-}13)$$

Figure 37 presents the amplitude of force transmissibility $|T_{fI0}|$ and $|T_{fII0}|$ against frequency ratio λ respectively at mass ratio $\mu = 0.03$; damping ratio $\boldsymbol{\xi}$= 0.15 and $v = 10$.

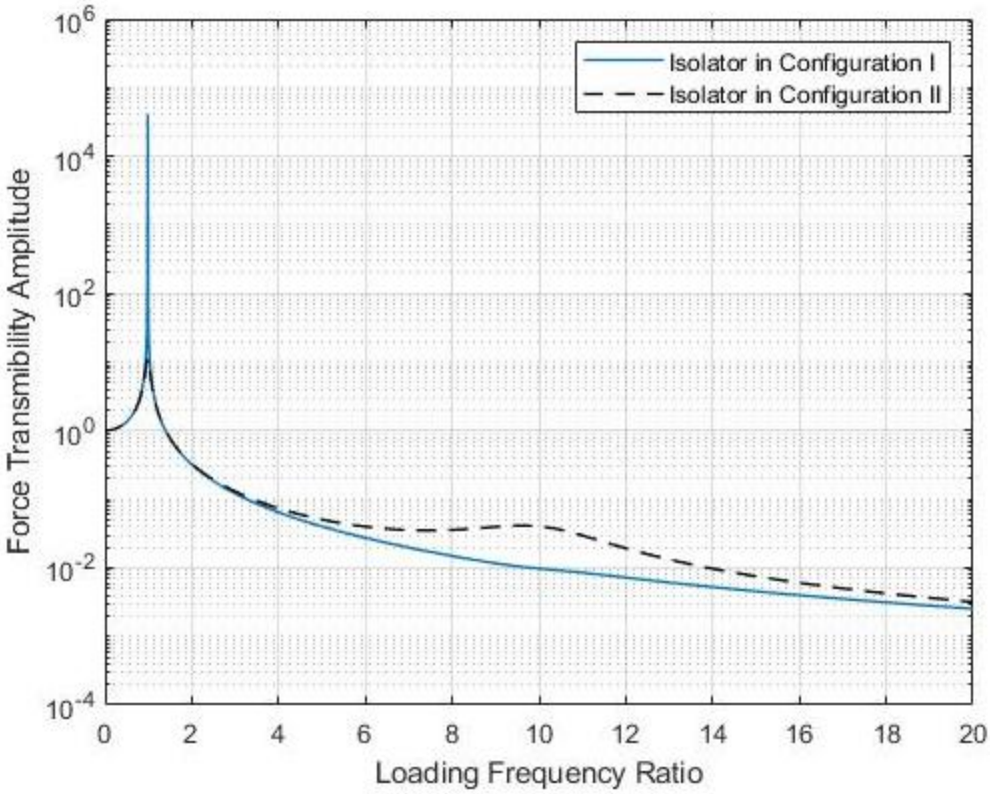

Figure 37 *- Force transmissibility |T_fI0 | and |T_fII0 | of the isolator in configuration I and configuration II at mass ratio μ=0.03; damping ratio* $\boldsymbol{\xi}$*= 0.15 and v=10.*

Figure 37 clearly shows the adding the three elements dynamic vibration absorber does not improve the isolator's performance at all, the very high peak, especially the peak of $|T_{fI0}|$, at λ close to 1. And $|T_{fI0}| < 1$ only when $\lambda > 1.4$. $|T_{fII0}| < 1$ only when $\lambda >$ 1.41. Therefore, simply attaching a three elements tuned mass damper to an isolator does not improve vibration isolation performance of the isolator. Tuning the damper to the isolator's frequency, *i.e.*, $v = 1$, could not change this fact fundmentaly. At mass ratio of

$\mu = 0.03$; damping ratio $\boldsymbol{\xi}$ = 0.15 and v = 1 , $|T_{fI0}|$ =11.5 when $\lambda = 0.96$ and $|T_{fII0}|$ = 1000 when $\lambda = 1$.

3.2.3 Displacement Transmissibility

For the system shown in Figure 34, with $F_e = 0$, the equations of motion for displacement excitation of the base X_e (the source of vibration) are:

$$\begin{cases} 4M\ddot{x}_1 + k_1(x_1 - X_e) + k_2(x_1 - x_2) + c_2(\dot{x}_1 - \dot{x}_2) = 0 & (3-14) \\ m\ddot{x}_2 + k_2(x_2 - x_1) + c_2(\dot{x}_2 - \dot{x}_1) + k(x_2 - X_{e)} = 0 & (3-15) \end{cases}$$

Eq. (3-14) and Eq. (3-15) can be rewritten as:

$$\begin{cases} \ddot{x}_1 + \frac{c_2}{M}\dot{x}_1 + \frac{k_1+k_2}{M}x_1 - \frac{c_2}{M}\dot{x}_2 - \frac{k_2}{M}x_2 = \frac{k_1}{M}X_e & (3-16) \\ \ddot{x}_2 + \frac{c_2}{m}\dot{x}_2 + \frac{k_2+k}{m}x_2 - \frac{c_2}{m}\dot{x}_1 - \frac{k_2}{m}x_1 = \frac{k}{m}X_e & (3-17) \end{cases}$$

Applying the definitions of parameters in Eq. (3-9) and Performing Fourier transform on Eq. (3-16) and Eq. (3-17), one gets:

$$\begin{cases} (-\omega^2 + 2j\xi\mu\omega_2\omega + \omega_1^2 + \mu\omega_2^2)X_1 - (2j\mu\xi\omega_2\omega + \mu\omega_2^2)X_2 = \omega_1^2 X_e & (3-18) \\ (-\omega^2 + 2j\xi\omega_2\omega + \omega_2^2 + \alpha\omega_2^2)X_2 - (2j\xi\omega_2\omega + \omega_2^2)X_1 = \alpha\omega_2^2 X_e & (3-19) \end{cases}$$

Solving Eq. (3-18) and Eq. (3-19), the displacement transmissibility of the isolator in configuration I can be obtained as:

$$T_{Id} = \frac{X_1}{X_e} = \frac{A + j\xi B}{C + j\xi D} \qquad (3\text{-}20)$$

Where:

$$A = -\lambda^2 + (1+\alpha)v^2 + \alpha\mu v^4 \qquad (3\text{-}21)$$
$$B = 2v\lambda(1 + \mu\alpha v^2) \qquad (3\text{-}22)$$
$$C = \lambda^4 - (1 + \mu v^2 + v^2 + \alpha v^2)\lambda^2 + v^2 + \alpha v^2 + \alpha\mu v^4 \qquad (3\text{-}23)$$
$$D = 2v\lambda[1 + \alpha\mu v^2 - (1+\mu)\lambda^2] \qquad (3\text{-}24)$$

Inserting Equations (3-21), (3-22), (3-23) and (3-24) into Eq. (3-20) and comparing the resulting displacement transmissibility of the isolator, T_{Id}, with the force transmissibility of the isolator, $T_{If,}$ presented in Eq. (3-10), It is easy to find that: $T_{Id} = T_{If}$, therefore, this isolator is a passive linear isolator. The displacement transmissibility function of the isolator in configuration II, T_{IId}, can be developed in similar procedures and it will meet the linear condition of $T_{IId} = T_{IIf}$.

Since the isolator presented includes a negative stiffness element, the stability of the isolator, a two-degree-of-freedom dynamic system, becomes a serious issue. The bound on the value of negative stiffness, within which the isolator (dynamic system) can keep operating stably, should be determined before any further analysis or design on the isolator.

According to the Routh-Hurwith stability criterion, a system is asymptotically stable if and only if all the eigenvalues lie in the left half of the complex plane. Donated by s , eigenvalues can be determined by the characteristic polynomial $P(s)$ of the two-degree-of-freedom system in the form of:

$$P(s) = s^4 + \sigma_1 s^3 + \sigma_2 s^2 + \sigma_3 s + \sigma_4 \tag{3-25}$$

The necessary and sufficient conditions needed to guarantee the stability of the two-degree-of-freedom system are:

$$\begin{cases} \sigma_1 > 0 \\ \sigma_2 > 0 \\ \sigma_3 > 0 \\ \sigma_4 > 0 \\ \sigma_1\sigma_2 > \sigma_3 \\ \sigma_1\sigma_2\sigma_3 > \sigma_3^2 + \sigma_1^2\sigma_4 \end{cases} \tag{3-26}$$

Where all real coefficients of the polynomial $P(s)$ corresponds to the ones in the dominator of the transmissibility function T, with $T = T_f = T_d$ for this isolator.

By inserting jλ=s into Eq. (3-10), the transmissibility function of the isolator in configuration I becomes:

$$T_I = T_{fI} = \\ = \frac{s^2+(1+\alpha)v^2+\alpha\mu v^4+2\xi v(1+\alpha\mu v^2)s}{s^4+(v^2+\alpha v^2+\mu v^2+1)s^2+(v^2+\alpha v^2+\alpha\mu v^4)+2\xi v(1+\mu)s^3+2\xi v(1+\alpha\mu v^2)s}$$

(3-27)

For configuration II, Eq. (11) yields：

$$T_{II} = T_{fII} = \\ = \frac{s^2+(1+\alpha)v^2+\alpha\mu v^4+2\xi v(1+\mu v^2)s}{s^4+(v^2+\alpha v^2+\alpha\mu v^2+1)s^2+(v^2+\alpha v^2+\alpha\mu v^4)+2\xi v(1+\mu)s^3+2\xi v(1+\mu v^2)s} \tag{3-28}$$

Therefore, for the isolator in configuration I：

$$\begin{cases} \sigma_1 = 2\xi v(1+\mu) \\ \sigma_2 = v^2 + \alpha v^2 + \mu v^2 + 1 \\ \sigma_3 = 2\xi v(1+\alpha\mu v^2) \\ \sigma_4 = v^2 + \alpha v^2 + \alpha\mu v^4 \end{cases} \tag{3-29}$$

For the isolator in configuration II:

$$\begin{cases} \sigma_1 = 2\xi v(1+\mu) \\ \sigma_2 = v^2 + \alpha v^2 + \alpha\mu v^2 + 1 \\ \sigma_3 = 2\xi v(1+\mu v^2) \\ \sigma_4 = v^2 + \alpha v^2 + \alpha\mu v^4 \end{cases} \tag{3-30}$$

By substituting Eq. (3-29) or Eq. (3-30) into Eq. (3-26), a unique constraint on the negative stiffness ratio α for the isolator both in configuration I and in Configuration II can be obtained as:

$$\alpha > -\frac{1}{1+\mu v^2} \tag{3-31}$$

The case $\alpha = -\frac{1}{1+\mu v^2}$ is the limiting case of stability. According to the definition given in Eq. (3-9), both mass ratio μ and frequency ratio v are positive. Figure 33 presents the stable region of the isolator, which is the grey shaded region enclosed by $v = 0$, $\alpha = 0$ and curve $\alpha = -\frac{1}{1+\mu v^2}$.

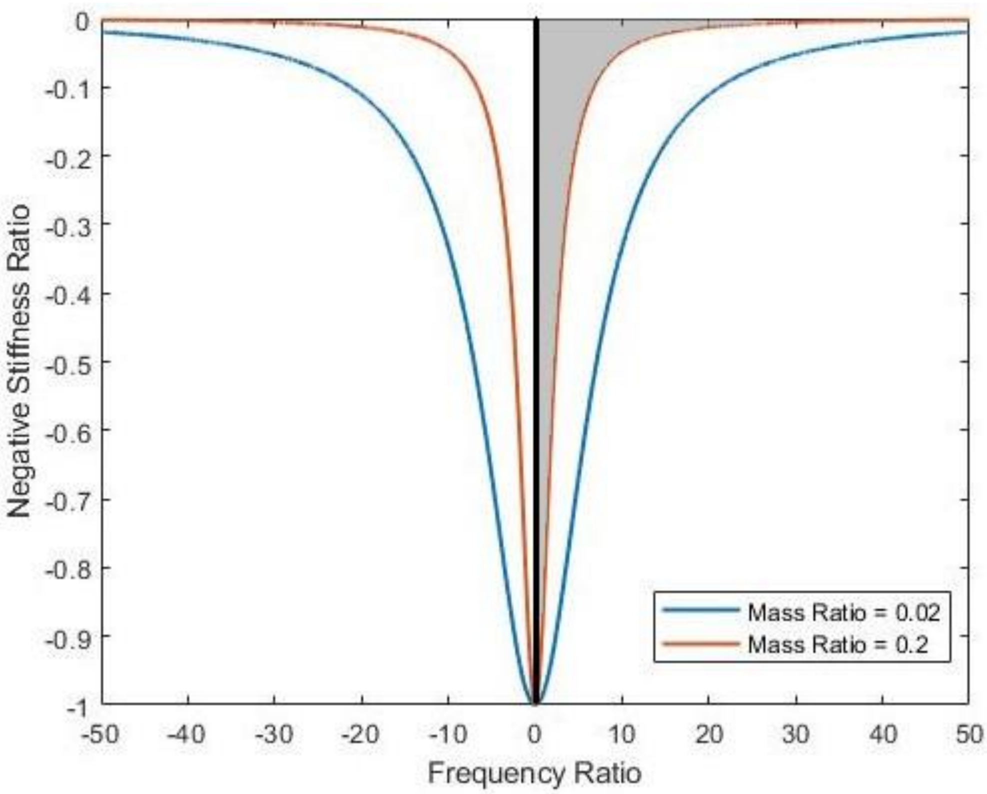

***Figure 38** - The stable region of the isolator and effect of mass ratio on stable region*

To ensure the isolator operates stably, in the design of the isolator, the parameters chosen must be in the stable region shown in Figure 38. For example, taking mass ratio $\mu = 0.01$ and frequency ratio $v = 10$, Eq. (3-31) yields the constraints on the negative stiffness ratio α as: $\alpha > -0.5$.

Figure 38 also shows the effect of mass ratio μ on the stable region of the isolator. It is observed that as the mass ratio increase from 2% to 20%, the stable region of the isolator is reduced significantly. Therefore, a smaller mass ratio is preferred for the isolator's stability. However, this does not mean mass ratio μ can be zero. If $\mu = 0$, *i.e.*, $m = 0$, the suggested isolator turned into a single-degree-of-freedom system. Especially, the isolator in configuration I is reduced to exactly the single-degree-of-freedom oscillator proposed and studied by Antoniadis et al [35]. According to the definition in Eq. (3-9), $m = 0$ leads to $\omega_2 \rightarrow \infty$ and $v \rightarrow \infty$. Making use of Eq. (3-10) and Eq. (3-11), the following can be obtained:

$$\lim_{v\to\infty} T_{fI} = \lim_{v\to\infty} T_{fII} = 1 \tag{3-32}$$

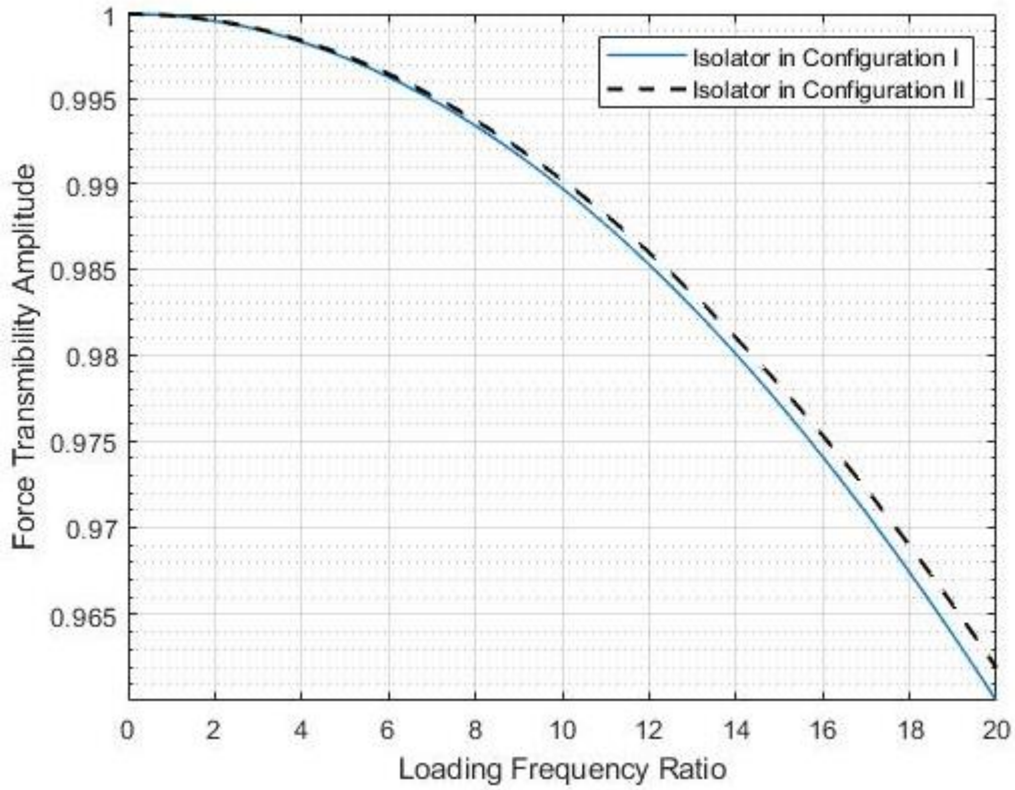

Figure 39 *- Force Transmissibility |TfI | and |TfII | of the isolator suggested at v=1000, μ=0.03, α=-0.25 and ξ=0.03*

Eq. (3-32) reveals that as $v \rightarrow \infty$, the transmissibility of the isolator suggested, configuration I or configuration II, goes to one, which means the isolator does not show any attenuation at all at any frequency. It should be noted that a large value of v, not to say infinity, can damage the performance of the isolator seriously. Figure 39 presents the transmissibility of the isolator suggested at $v = 1000$ while $\mu = 0.03$; $\alpha = -0.25$ and $\xi = 0.03$. Figure 39 clearly shows that for $0 < \lambda < 20$, the maximum reducing in transmissibility is only 4%, therefore, almost no attenuation achieved. In the design of the suggested isolator, mass ratio μ should be chosen from the range of 1% to 5%.

3.3 Numerical simulations and discussion

3.3.1 Performance of the vibration isolator

The suggested isolator, for both configuration I or configuration II, has three linear spring elements. The system's static stiffness, k_s, is determined by these spring elements to be:

$$k_s = k_1 + \frac{k_2 k}{k_2 + k} \tag{3-33}$$

The system's static stiffness should meet the requirements of static load bearing capacity and the limit on static displacement. In the design of such an isolator, firstly, we evaluate the static stiffness required to support the static load and meet the condition of static displacement limit. Once the static stiffness, k_0, is obtained after evaluation, the following relationship should be held to meet the requirement of static load capacity:

$$k_s = k_1 + \frac{k_2 k}{k_2 + k} = k_0 \tag{3-34}$$

By Inserting the following definition and relationships into Eq. (3-34):

$\mu = \frac{m}{M}$, $\alpha = \frac{k}{k_2}$ and $\frac{k_2}{k_1} = \frac{m\omega_2^2}{M\omega_1^2} = \mu v^2$

We obtain:

$$k_1 = \frac{1+\alpha}{1+\alpha+\alpha\mu v^2} k_0 \tag{3-35}$$

And

$$k_2 = \mu v^2 k_1 = \frac{(1+\alpha)\mu v^2}{1+\alpha+\alpha\mu v^2} k_0 \tag{3-36}$$

In practice, a safety margin ε should be given for the selection of negative stiffness k in the design of such an isolator. To enable the isolator to operate close to the dynamically neutral stable point, the following equation should be valid:

$$k_1 + \frac{k_2(1+\varepsilon)k}{k_2+(1+\varepsilon)k} = 0 \tag{3-37}$$

For the system to be statically stable, it is assumed that $\varepsilon > 0$.

3.3.2 Numerical Optimisation and Analysis

The following example demonstrates the suggested approach for the design of such an isolator. The static load is M = 500kg. The static displacement limit is $\delta = 0.01m$. The required system static stiffness can be evaluated as: $k_0 \geq 490000N/m$. Therefore, the systems static stiffness can be taken as: $k_0 = 500000N/m$. Setting the design safety margin $\varepsilon = 0.02$, the estimated negative stiffness achievable is $(1+\varepsilon)\alpha = -0.25$. Choosing mass ratio $\mu = 0.03$, and making use of the limit condition of stability: $-0.25 = -\frac{1}{1+\mu v^2}$, the value of v can be taken as: $v = 10$. Then, the other parameters of the isolator can be designed as following: the mass of the dynamic vibration absorber $m = \mu M = 15kg$. The design value of negative stiffness ratio $\alpha = -0.2451$. Making use of Eq. (3-35) and Eq. (3-36), the following stiffness can be determined:

$$k_1 = \frac{(1+\alpha)}{1+\alpha+\alpha\mu v^2} k_0 = 38.5153k_0$$
$$k_2 = \frac{(1+\alpha)\mu v^2}{1+\alpha+\alpha\mu v^2} k_0 \quad = 115.5459k_0$$

The negative stiffness designed $k = \alpha k_2 = -0.2451 \times 115.5459 k_0 = -28.32 k_0$. Inserting k_1, k_2 and k into Eq. (3-34), the static stiffness of the designed isolator can be found to be $k_s = 1.0005 k_0$, which confirms the static load capacity required is met. It should be noticed that the negative stiffness realized, with 2% safety margin, is $(1+\varepsilon)k = 28.8865 k_0$

Setting $\xi = 0.03$, $c_2 = 1766.3$. Figure 40 presents the transmissibility of this isolator, in configuration I and configuration II, respectively.

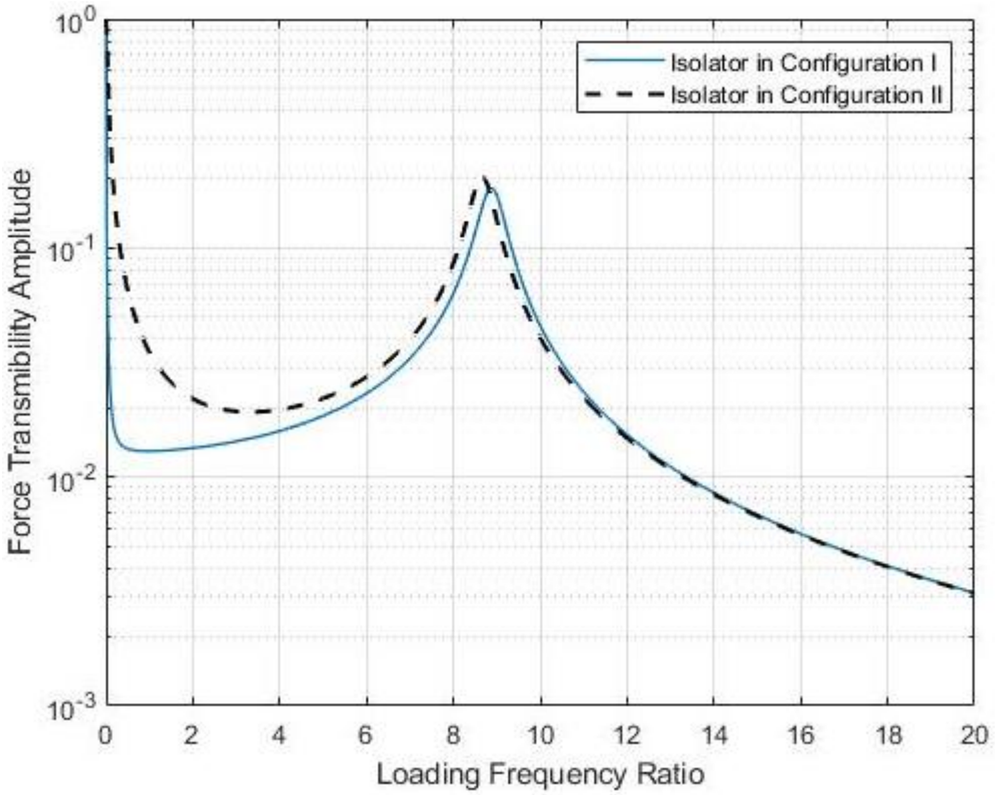

Figure 40 *- Force Transmissibility |TfI | and |TfII | of the isolator designed at ν=10, μ=0.03, α=-0.25 and ξ=0.03*

A numerical simulation was performed on this isolator to check results obtained above. The 4th order Runge-Kutta method (RK4) was employed in the numerical simulation. Suppose that a harmonic load Acting on M, $F_e = 100\cos\omega t$ (N), For the isolator in configuration I, the force transmitted to the base is : $F_T = k_1 x_1 + k x_2$ with x_1 and x_2 being determined numerically, F_T and further the transmissibility of the isolator $T = \frac{F_T}{F_e}$ can be determined from the results. For the isolator in configuration II, $F_T = k_1 x_1 + k_2 x_2$. In order to solve for the unknown parameters, we first let the loading frequency $\omega = \omega_1 = 196.25\ 1/s$, *i.e.*, $\lambda = 1$, to allow the numerical simulations to be performed on the isolator designed above, for both configuration I and configuration II respectively.

Figure 41 presents the simulated force transmitted to the base, F_T, for the isolator in configuration I. It can be found that the peak value of F_T, when the system stabilises, is about 1.296N. The peak value of F_e is 100N. Therefore, the transmissibility at $\lambda = 1$ is $T = 0.01296$, which is exactly same as $T_r = 0.01296$ obtained from the transmissibility at $\lambda = 1$ from the transmissibility graph of the isolator in configuration I in Figure 40.

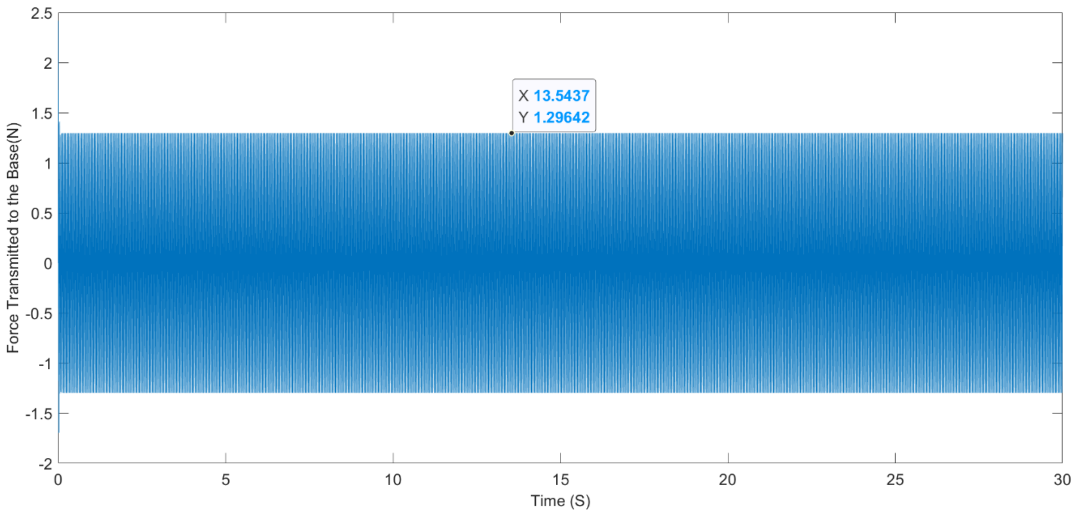

Figure 41 *- The force transmitted to the base*

The transmissibility of the isolator at $\lambda = 0.01$ and $\lambda = 8.877$ were determined by numerical simulation and transmissibility were determined as T= 0.1853 and T= 0.1828, respectively. These are equal to the transmissibility values given by the transmissibility graph at the same value of λ in Figure 40, though the simulated force transmitted to the base will not be presented here to save space. For the isolator in configuration II, numerical simulation can be performed and transmissibility at any value of λ and can be determined in the same way and checked against the transmissibility graph presented in Figure 40.

It is highlighted that, in the design of the isolator presented above, the limit condition of stability was employed. The isolator produced operates close to the dynamically neutral stable point. Intensive numerical simulation on the effect of parameters of the isolator on the transmissibility of the isolator was performed and it is proven that such a design is an optimal design.

Figure 37 presents the transmissibility of the isolator in configuration I and II at mass ratio $\mu = 0.035$; negative stiffness ratio $\alpha = -0.25$; damping ratio $\boldsymbol{\xi} = 0.03$ and $v = 10$. It can be observed that as mass ratio increases from 0.03 to 0.035 while keeping the other parameters constant, the transmissibility, especially the transmissibility of the isolator in configuration I, drops but not so abruptly as that shown in Figure 7, though $T_r \leq 1$ at any frequency and $T_r = 1$ only at $\lambda = 0$.

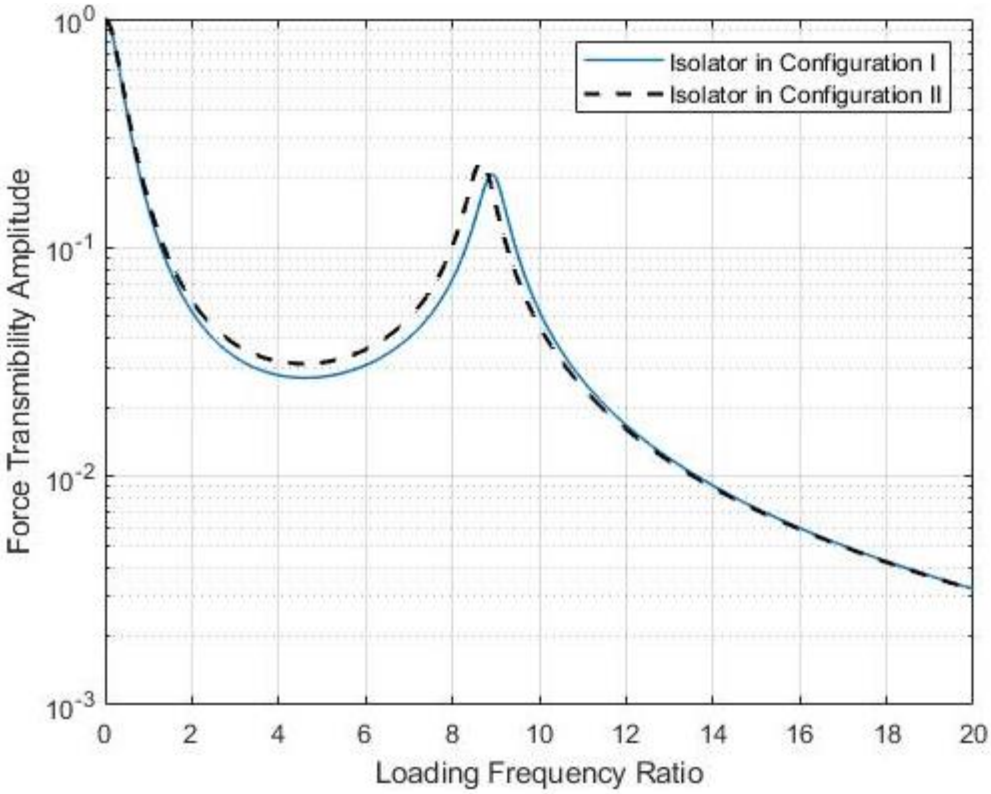

Figure 42 *- Force Transmissibility |TfI | and |TfII | of the isolator in configuration I and II at mass ratio μ=0.035; negative stiffness ratio α=-0.25; damping ratio ξ = 0.03 and v=10.*

If the mass ratio is decreased from $\mu = 0.03$ to $\mu = 0.025$ while keeping the other parameters constant, the transmissibility of the isolator in configuration I and configuration II is presented in Figure 53. It is observed that the transmissibility, especially the transmissibility of the isolator in configuration I, gets a very high peak, not to say vibration attenuation.

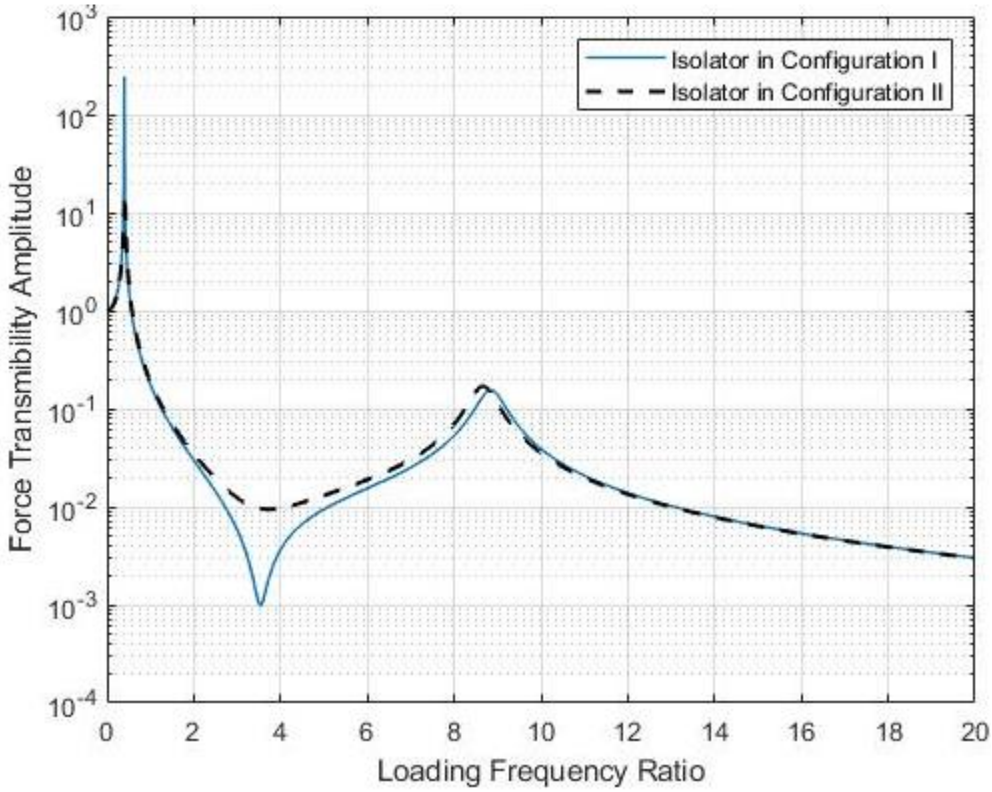

Figure 43 *- Force Transmissibility |TfI | and |TfII | of the isolator in configuration I and II at mass ratio μ=0.025; negative stiffness ratio α=-0.25; damping ratio* ξ *= 0.03 and v=10*

The effect of parameter v on transmissibility of the isolator is similar to that of parameter μ. Increasing from $v = 10$ to $v = 12$ while keeping the value of other parameters constant, the transmissibility of the isolator becomes that shown in Figure 44. Comparing Figure 44 with Figure 40 ($v = 10$), it can be found that the transmissibility in Figure 44 does not drop as abruptly, and the second peak moved to higher frequency. On the other hand, decreasing the value of v, for example to $v = 9$, will leads to very high first peak on transmissibility.

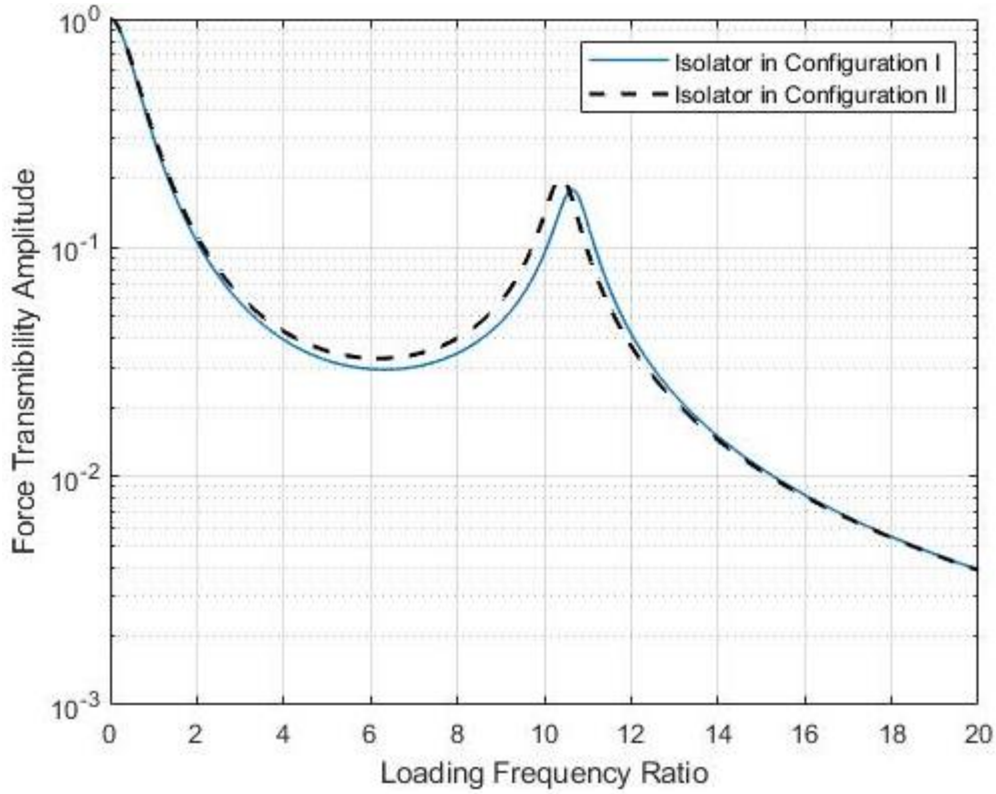

Figure 44 *- Force Transmissibility |TfI | and |TfII | of the isolator in configuration I and II at mass ratio μ=0.03; negative stiffness ratio α=-0.25; damping ratio **ξ** = 0.03 and ν=12*

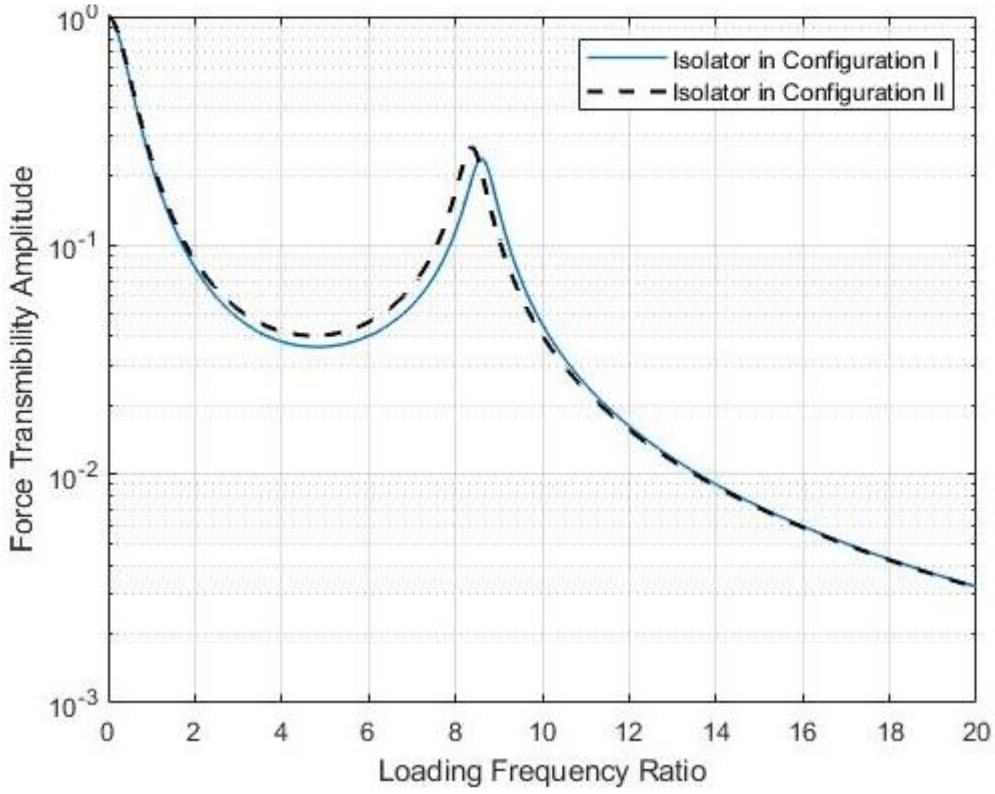

Figure 45 *- Force Transmissibility |TfI | and |TfII | of the isolator in configuration I and II at mass ratio μ=0.03; negative stiffness ratio α=-0.3; damping ratio **ξ** = 0.03 and ν=10*

If the absolute value of negative stiffness ratio is increased from 0.25 to 0.3($\alpha = -0.3$) while keeping the values of other parameters constant, the transmissibility becomes that as shown in Figure 45. If the absolute value of α is decreased, the system will become unstable, and the transmissibility will get a very high first peak.

The damping ratio $\boldsymbol{\xi}$ plays a very interesting role in the isolator. From Figure 40 it can be observed that without employing high damping ($\boldsymbol{\xi}$ = 0.03), the designed isolator can achieve very good vibration isolation. If the damping ratio is reduced to $\boldsymbol{\xi}$= 0.01 while keeping the values of other parameters constant, the transmissibility of the isolator becomes that shown in Figure 46. And by comparing Figure 46 with Figure 40, it can be observed that a smaller damping ratio makes the transmissibility drops more suddenly, especially the transmissibility of the isolator in configuration II. However, a smaller damping ratio leads to higher second peak on the transmissibility. If $\boldsymbol{\xi}$ = 0, that means that there is no dash port (C_2), or no damping at all, the transmissibility of the isolator is presented in Figure 42. It can be observed that transmissibility $T_r < 0.015$ in a large frequency range from 0 to $8.4\omega_1$, though the transmissibility got a very high second peak. This means that if the loading frequencies in the range of 0 to $8.4\omega_1$, without any damping, the isolator can still achieve excellent vibration isolating.

If the damping ratio is increases to $\boldsymbol{\xi}$ = 0.1 while the values of the other parameters are kept constant, the transmissibility of the isolator becomes that shown in Figure 48. And by comparing Figure 48 with Figure 40, it can be observed that heavy damping does not produce significant improved vibration isolation performance of the isolator except reducing the second peak of the transmissibility. The effect of each parameter on the performance of the suggested isolator should be taken into consideration in the design of such an isolator, especially when determining the tolerance of each parameter. The optimal design of the suggested isolator is one that allows the isolator to operate on or close to the dynamically neutral stable point. For example, consider the optimal mass ratio of the designed isolator above which is $\mu = 0.03$.

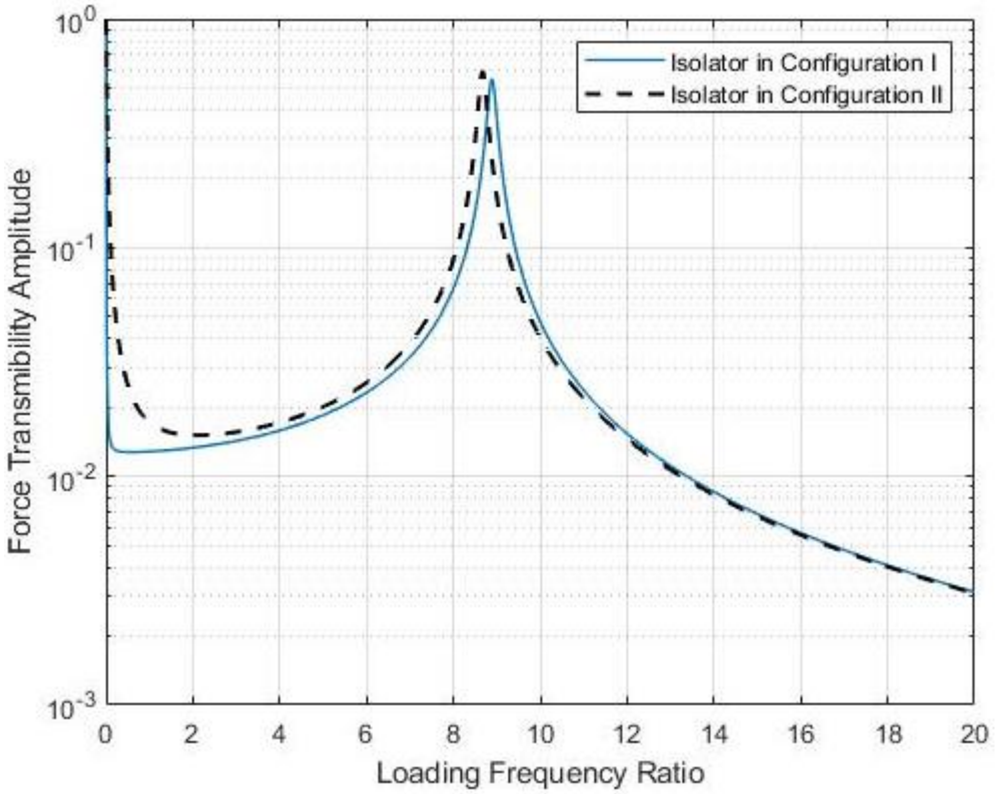

Figure 46 *- Force Transmissibility |TfI | and |TfII | of the isolator in configuration I and II at mass ratio μ=0.03; negative stiffness ratio α=-0.25; damping ratio ξ = 0.01 and v=10*

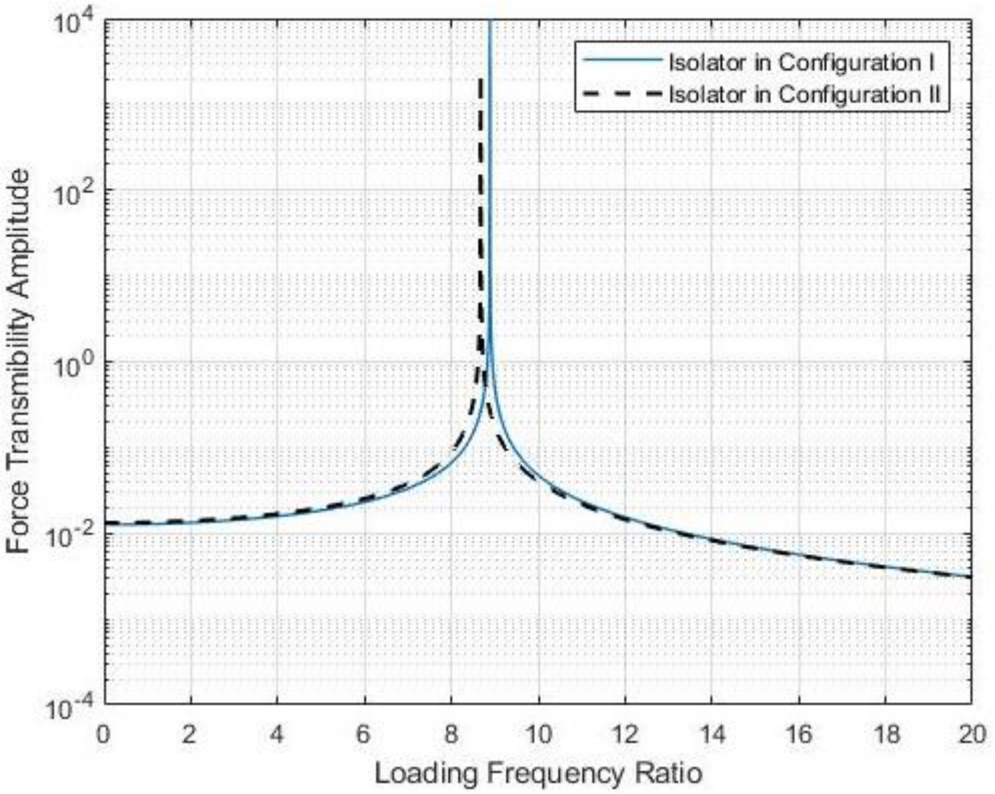

Figure 47 *- Force Transmissibility |TfI | and |TfII | of the isolator in configuration I and II at mass ratio μ=0.03; negative stiffness ratio α=-0.25; damping ratio ξ = 0 and v=10*

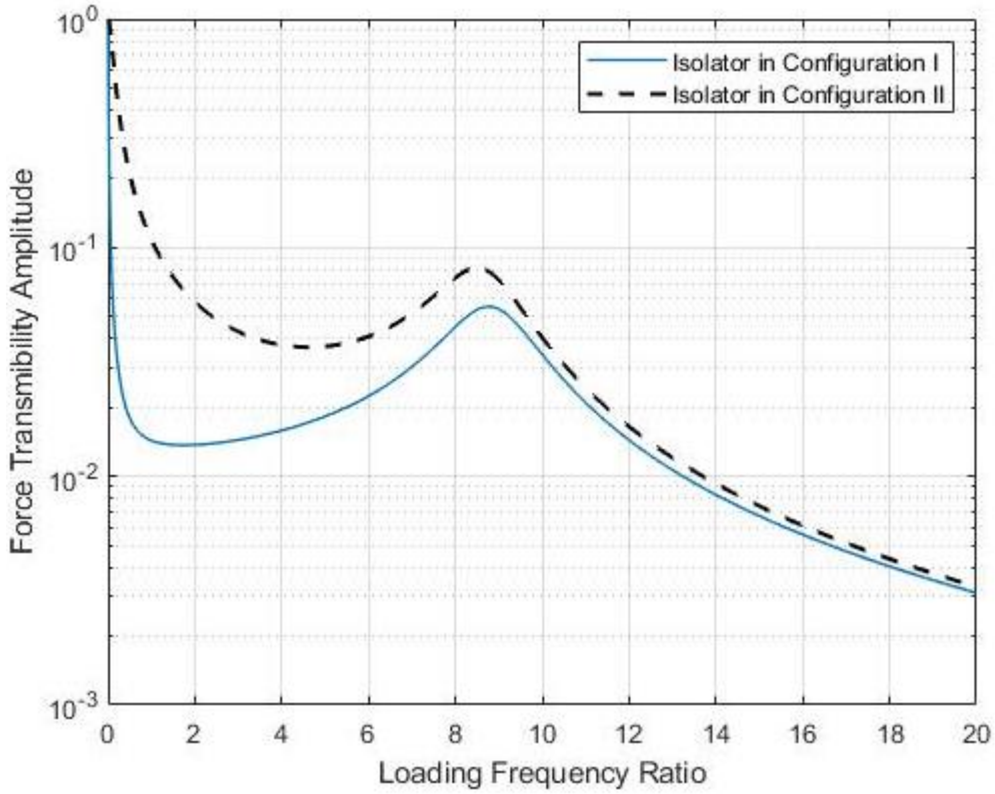

Figure 48 *- Force Transmissibility |TfI | and |TfII | of the isolator in configuration I and II at mass ratio μ=0.03; negative stiffness ratio α=-0.25; damping ratio ξ=0.1 and v=10*

If the mass ratio is increased to 0.032, the isolator can still perform very well. However, if the mass ratio realized at the end is 0.02, the system could become unstable. It should be noted that the changing of one parameter, for example μ, could result in changing of other parameters, such as α. Numerical simulation also confirmed the requirement on the negative stiffness ratio is: $\alpha \geq -\frac{1}{1+\mu v^2}$, for the isolator in both configuration I and configuration II. Especially, when $\alpha = -\frac{1}{1+\mu v^2}$, the isolator, in configuration I or II, is stable and performs very well, though the isolator in configuration I performs even better than the isolator in configuration II. Numerical simulation clearly shows that if this condition for stable running of the isolator is not met, divergence will occur in the response of M, $x_1(t)$, and displacement of m, $x_2(t)$, soon after initialization of the system, which means the isolator cannot operate stably.

3.3.3 Simulation under sinusoidal, random and white-noise loading

A computer simulation was performed on this isolator to check results obtained above. The MATLAB Simulink platform was employed in the numerical simulation. Suppose that a harmonic load Acting on M, $F_e = 100\cos\omega t$ (N), For the isolator in configuration I, the force transmitted to the base is : $F_T = k_1x_1 + kx_2$ with x_1 and x_2 being determined numerically, F_T and further the transmissibility of the isolator $T = \frac{F_T}{F_e}$ can be determined from the results. For the isolator in configuration II, $F_T = k_1x_1 + k_2x_2$.

The static load is M = 500kg. The static displacement limit is $\delta = 0.01m$. The required system static stiffness can be evaluated as: $k_0 \geq 490000N/m$. Therefore, the systems static stiffness can be taken as: $k_0 = 500000N/m$. Setting the design safety margin $\varepsilon = 0.02$, the estimated negative stiffness achievable is $(1+\varepsilon)\alpha = -0.25$. Choosing mass ratio $\mu = 0.03$, and making use of the limit condition of stability: $-0.25 = -\frac{1}{1+\mu v^2}$, the value of v can be taken as: $v = 10$. Then, the other parameters of the isolator can be designed as following: the mass of the dynamic vibration absorber $m = \mu M = 15kg$. The design value of negative stiffness ratio $\alpha = -0.2451$. Making use of Eq. (3-35) and Eq. (3-36), the following stiffness can be determined:

$$k_1 = \frac{(1+\alpha)}{1+\alpha+\alpha\mu v^2} k_0 = 38.5153 k_0 = 19\ 257\ 650 N/m$$
$$k_2 = \frac{(1+\alpha)\mu v^2}{1+\alpha+\alpha\mu v^2} k_0 \quad = 115.5459 k_0 = 57\ 772\ 950\ N/m$$

The negative stiffness designed $k = \alpha k_2 = -0.2451 \times 115.5459 k_0 = -28.32 k_0 = 14\ 160\ 000\ N/m$

Inserting k_1, k_2 and k into Eq. (3-34), the static stiffness of the designed isolator can be found to be $k_s = 1.0005 k_0$, which confirms the static load capacity required is met. It should be noticed that the negative stiffness realized, with 2% safety margin, is $(1+\varepsilon)k = 28.8865 k_0$

Setting $\xi = 0.03,\ c_2 = 1766.3$.

The results obtained from the Simulink analysis were compared against a traditional isolator system in order to draw a concise comparison of the effect of the inclusion of the additional damping mass and the system's configuration as to ascertain the level of improvement of the proposed configuration. Three key performance areas were identified in order to provide a comprehensive comparison of advantages of the proposed system as compared to the traditional single stage isolator. For the purpose and integrity of the analysis, key parameters of the primary system were kept constant whereas the proposed system's parameters were optimised according to the optimisation techniques derived and discussed in the preceding sections, namely, these parameters are:

$M = 500kg;\ k_1 = 19\ 257\ 650\ N/m$

Taking $\xi = 0.03$, then, $c = 2\xi\sqrt{k_1 M} = 2 \times 0.03 \times \sqrt{19\ 257\ 650 \times 500} = 5887.59$

For the purposes of seismic analysis, the uniform random and white-noise loading were analysed as seismic loading inputs whereas the loading on the primary system was modelled as:

$$M\ddot{x} + c\dot{x} + k_1 x = -M\ddot{x}_g$$

The gravitation acceleration due to gravity was assumed to be constant at a value of:

$$g = 9.8\ m/s^2$$

For the traditional isolator, the force transmitted to the base is : $F_T = k_1 x_1 + c\dot{x}_1$.

3.3.3.1 Sinusoidal Loading

Suppose that a harmonic load is acting on M is $F_e = 100\sin\omega t$ (N).

Where the loading frequency $\omega = \omega_1 = 196.25$ rad/s

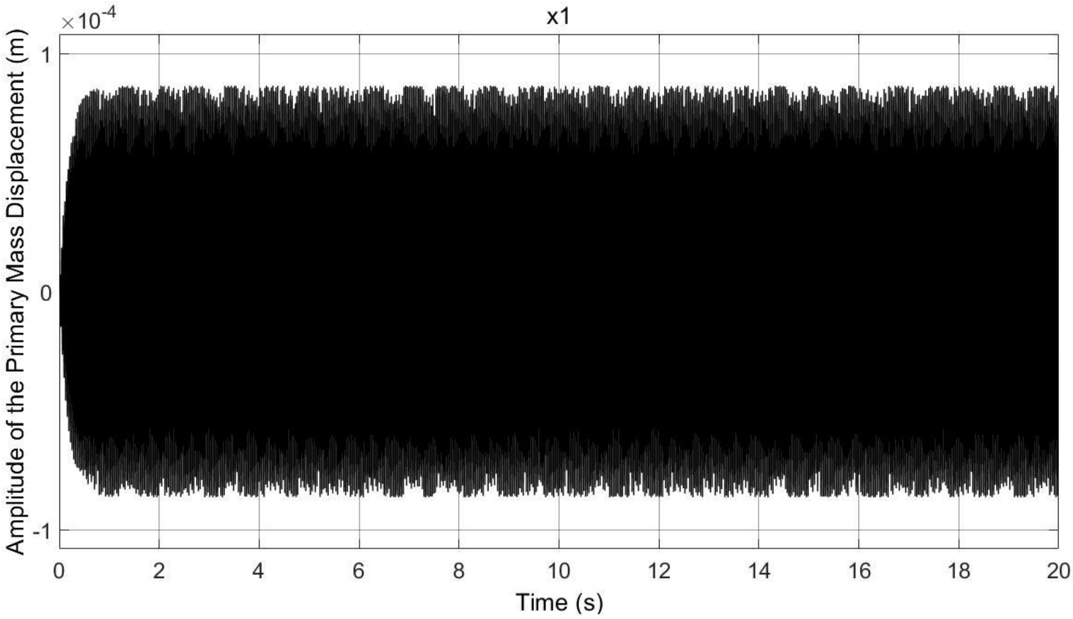

Figure 49 *– Simulated Primary Mass Displacement for Primary System with the Traditional Isolator under Sinusoidal Loading*

Figure 49 shows the simulated displacement response of the primary system with a traditional isolator shown in Figure 6. The displacement of the primary mass shows a rapid increase in amplitude as the system initialises, the displacement shows a stable period in oscillations due to the imposed sinusoidal loading, the plot indicates that the system requires an short time lapse in order to stabilise into a steady state condition with the imposed loading due to the high loading frequency, the system is observed to stabilise at a time lapse of 1.206 seconds. A peak amplitude of 8.698×10^{-5} metres is observed within the simulated timeframe of the analysis.

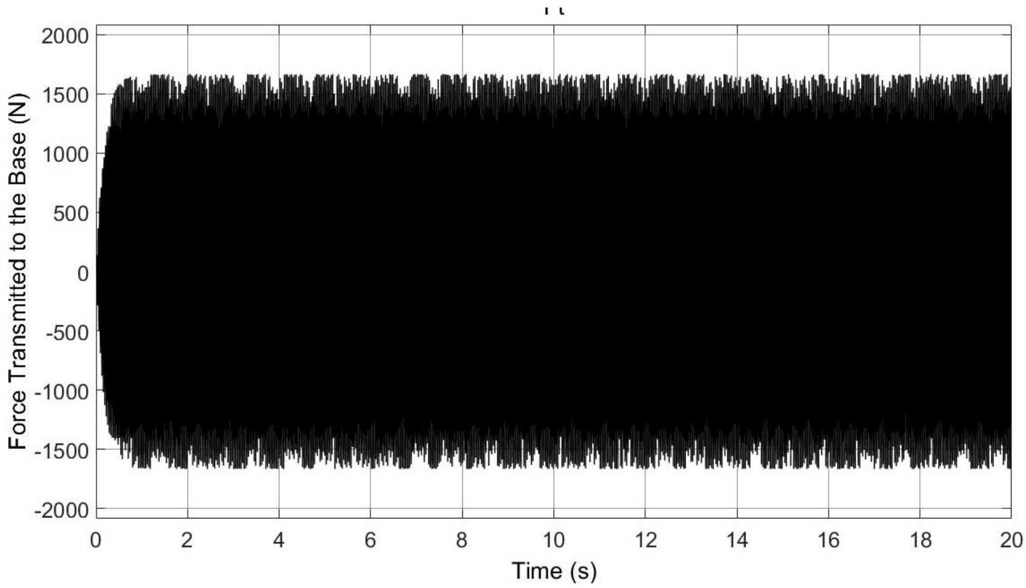

Figure 50 *- Simulated Forces Transmitted to the Base for the Primary System with the Traditional Isolator under Sinusoidal Loading*

Figure 50 shows the simulated loads transferred to the base of a system with a traditional isolator shown in Figure 6. The loads transferred to the base of the primary system also shows a rapid increase in amplitude as the system initialises and stabilises at a time lapse of 1.206 seconds achieving a maximum load transfer of 1663.3N.

3.3.3.1.1 Configuration I

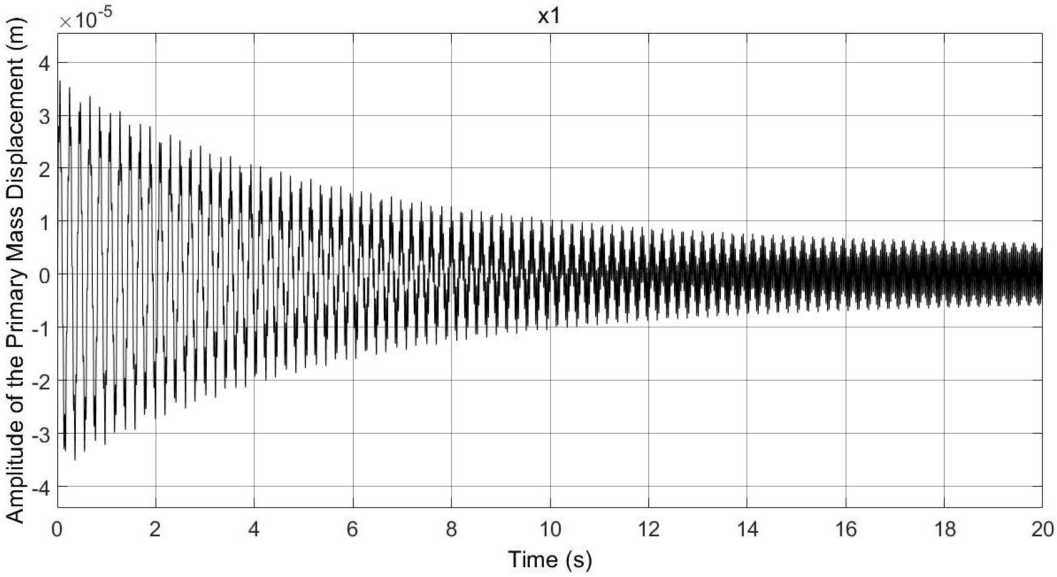

Figure 51 *- Simulated Primary Mass Displacement for Vibrational Isolator Integrated with a Negative Stiffness Element under Sinusoidal Loading*

Figure 51 shows the simulated displacement response of the primary system with configuration I of the vibrational isolator with a negative stiffness element shown in Figure 34. The displacement of the primary mass shows a gradual decrease in amplitude of the displacement with the peak displacement recorded at a time lapse of 0.052 seconds at

3.662×10^{-5} metres which is a reduction of 57.91% in the peak displacement, however, we observe that primary system begins to stabilise at a later time lapse of 17.979 seconds at a steady-state displacement of 6.428×10^{-6} metres. This is an effect of the negative stiffness element which displays continuous vibration isolation with time thus the delayed stabilisation of the primary mass displacement.

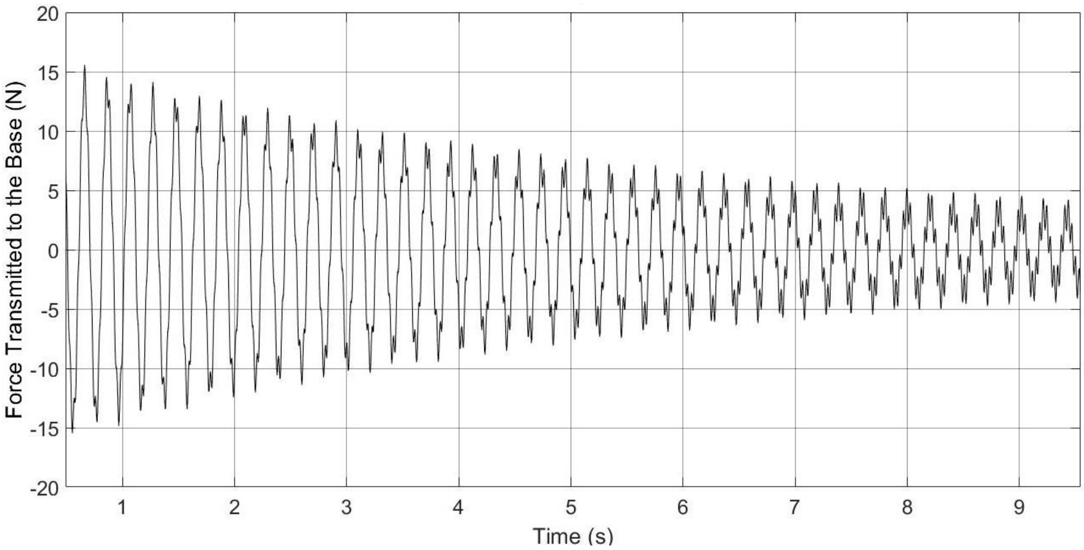

Figure 52 *- Simulated Loads Transmitted to the Base of the Primary System with the Vibration Isolator Integrated with a Negative Element under Sinusoidal Loading*

Figure 52 shows the simulated loads transmitted to the base of the primary system with configuration I of the vibrational isolator with a negative stiffness element shown in Figure 34. The loads transmitted to the base show a gradual decrease in amplitude of the displacement with the peak load transmitted is recorded at a time lapse of 0.0659 seconds at 15.644N which is a reduction of 99.06% in the peak load transmitted, however, we observe that primary system begins to stabilise at a later time lapse of 18 seconds at a steady-state displacement of 1.971N. This is an effect of the negative stiffness element which displays continuous vibration isolation with time thus the delayed stabilisation of the primary mass displacement. The proposed isolator displays enhanced vibration isolation thus offering significant protection of the primary system.

3.3.3.1.2 Configuration II

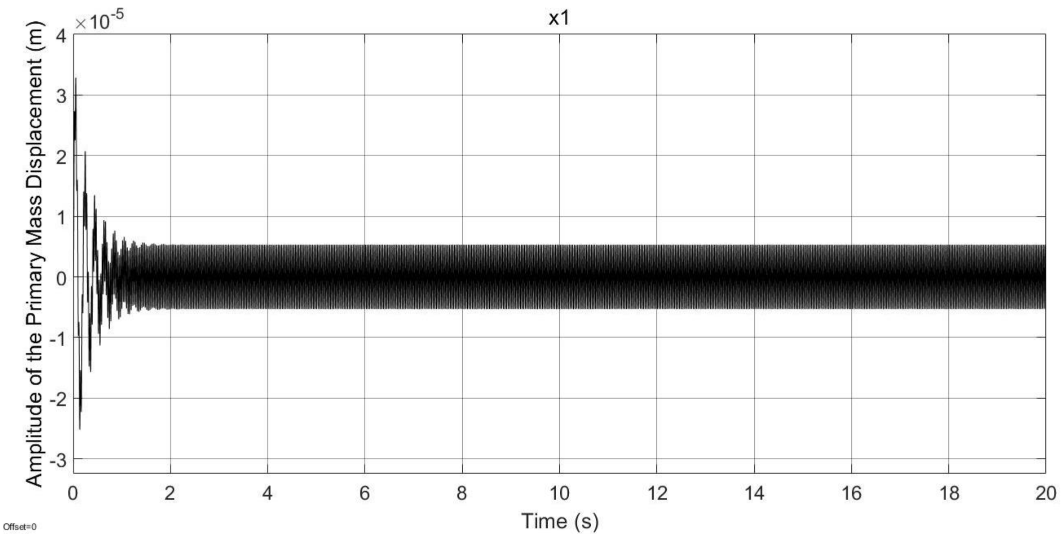

Figure 53 *- Simulated Primary Mass Displacement for Vibrational Isolator Integrated with a Negative Stiffness Element under Sinusoidal Loading*

Figure 53 shows the simulated displacement response of the primary system with configuration II of the vibrational isolator with a negative stiffness element shown in Figure 35. The displacement of the primary mass shows a gradual decrease in amplitude of the displacement with the peak displacement recorded at a time lapse of 0.052 seconds at 3.275×10^{-5} metres which is a reduction of 62.34% in the peak displacement, however, we observe that primary system begins to stabilise at time lapse of 2.231 seconds at a steady-state displacement of 5.289×10^{-6} metres.

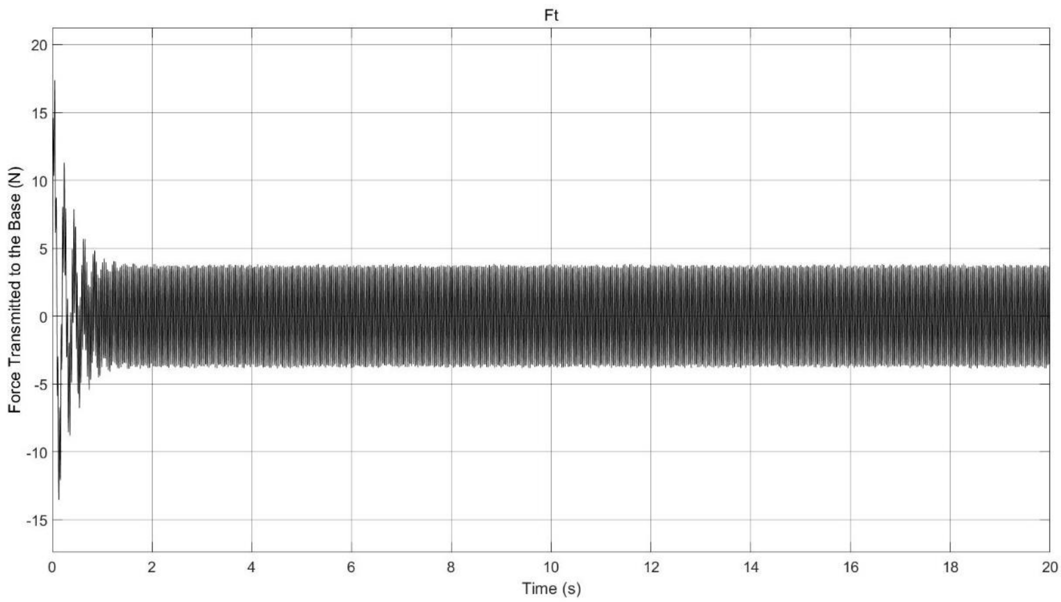

Figure 54 *- Simulated Loads Transmitted to the Base of the Primary System with the Vibration Isolator Integrated with a Negative Element under Sinusoidal Loading*

Figure 54 shows the simulated loads transmitted to the base of the primary system with the configuration II of the vibrational isolator with a negative stiffness element shown in Figure 35. The loads transmitted to the base show a rapid decrease in amplitude of the displacement with the peak displacement recorded at a time lapse of 0.048 seconds at 17.3621N. However, we observe that primary system begins to stabilise at a lapse of 1.9048 seconds at a steady-state transmitted load of 1.971N. The second configuration of the proposed isolator also displays enhanced vibration isolation thus offering significant protection of the primary system as a reduction of 98.96% is observed from the loads transmitted to the base of the primary system with a traditional vibration isolator.

3.3.3.1.3 Discussion

Both configurations of the proposed isolator display significant vibration isolation as compared to the traditional vibration isolator. Configuration I is observed to stabilise at later time lapses as compared to configuration II, whereas the configuration II displays 4.37% greater vibration isolation than configuration I. This is attributed to the position of the negative stiffness element which provides support to both the primary mass and secondary mass as shown in Figure 35. This arrangement limits the deflection of the primary mass; however, configuration I displays better load dissipation for the loads transmitted to the base of the primary system, which is also attributed to the position of the negative stiffness element as shown in Figure 34. The marginals of difference are minimal but indicate that the position of the negative stiffness has a large impact on the response of the primary system, which is also evident in when assessing the difference in time lapse required for the system to stabilise into a steady-state displacement and load transmission.

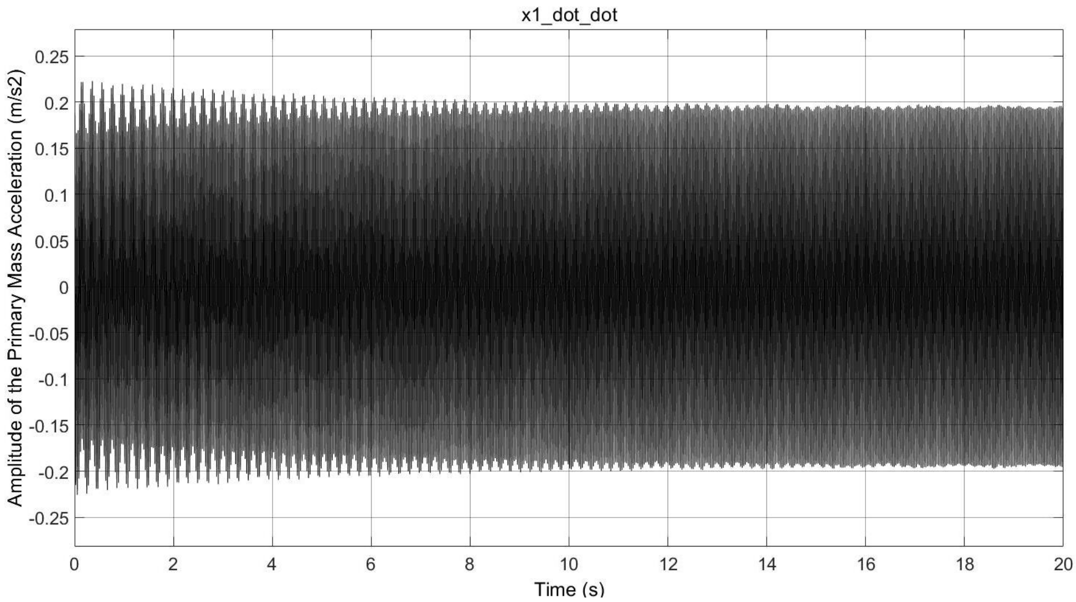

Figure 55 *- Simulated Acceleration of the Primary Mass for the System with Configuration I Vibration Isolator Integrated with a Negative Element under Sinusoidal Loading*

Figure 55 shows the simulated acceleration response of the primary system with configuration I of the vibrational isolator with a negative stiffness element shown in Figure 34. The acceleration of the primary mass shows a slight decrease in amplitude of the with the peak acceleration recorded at a time lapse of 0.059 seconds at 0.224 m/s^2. We observe that primary system begins to stabilise at time lapse of 14.037 seconds at a steady-state acceleration of 0.199 m/s^2.

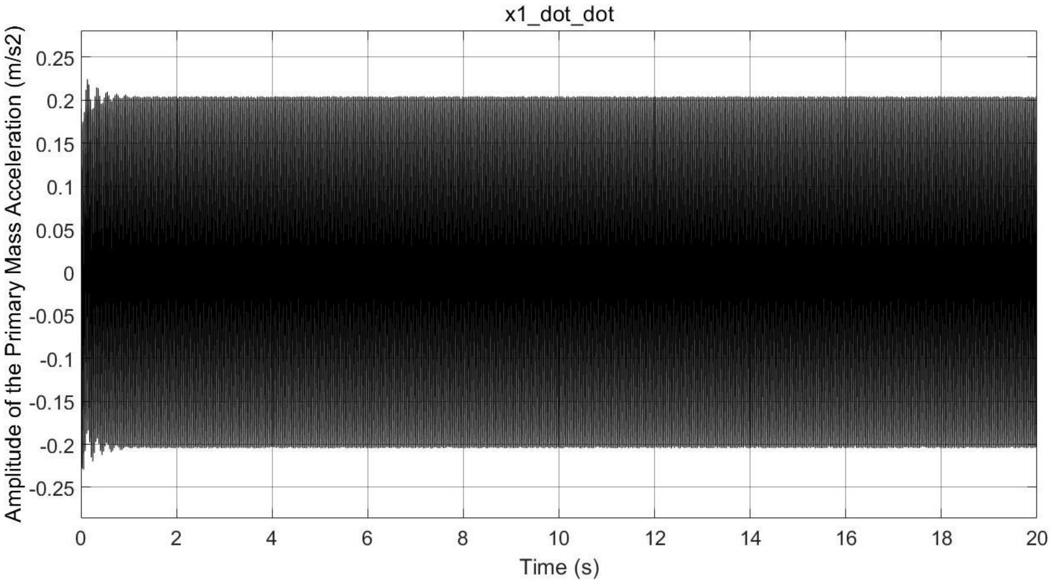

Figure 56 *- Simulated Acceleration of the Primary Mass for the System with Configuration II Vibration Isolator Integrated with a Negative Element under Sinusoidal Loading*

Figure 56 shows the simulated acceleration response of the primary system with configuration II of the vibrational isolator with a negative stiffness element shown in Figure 35. The acceleration of the primary mass shows a slight decrease in amplitude of the with the peak acceleration recorded at a time lapse of 0.069 seconds at 0.229 m/s^2. We observe that primary system begins to stabilise at time lapse of 0.936 seconds at a steady-state acceleration of 0.207 m/s^2.

Configuration II stabilises significantly far more rapidly as compared to configuration I as shown in Figure 55 and Figure 56 thus making ideal for remote applications whereas rapid system equilibrium is emphasised such as in cases of automotive and aeronautical applications where end-user comfort is a priority or priority structures which are sensitive to deflections. However, configuration I displays lower peak acceleration of the primary mass, although marginal, when compared to the configuration II. Configuration I however, is ideal in cases whereas limiting loads to the base is of a higher priority than deflections for systems imposed with a sinusoidal load.

3.3.3.2 Random Loading

Suppose that a uniform random load is acting on M

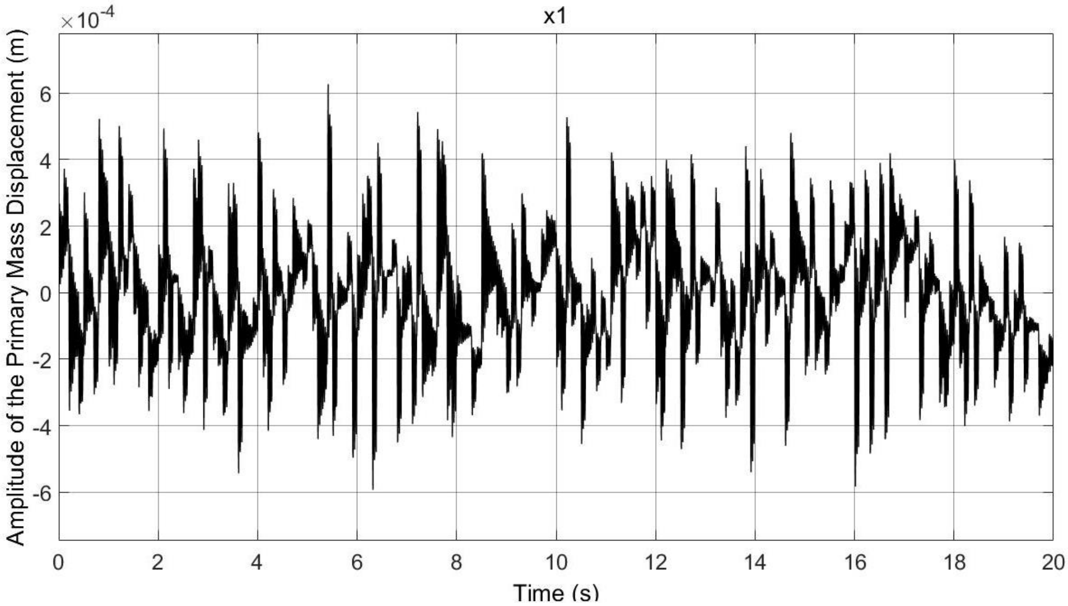

Figure 57 *- Simulated Primary Mass Displacement for the Primary System with the Traditional Isolator under Random Loading*

Figure 57 shows the simulated displacement response of the primary system with a traditional isolator shown in Figure 6. The displacement of the primary mass shows a varied amplitude response throughout the time lapse. A peak amplitude of 6.308×10^{-4} metres is observed at a time lapse of 5.406 seconds.

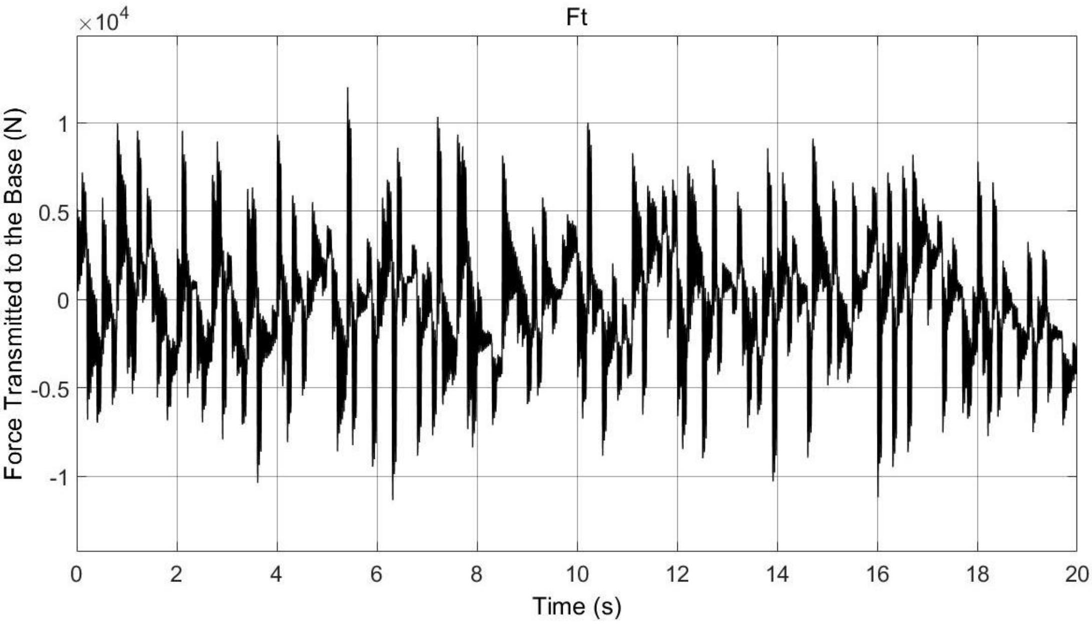

Figure 58 -. *Simulated Forces Transmitted to the Base for the Primary System with the Traditional Isolator under Random Loading*

Figure 58 shows the simulated loads transferred to the base of a system with a traditional isolator shown in Figure 6. The loads transferred to the base of the primary system also shows a varied amplitude throughout the time lapse. The peak load transmitted is recorded at a time-lapse of 5.413 seconds achieving a maximum load transfer of 12 081N.

3.3.3.2.1 Configuration I

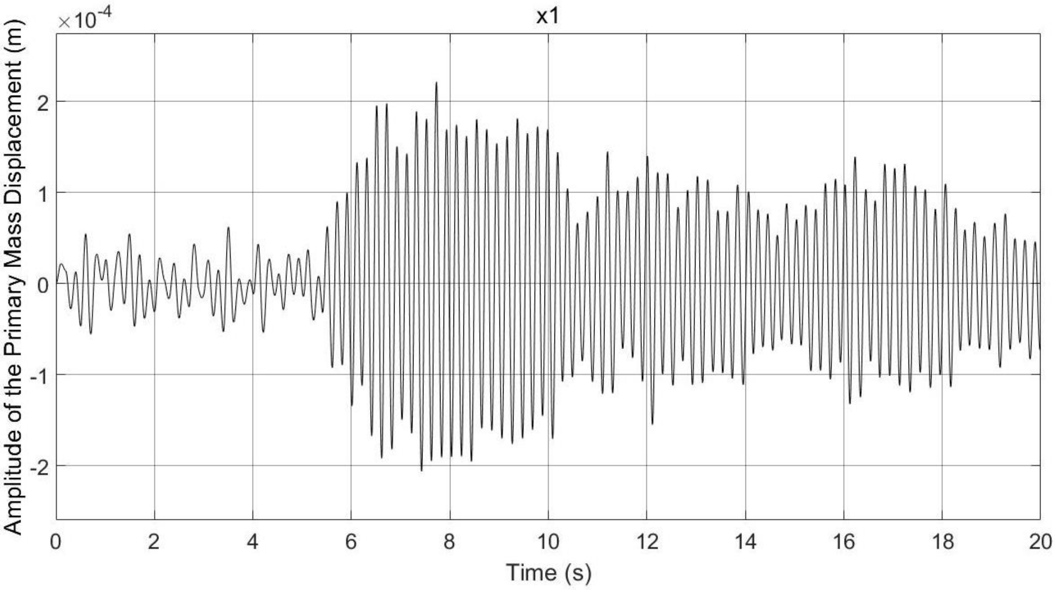

Figure 59 *- Simulated Primary Mass Displacement for Vibrational Isolator Integrated with a Negative Stiffness Element under Random Loading*

Figure 59 shows the simulated displacement response of the primary system with configuration I of the proposed vibration isolator integrated with a negative stiffness element shown in Figure 34. The displacement of the primary mass shows a varied amplitude response throughout the time lapse. A peak amplitude of 2.221×10^{-4} metres is observed at a time lapse of 7.728 seconds. This constitutes a reduction of 64.79% to the peak displacement recorded for the primary system with the traditional vibrational isolator. Figure 59 displays a low response as the system initialises of which abruptly starts to increase at a time lapse of 5.713 seconds which can be attributed to the negative stiffness element initialisation which is affected by the random loading imposed on to the primary system thus the increase is a result of the recalibration of the negative stiffness element to the varying load.

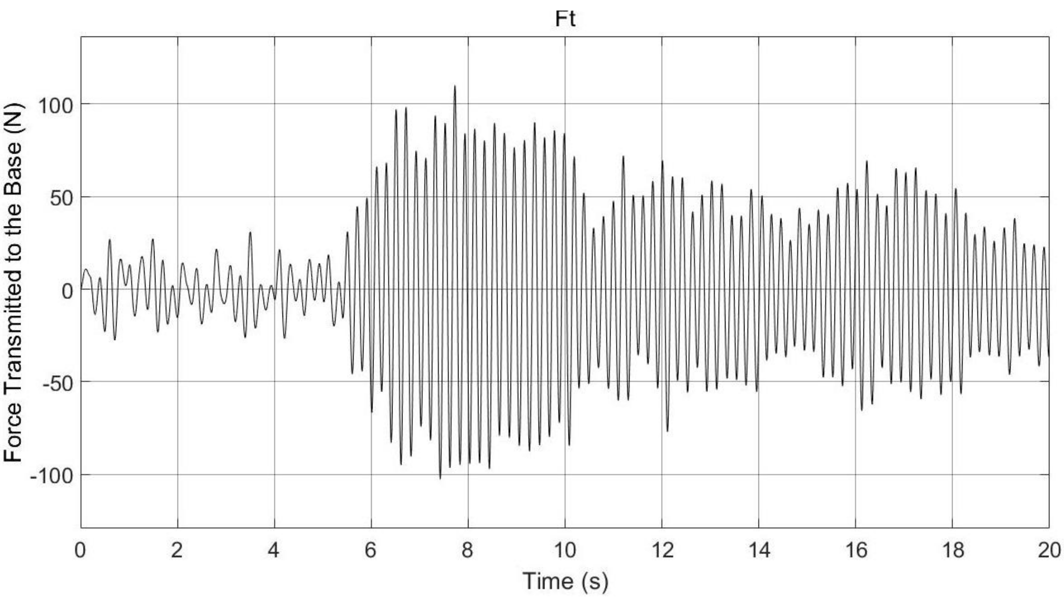

Figure 60 - *Simulated Loads Transmitted to the Base of the Primary System with the Vibration Isolator Integrated with a Negative Element under Random Loading*

Figure 60 shows the simulated displacement response of the primary system with configuration I of the proposed vibration isolator integrated with a negative stiffness element shown in Figure 34. The recorded response of the loads transmitted to the base of the primary system shows a varied amplitude response throughout the time lapse. A peak load transfer of 110.203N metres is observed at a time lapse of 7.728 seconds. This constitutes a reduction of 99.16% to the peak load transmitted to the base of the primary system with the traditional vibrational isolator. Figure 60 displays a low response as the system initialises of which abruptly starts to increase at a time lapse of 5.711 seconds similar to the response of the primary mass defection shown in Figure 59, which can also be attributed to the negative stiffness element initialisation which is affected by the random loading imposed on to the primary system thus the increase is a result of the recalibration of the negative stiffness element to the varying load.

3.3.3.2.2 Configuration II

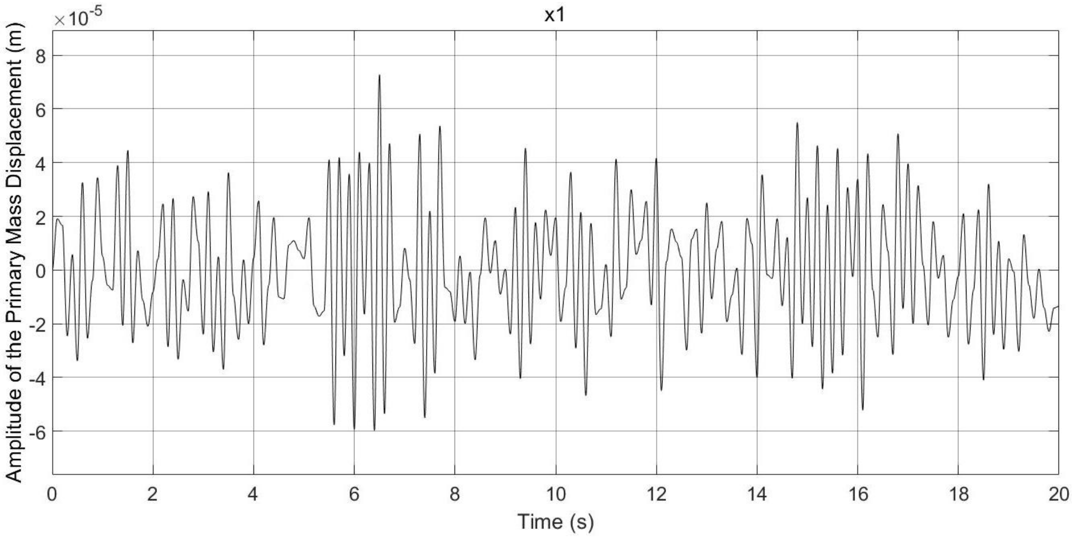

Figure 61 *– Simulated Primary Mass Displacement for Vibrational Isolator Integrated with a Negative Stiffness Element under Random Loading*

Figure 61 shows the simulated displacement response of the primary system with configuration II of the proposed vibration isolator integrated with a negative stiffness element shown in Figure 35. The displacement of the primary mass shows a varied amplitude response throughout the time lapse. A peak amplitude of 7.315×10^{-5} metres is observed at a time lapse of 6.495 seconds. This constitutes a reduction of 88.40% to the peak displacement recorded for the primary system with the traditional vibrational isolator.

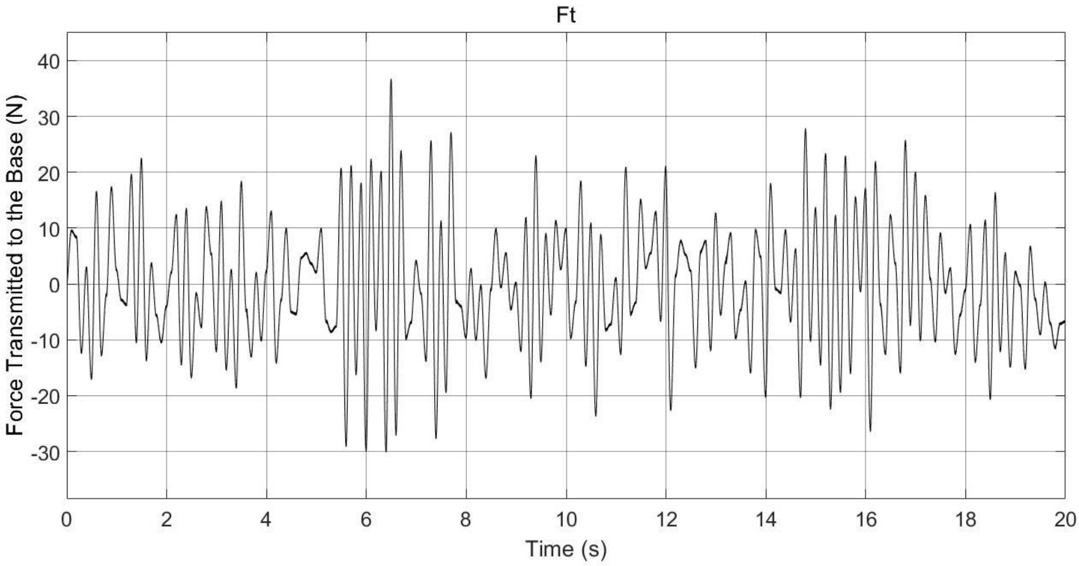

Figure 62 *- Simulated Loads Transmitted to the Base of the Primary System with the Vibration Isolator Integrated with a Negative Element under Random Loading*

Figure 62 shows the simulated displacement response of the primary system with configuration II of the proposed vibration isolator integrated with a negative stiffness element shown in Figure 35. The recorded response of the loads transmitted to the base of the primary system shows a varied amplitude response throughout the time lapse. A peak load transfer of 36.812N metres is observed at a time lapse of 6.494 seconds. This constitutes a reduction of 99.70% to the peak load transmitted to the base of the primary system with the traditional vibrational isolator

3.3.3.2.3 Discussion

Both configurations of the proposed vibrational isolator integrated with a negative stiffness element display enhanced vibration isolation when compared to the traditional vibrational isolator shown in Figure 6. Configuration II displays enhanced performance for both the displacement of the primary mass and the loads transferred to the base of the primary system.

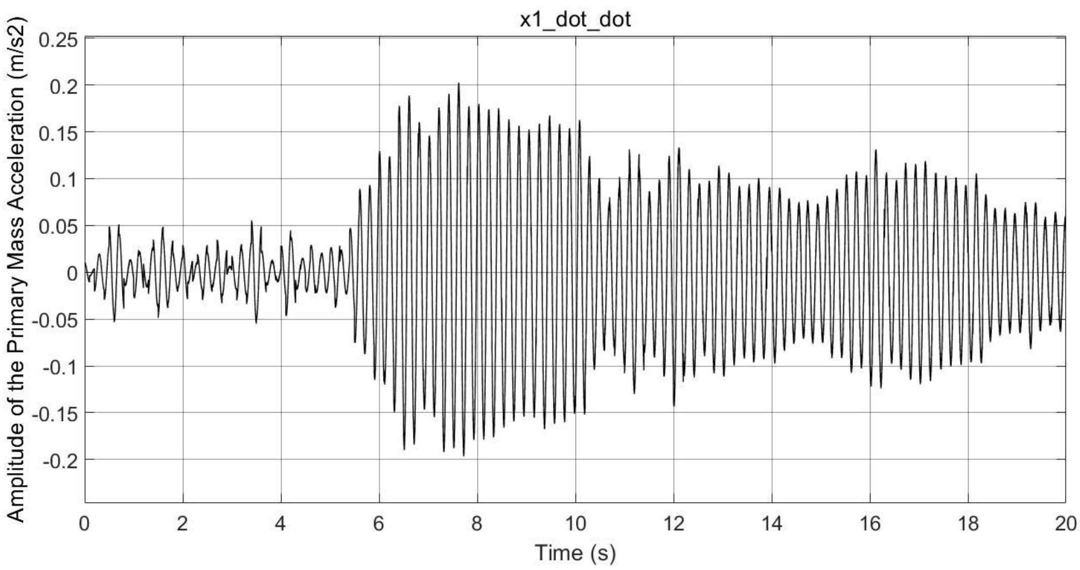

__Figure 63__ - Simulated Acceleration of the Primary Mass for the System with Configuration I Vibration Isolator Integrated with a Negative Element under Random Loading

Figure 63 shows the simulated displacement response of the primary system with configuration I of the vibrational isolator with a negative stiffness element shown in Figure 34. The acceleration of the primary mass shows a varied amplitude of the acceleration with the peak acceleration recorded at a time lapse of 7.609 seconds at 0.202 m/s^2.

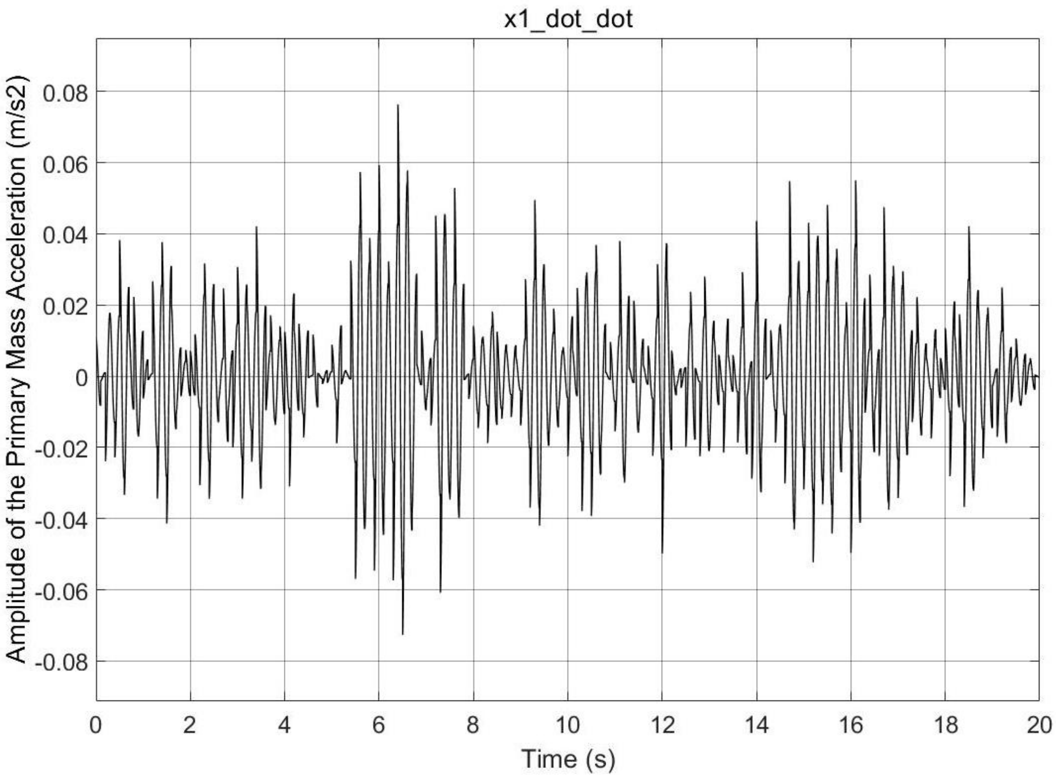

__Figure 64__ - Simulated Acceleration of the Primary Mass for the System with Configuration II Vibration Isolator Integrated with a Negative Element under Random Loading

Figure 64 shows the simulated displacement response of the primary system with configuration II of the vibrational isolator with a negative stiffness element shown in Figure 35. The acceleration of the primary mass also shows a varied amplitude of the acceleration with the peak acceleration recorded at a time lapse of 6.399 seconds at 0.077 m/s^2.

Configuration II also displays a relatively consistent load sequence and a significantly lower rate of oscillation of the primary mass when compared to configuration I, which is essential for application in remote and user-centric industries such as for the automotive and aeronautical sectors as the response must be consistent to prevent discomfort.

3.3.3.3 White-Noise Loading

Suppose that a seismic (white-noise band) load is acting on M

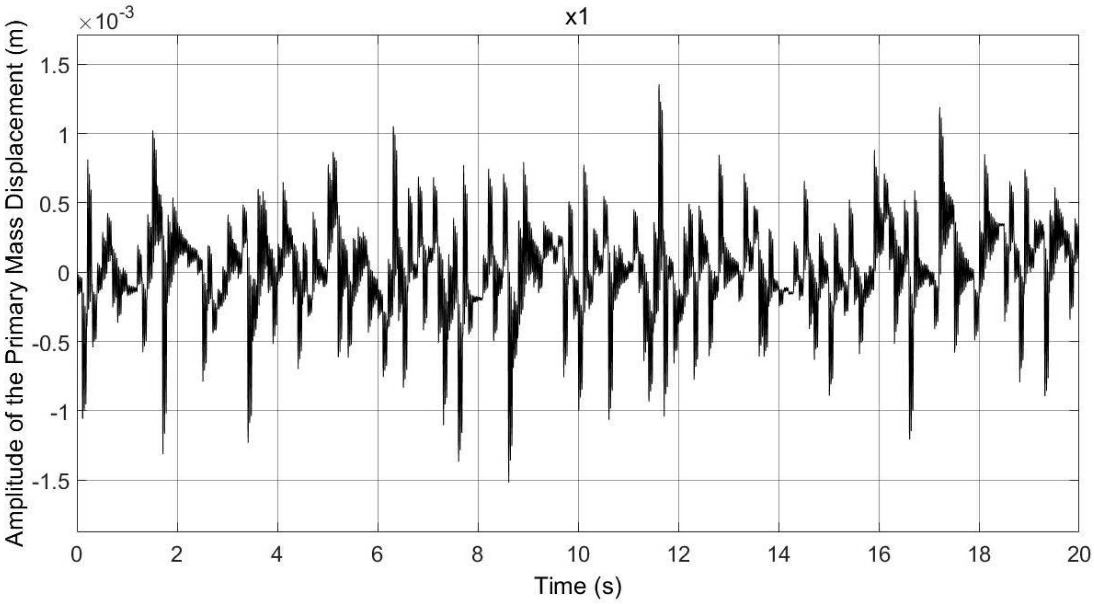

***Figure 65** – Simulated Primary Mass Displacement for Traditional Isolator under a White-Noise Frequency Band Loading*

Figure 65 shows the simulated displacement response of the primary system with a traditional isolator shown in Figure 6. The displacement of the primary mass shows a varied amplitude response throughout the time lapse. A peak amplitude of 0.002 metres is observed at a time lapse of 8.611 seconds.

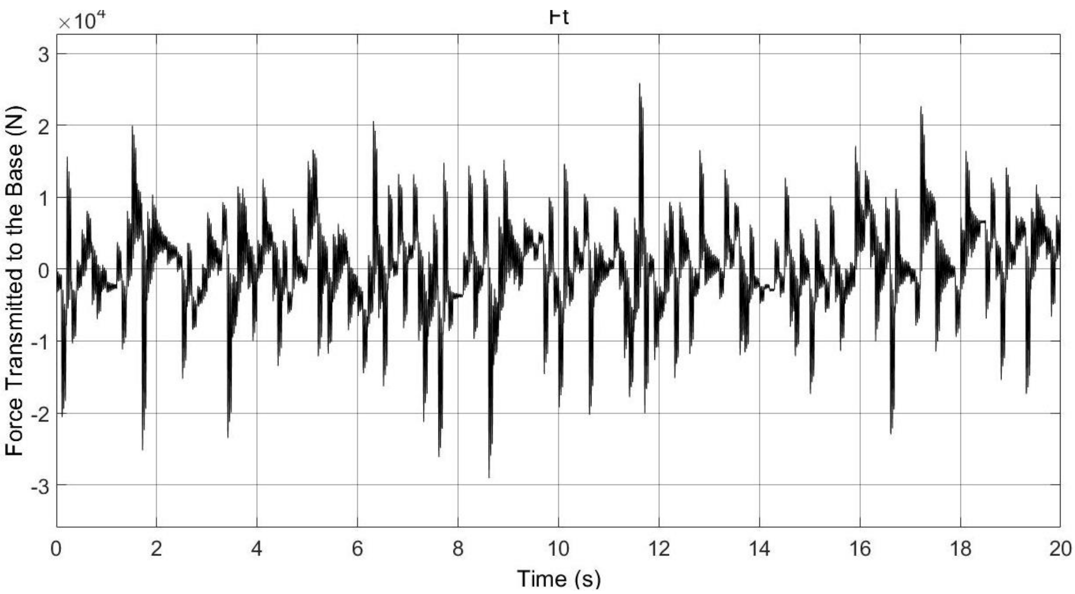

***Figure 66** – Simulated Forces Transmitted to the Base for the Primary System with the Traditional Isolator under Sinusoidal Loading*

Figure 66 shows the simulated loads transferred to the base of a system with a traditional isolator shown in Figure 6. The loads transferred to the base of the primary system also shows a varied amplitude throughout the time lapse. The peak load transmitted is recorded at a time-lapse of 8.613 seconds achieving a maximum load transfer of 28 780N.

3.3.3.3.1 Configuration I

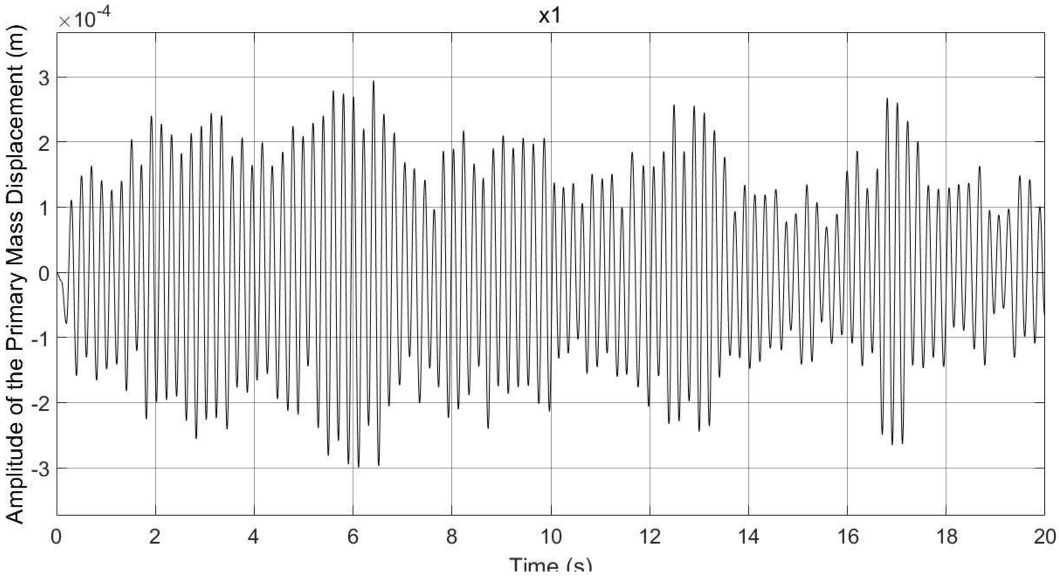

Figure 67 *– Simulated Primary Mass Displacement for Vibrational Isolator Integrated with a Negative Stiffness Element under a White Noise Frequency Loading*

Figure 67 shows the simulated displacement response of the primary system with configuration I of the proposed vibration isolator integrated with a negative stiffness element shown in Figure 34. The displacement of the primary mass shows a varied amplitude response throughout the time lapse. A peak amplitude of 2.997×10^{-4} metres is observed at a time lapse of 6.122 seconds. This constitutes a reduction of 80.02% to the peak displacement recorded for the primary system with the traditional vibrational isolator.

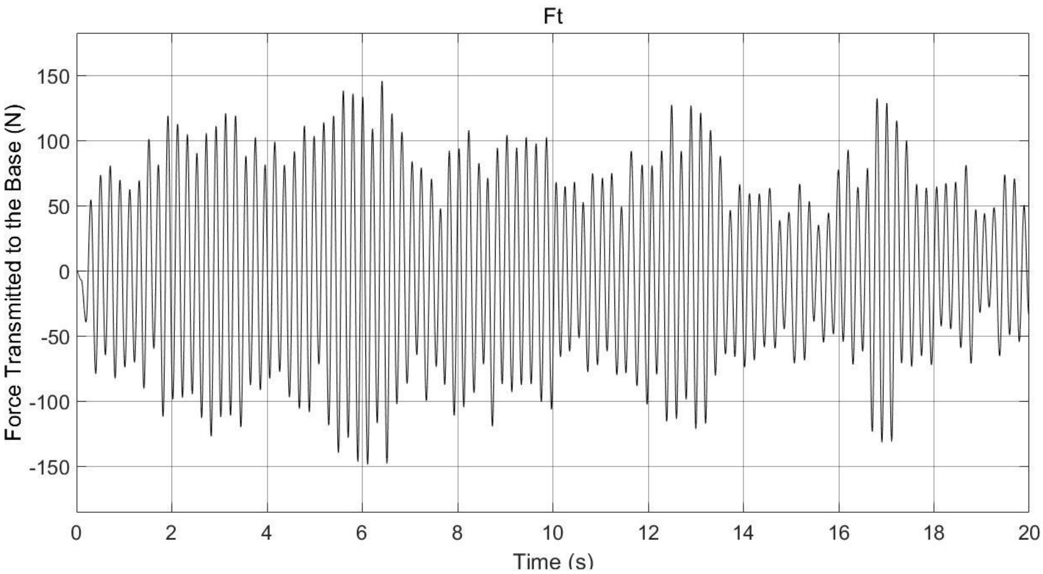

Figure 68 *– Simulated Loads Transmitted to the Base of the Primary System with the Vibration Isolator Integrated with a Negative Element under a White Noise Frequency Band Loading*

Figure 68 shows the simulated displacement response of the primary system with configuration I of the proposed vibration isolator integrated with a negative stiffness element shown in Figure 34. The recorded response of the loads transmitted to the base of the primary system shows a varied amplitude response throughout the time lapse. A peak load transfer of 147.706N metres is observed at a time lapse of 6.117 seconds. This constitutes a reduction of 99.49% to the peak load transmitted to the base of the primary system with the traditional vibrational isolator

3.3.3.3.2 Configuration II

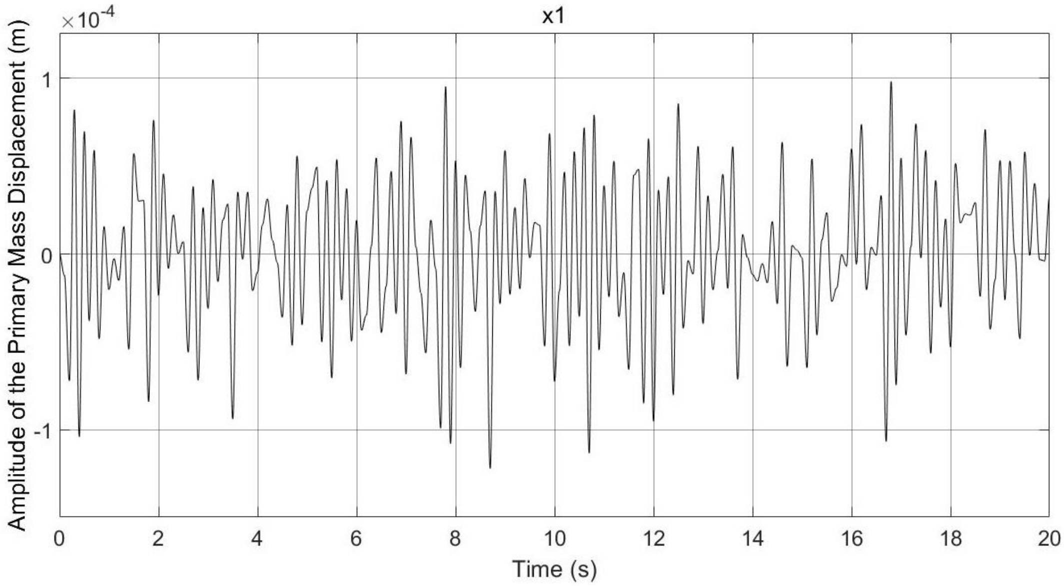

Figure 69 *– Simulated Primary Mass Displacement for Vibrational Isolator Integrated with a Negative Stiffness Element under a White Noise Frequency Loading*

Figure 69 shows the simulated displacement response of the primary system with configuration II of the proposed vibration isolator integrated with a negative stiffness element shown in Figure 35. The displacement of the primary mass shows a varied amplitude response throughout the time lapse. A peak amplitude of 1.121×10^{-4} metres is observed at a time lapse of 8.688 seconds. This constitutes a reduction of 92.52% to the peak displacement recorded for the primary system with the traditional vibrational isolator.

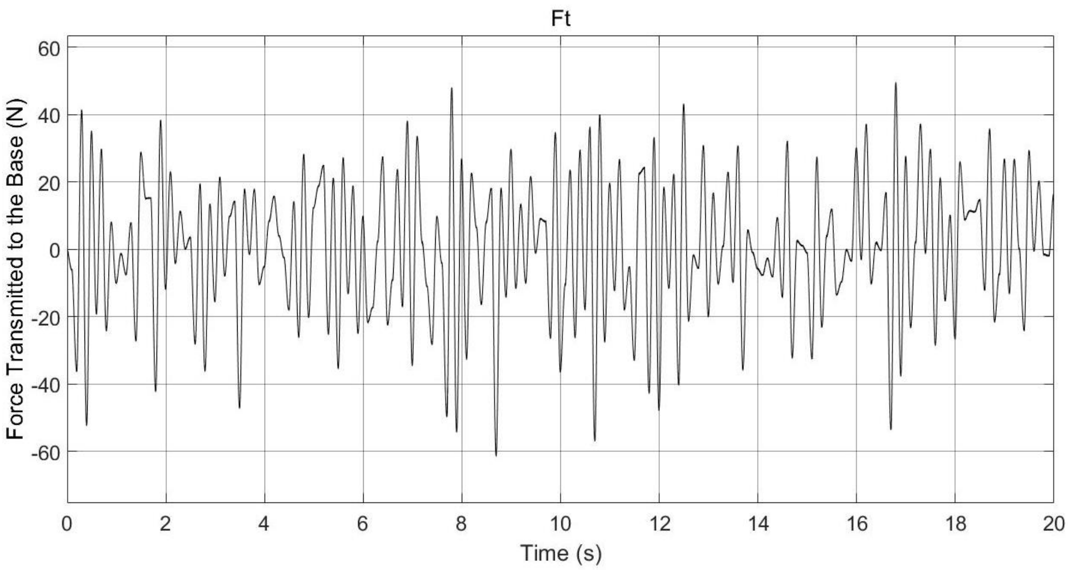

Figure 70 *– Simulated Loads Transmitted to the Base of the Primary System with the Vibration Isolator Integrated with a Negative Element under a White Noise Frequency Band Loading*

Figure 70 shows the simulated displacement response of the primary system with configuration II of the proposed vibration isolator integrated with a negative stiffness element shown in Figure 35. The recorded response of the loads transmitted to the base of the primary system shows a varied amplitude response throughout the time lapse. A peak load transfer of 61.144N metres is observed at a time lapse of 8.682 seconds. This constitutes a reduction of 99.79% to the peak load transmitted to the base of the primary system with the traditional vibrational isolator

3.3.3.3.3 Discussion

Both configurations of the proposed vibrational isolator integrated with a negative stiffness element display enhanced vibration isolation when compared to the traditional vibrational isolator shown in Figure 6. Configuration II displays enhanced performance for both the displacement of the primary mass and the loads transferred to the base of the primary system.

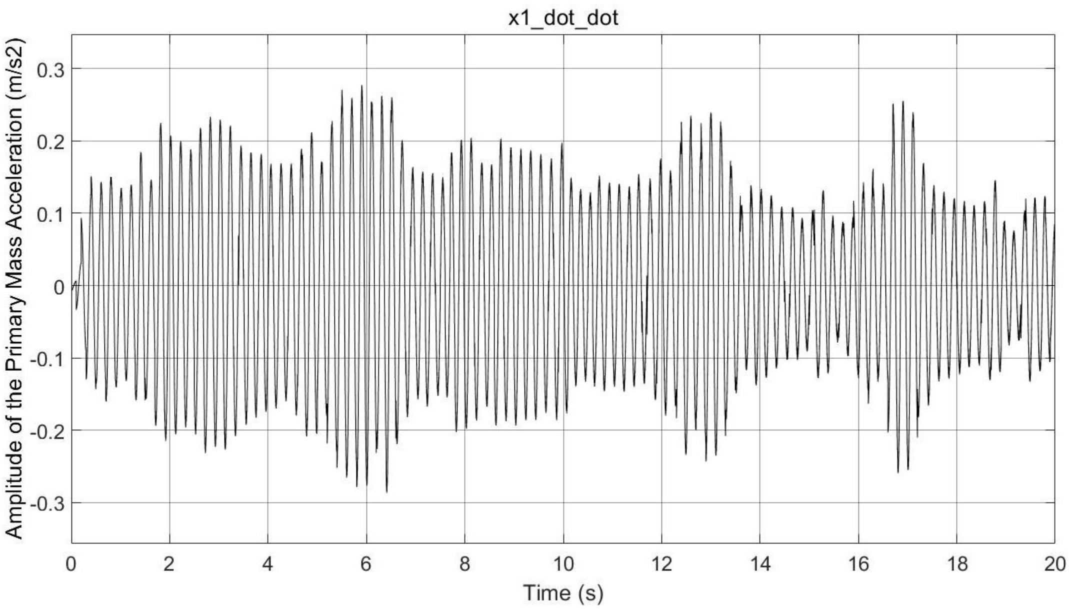

Figure 71 *- Simulated Acceleration of the Primary Mass for the System with Configuration I Vibration Isolator Integrated with a Negative Element under a White Noise Frequency Band Loading.*

Figure 71 shows the simulated displacement response of the primary system with configuration I of the vibrational isolator with a negative stiffness element shown in Figure 34. The acceleration of the primary mass also shows a varied amplitude of the acceleration with the peak acceleration recorded at a time lapse of 6.422 seconds at 0.287m/s^2.

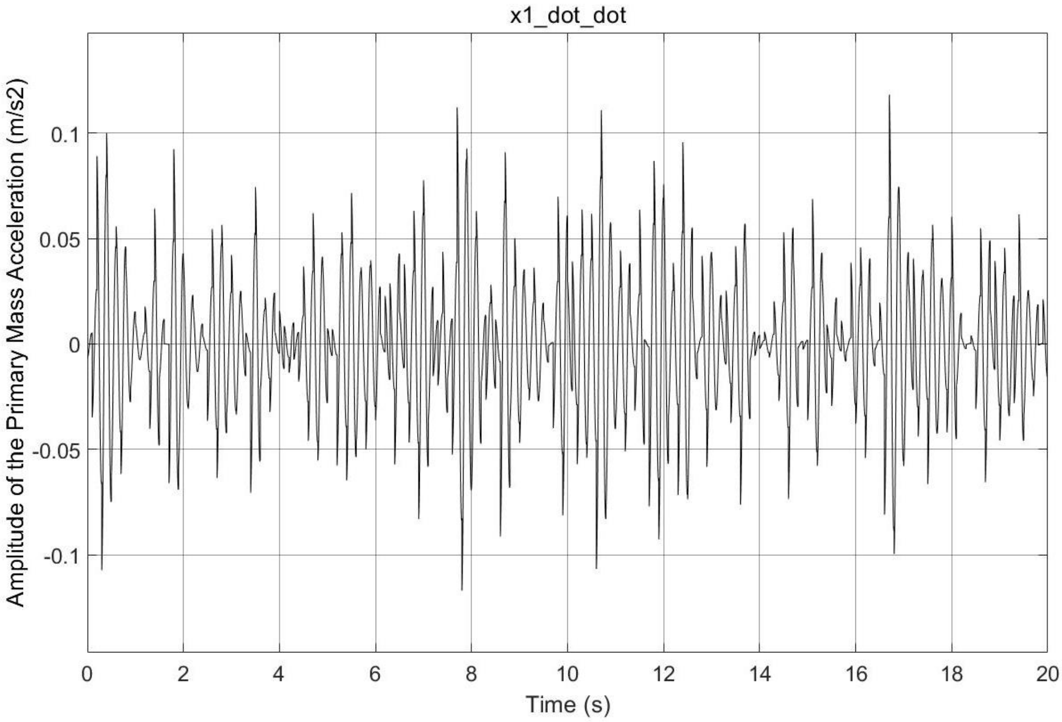

Figure 72 *- Simulated Acceleration of the Primary Mass for the System with Configuration II Vibration Isolator Integrated with a Negative Element under a White Noise Frequency Band Loading.*

Figure 72 shows the simulated displacement response of the primary system with configuration II of the vibrational isolator with a negative stiffness element shown in Figure 35. The acceleration of the primary mass also shows a varied amplitude of the acceleration with the peak acceleration recorded at a time lapse of 16.696 seconds at 0.118m/s^2.

Configuration II also displays a relatively consistent load sequence and a significantly lower rate of oscillation of the primary mass when compared to configuration I, which is essential in remote and user-centric applications such as in the automotive and aeronautical industries as the response must be consistent to prevent discomfort.

3.4 Conclusion

A vibration isolator integrated a dynamic vibration absorber with a negative stiffness spring was suggested, in two configurations, I and II. The force and displacement transmissibility, which are a common measure of a vibration isolator, were derived, based on the two-degree-of-freedom model of the isolator. It has been proven that the isolator suggested is a linear isolator, for its force transmissibility is exactly same as its displacement transmissibility.

A unique constraint on the negative stiffness ratio α of the isolator for both in configuration I and in Configuration II to run stably was developed and verified using numerical simulations. The stable region for the isolator’s operation is presented and the effect of each parameter on the stable region is reviewed and discussed, which is of benefit in the initial design or parameter selection of such an isolator. The optimal design of such an isolator was demonstrated with a design example and extensive numerical study was performed on the suggested isolator.

The suggested isolator can achieve vibration attenuation over any frequency rather than only when the frequency higher than $\sqrt{2}$ times the basic natural frequency of the isolator. Therefore, the traditional conflict requirements on an isolator of a high static stiffness required to bear high static load or limit static displacement and low or even zero dynamic stiffness to reduce the basic natural frequency so that the frequency range over which attenuation ($T < 1$) occur can be increased, is completely eliminated. Now, the static stiffness can be designed according to the requirement on static load bearing capacity only, without any worrying about the requirement of low or zero dynamic stiffness. Moreover, this isolator is a linear passive isolator. There is no nonlinear element involved.

Simulations conducted displayed enhanced vibration isolation for the vibration isolator integrated with a negative stiffness element. Significant reductions were observed for both the primary mass displacements and the load transmitted to the base of the primary structure when compared with the performance of the traditional vibration isolator. Configuration II of the proposed isolator displayed greater performance with regards to displacement and load transmission, additionally, configuration II displayed greater stability under sinusoidal, random and white-noise frequency band loading when compared to configuration I due to the position of the negative stiffness element. It can be deduced from the simulations that negative stiffness elements provide greater isolation properties when placed between the primary and secondary mass as the isolation is distributed into both masses thus improving the overall isolation performance of the system.

The theoretical and numerical analysis undertaken confirms the enhance vibration isolation performance of both configurations of the proposed linear vibrational isolator as compared to the traditional vibration isolator and provides a system that is not subject to the requirement of an impractical fundamental natural frequency value that would not be able to meet the static load requirements for practical implementation of the proposed isolator. However, the optimal design under different type of loading needs to be investigated further in detail. Prototype developing and experimental investigation should be performed in order to develop design guideline for practical application of the proposed isolator.

CHAPTER FOUR – DYNAMIC PERFORMANCE DRIVEN OPTIMAL DESIGN ON A PASSIVE TWO STAGE VIBRATION ISOLATOR

4.1 Introduction

A vibration isolator is employed to isolate the source of vibration from the object to be protected. Figure 73 presents the single-degree-of-freedom model of a single-stage traditional vibration isolator. There are mainly two distinct cases for vibrational loading, the first case is referred to as the force transmissibility problem discussed in the preceding chapters. The ultimate function of a vibration isolator is to minimize the transmitted vibration transmitted to the payload. The non-dimensional parameter which is used to quantify the effectiveness of an isolation system is transmissibility.

Figure 74 presents the transmissibility, using Eq. (2-1), of a single-stage passive linear isolator, as shown in Figure 1. It is observed that vibration can only be attenuated at frequencies above the square root of two times the fundamental natural frequency of the system, i.e., $T_r < 1$ only happens as $\lambda > \sqrt{2}$ or $\omega > \sqrt{2}\omega_1$. Therefore, to design a isolator start isolating vibration at lower frequency, the fundamental natural frequency of the system, ω_1, should approximate zero.

As discussed previously, this requirement imparts an impractical limitation on the use of a vibration isolator. In this chapter, a novel two-stage vibrational isolator is proposed in order to present a viable alternative to the traditional vibration isolator that provides enhanced vibrational isolation performance and is not subjective any restrictive requirements on the fundamental natural frequency of the primary system. Extensive analytical and numerical analysis is undertaken in order to evaluate the proposed isolators performance against the traditional vibrational isolator under varied boundary conditions. A sensitivity analysis is undertaken in order to determine an optimal range of the governing parameters by observing and recording their influence on the transmissibility of the proposed two-stage isolator. The results of which are used to determine optimal parameter values for the numerical simulations undertaken using the Simulink platform on the MATLAB suite of applications. The numerical simulations are used as a practical evaluation of the performance of the proposed linear isolator against a traditional vibrational isolator depicted in Figure 73.

4.2 A two-stage vibration isolator

4.2.1 Proposed vibration isolator

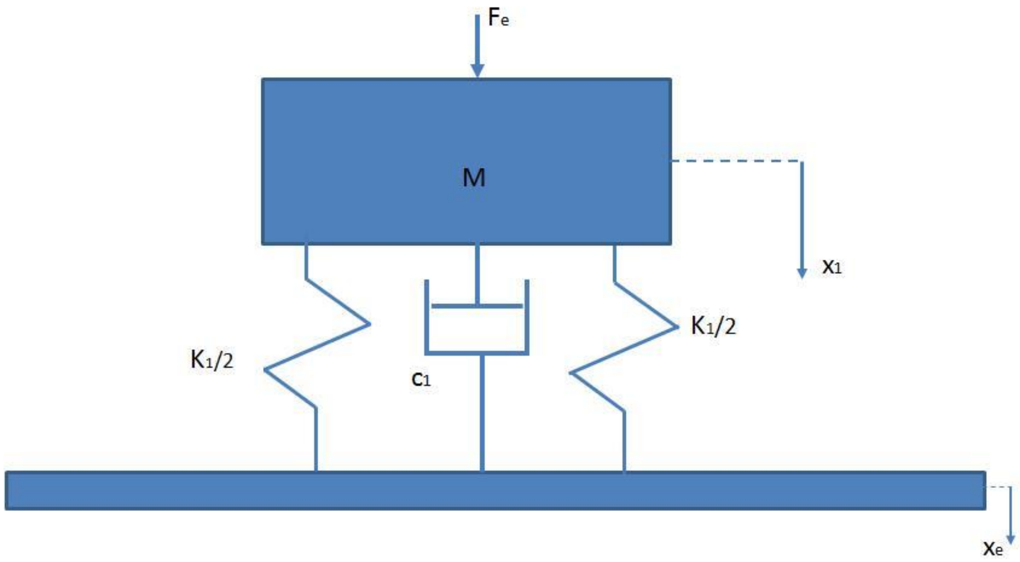

Figure 73 *- Model of a single-stage traditional vibration isolator*

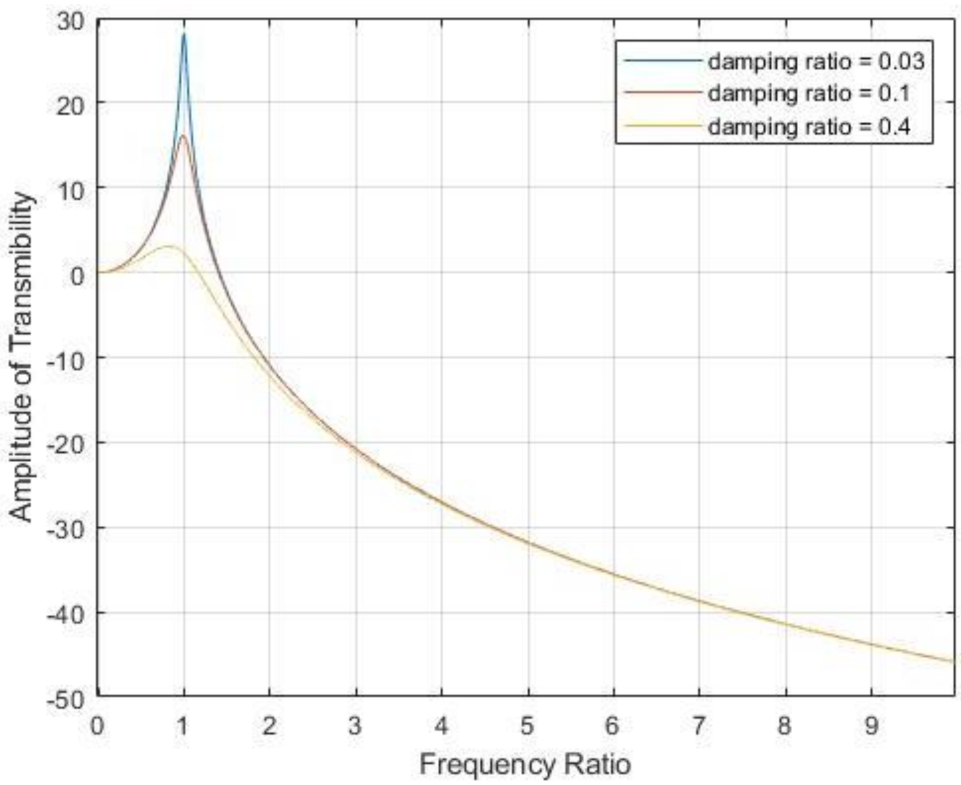

Figure 74 *- Transmissibility of a single-stage vibration isolator at different damping ratios*

Figure 74 clearly depicts that the significant effect of damping of a single-stage passive linear isolator on its isolating performance. Heavy damping is required to reduce the peak of transmissibility of such an isolator. However, increasing of damping will inevitably increase the transmissibility at higher frequencies.

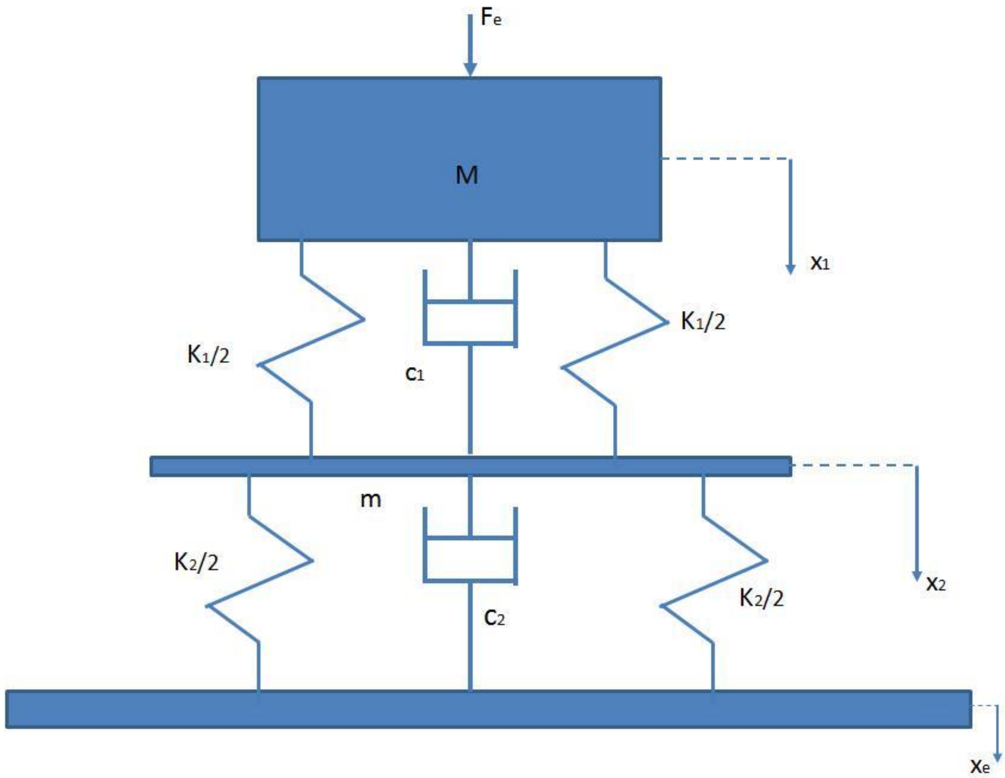

Figure 75 *- Model of a two-stage vibration isolator*

To improve the isolating performance at higher frequencies, a two-stage vibration isolator was introduced and studied [59]. Figure 75 depicts the two-degree-of-freedom model of a two-stage passive vibration isolator. It can be observed that the single-stage isolator consisting of auxiliary mass *m*, stiffness k_2 and dashpot c_2 inserts into another single- stage isolator of mass *M*, stiffness k_1 and dashpot c_1. Figure 4 presents the typical transmissibility of a linear two-stage passive vibration isolator in contrast with the transmissibility of a single stage-isolator. Figure 76 also shows that a two-stage isolator can reduce the transmissibility at higher frequencies significantly. However, the transmission of low-frequency vibration in a two-stage isolator is generally no better than that of an equivalent single-stage isolator, or even worse. Another drawback of a two-stage isolator lies in the fact that in order to extend the high-frequency vibration isolation effectiveness further into low frequencies, the auxiliary mass (*m* in Figure 75) has to be increased significantly, which results in an excessive weight penalty that is a critical issue in vehicular applications. In order to improve the performance of a linear two-stage isolator, extensive research has been performed.

Nonlinearity and semi-active elements were also introduced and studied as a measure to improve the performance of a two-stage isolator [60, 61, 62, 63]. However, such measures do not improve the performance of a linear two-stage isolator significantly. For example, the inclusion of a nonlinear stiffness element such as a spring in a two-stage nonlinear vibration isolator just makes the transmissibility at the lower resonance frequency to bend to the right, which does not benefit the isolation at lower frequencies. Additional measures such as the inclusion of an inerter and switchable stiffness control were adopted in an attempt to improve the isolating performance of a linear two-stage isolator [64, 65]. These efforts yielded some improvement on the transmissibility, but the improvement was not significant.

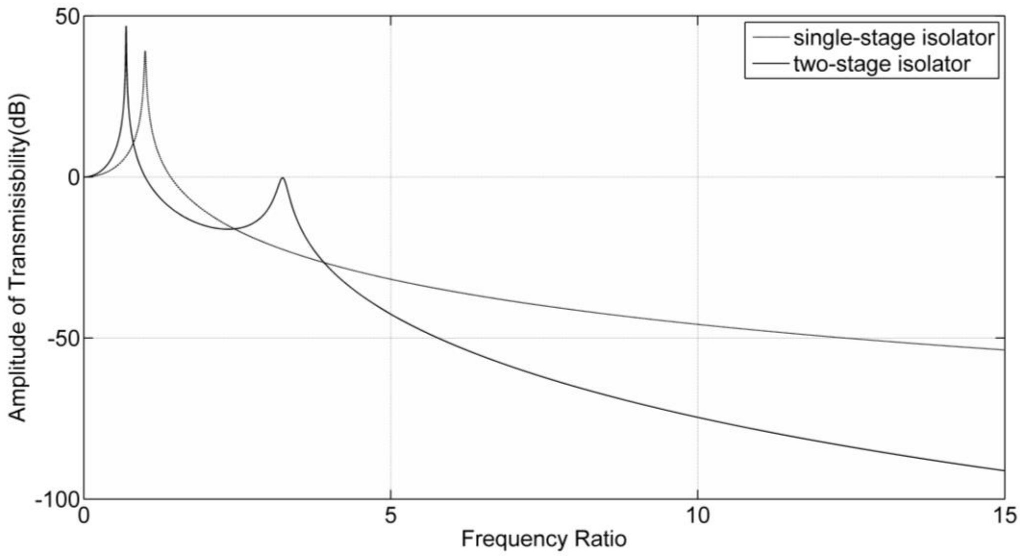

Figure 76 *- Transmissibility of a two-stage isolator vs. transmissibility of a single-stage isolator*

It has been observed that the effectiveness of a two-stage vibration isolator is largely dependent on the structural parameters of the isolator and the optimization of such parameters was performed [64]. However, it should be noted that in most of the designs and studies of the two-stage isolator, the plain idea of equivalent single-stage isolator limited the effectiveness of the design or study. In order to have the same static deflection as that of a single-stage isolator, the stiffness of the mounts in a two-stage isolator should be twice of the stiffness of the mount in an equivalent single-stage isolator. Based on this, $k_2 > k_1$ is taken for granted in almost all previous designs, research and even optimization of a two-stage isolators [65]. Additionally, the mass ratio of the ratio of auxiliary mass *m* to the main mass *M*, is limited to a range of 0.2 - 2 in most of the designs or research of two-stage isolators conducted. It is worthwhile then to study a two-stage isolator designed without such limitations.

4.2.2 Force Transmissibility

The passive two-stage vibration isolator is modelled as a two-degree-of-freedom system, as shown in Figure 75. For this system, with $x_e = 0$, the equations of motion, when M under harmonic force excitation, are given by:

$$\begin{cases} M\ddot{x}_1 + c_1(\dot{x}_1 - \dot{x}_2) + k_1(x_1 - x_2) = F_e\cos(\omega t) & (4-1) \\ m\ddot{x}_2 + k_2x_2 + c_2\dot{x}_2 + k_1(x_2 - x_1) + c_1(\dot{x}_2 - \dot{x}_1) = 0 & (4-2) \\ F_t = k_2x_2 + c_2\dot{x}_2 & (4-3) \end{cases}$$

F_t is the force transmitted to the base from machine M. The force transmissibility of the two-stage isolator can be derived from equations (4-1), (4-2) and (4-3) as:

$$T_{rf} = \frac{F_t}{F_e} = \frac{(j\omega c_1 + k_1)(j\omega c_2 + \mathrm{k}_2)}{[-M\omega^2 + j\omega c_1 + k_1](-m\omega^2 + j\omega c_1 + j\omega c_2 + k_1 + k_2) - (j\omega c_1 + k_1)^2} \quad (4\text{-}4)$$

Introducing:

$$\mu = \frac{m}{M}; \omega_1 = \sqrt{\frac{k_1}{M}}\ ; \ \omega_2 = \sqrt{\frac{k_2}{m}}; v = \frac{\omega_2}{\omega_1}; \alpha = \frac{c_2}{c_1}; \xi = \frac{c_1}{2\sqrt{k_1 M}} \tag{4-5}$$

Here μ is defined as mass ratio and α is damping ratio of the the parameters c_2 to c_1. Now the force transmissibility of the two-stage isolator, Eq (4-4), can be reduced to:

$$T_{rf} = \frac{-4\xi^2\alpha\lambda^2+\mu v^2+2j\xi\lambda(\alpha+\mu v^2)}{\mu\lambda^4-(\mu v^2+4\alpha\xi^2+\mu+1)\lambda^2+\mu v^2+2j\xi\lambda[\mu v^2+\alpha-(1+\mu+\alpha))\lambda^2]} \tag{4-6}$$

Where $\lambda = \frac{\omega}{\omega_1}$ is defined as frequency ratio while ω is the frequency of excitation force/loading.

The same system shown in Figure 75 is now under displacement excitation from the base (the source of vibration) x_e while $F_e = 0$ (M is the objected to be isolated from vibration). Using similar procedures, the displacement transmissibility of the two-stage isolator can be obtained as:

$$T_{rd} = \frac{X_1}{X_e} = \frac{A+j\xi B}{C+j\xi D} \tag{4-7}$$

Where:

$$A = -4\xi^2\alpha\lambda^2 + \mu v^2 \tag{4-8}$$

$$B = 2\lambda(\mu v^2 + \alpha) \tag{4-9}$$

$$C = \mu\lambda^4 - (1 + \mu v^2 + \mu + 4\alpha\xi^2)\lambda^2 + \mu v^2 \tag{4-10}$$

$$D = 2\lambda[\alpha + \mu v^2 - (1 + \alpha + \mu)\lambda^2] \tag{4-11}$$

Inserting equations (4-8), (4-9), (4-10) and (4-11) into Eq. (4-7) and comparing the resulting displacement transmissibility of the two-stage isolator, T_{rd}, with the force transmissibility of the isolator, T_{rf} presented in Eq. (4-6), it is then easy to observe that: $T_{rd} = T_{rf}$, therefore, this isolator is a linear isolator

4.3 Numerical simulations and discussion

Transmissibility is a tool employed to quantify the effectiveness of an isolating system. The transmissibility of a passive linear two-stage vibration isolator, as is given by Eq. (4-6), is a function of variable λ and parameters μ, v, α and ξ. The Minimax optimization has been previously successfully applied in the tuning of a tuned mass damper (TMD). A Minimax algorithm, implemented in a MATLAB environment, is developed for the proposed two-stage isolator. The transmissibility is set as the objective function. The goal of the Minimax algorithm is to minimize the worst case, in terms of maximum values, of a set of multi-variable functions, given an initial estimation, limited by lower and upper bounds on the optimization variables. Within the present context, the Minimax problem may be stated as follows:

$$\min \max Tr(\mathrm{p}),\ \mathrm{lb} \le \mathrm{p} \le \mathrm{ub} \tag{4-12}$$

p F

Where p is the vector of the variables, Tr(p) is the objective function, lb and ub are the lower and upper bound vectors of the variables respectively. Here, the task of the numerical algorithm is employed in the minimization of the maximum value (peak value) of the transmissibility, which obviously depends on the parameters of the isolator. Although in principle, the method would allow for the optimization of all the four parameters μ, v, α and ξ, the following approach has been adopted: for a given fixed mass ratio μ, the algorithm seeks the optimal values of parameters v, α and ξ, which results in the optimal performance of the proposed isolator. Thus, parameters v, α and ξ are here the three assumed free variables of the optimization process, listed in a (3 × 1) vector p. It should be highlighted that in order to initiate the optimization process, it is necessary to initialize the values of the three variable parameters v, α and ξ.

4.3.1 Performance of the vibration isolator

The performance of a linear passive two-stage isolator depends on the parameters of the isolator. Previously conducted research revealed that a two-stage isolator can only reduce transmissibility at higher frequencies as shown in Figure 76. The parameters of the two-stage isolator producing transmissibility shown in Figure 4 are : $\mu = 0.2, v = 2.2361, \alpha = 0.4472$ and $\xi = 0.01$. The damping ratio of the single-stage isolator is taken as $\xi = 0.01$.

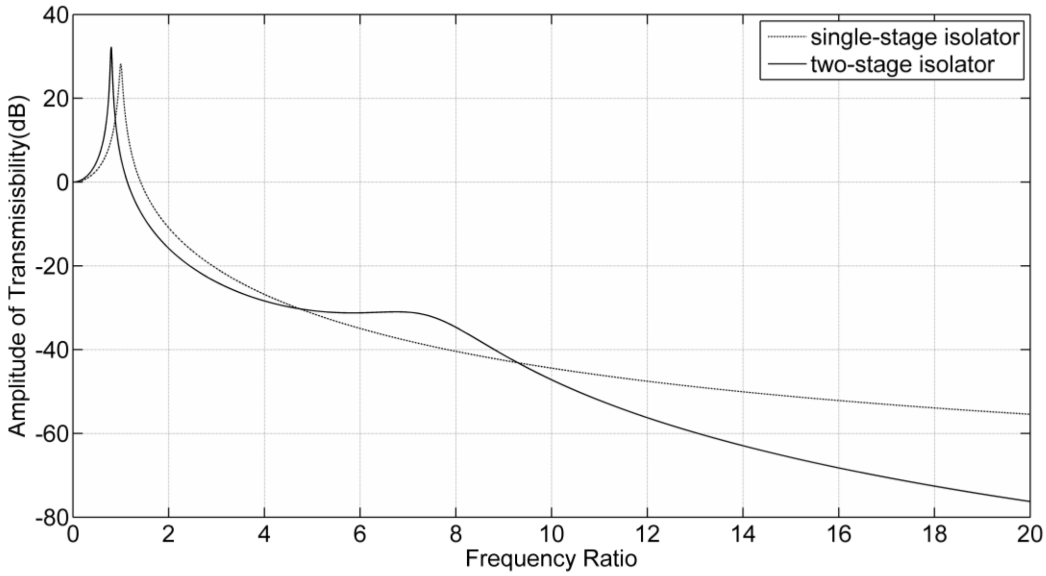

Figure 77 *- Transmissibility of a two-stage isolator at $\mu = 0.05$, $v = 6$, $\alpha = 1$ and $\xi = 0.03$ against the transmissibility of a single-stage isolator at $\xi = 0.03$*

The critical question behind the design and research of this proposed two-stage isolator is if the range of parameter value, limits or conditions applied in the design, research and optimization of a two-stage isolator are all ignored, could a new linear passive two-stage isolator with significantly different performance be realized? Figure 77 presents the transmissibility of a two-stage isolator at $\mu = 0.05$, out of the range 0.2 to 2 investigated before, $v = 6$, $\alpha = 1$ and $\xi = 0.03$ against the transmissibility of a single-stage isolator at $\xi = 0.03$. Figure 5 does not show significant improvement on the performance of previously proposed two-stage isolators. Whereas it can be observed that the first peak, occurring at $\lambda = 0.8$, is still slightly higher than the sole peak of a single-stage isolator, which occurs at $\lambda = 1$. The second peak, occurring at $\lambda = 6.75$, is slightly higher than the corresponding performance value of the single-stage isolator at the same λ value.

Maintaining the mass ratio at $\mu = 0.05$, the Minimax optimization presented in 2.2 was performed on the proposed two-stage isolator. In the optimization, p=$\{\alpha, \ \xi, \ v\}^T$, the lower bound is lb=$\{0, \ 0.01, \ 1\}^T$ and the upper bound is set as: ub=$\{2, \ 0.1, \ 10\}^T$. To start the optimization process, the initial value of the three variable parameters are set as: p_0=$\{0, 0.05, 4\}^T$. The optimized value of the three parameters yielded from the optimization process is: p_{opt}=$\{1.9998, 0.1, 1\}^T$.

Figure 78 presents the transmissibility of the optimized two-stage isolator versus the transmissibility of a single-stage isolator at the same damping ratio $\xi = 0.1$. The transmissibility of the optimized two-stage isolator has only one peak occurring at $\lambda = 0.175$ and the peak value is only about 10% of that of the peak of transmissibility, occurring at $\lambda = 1$, of the single-stage isolator. More importantly, it can be observed that the optimized two-stage isolator starts attenuation (transmissibility $T_r \leq 0$ dB) from a frequency ratio value of $\lambda = 0.346$, which is significantly lower than the corresponding attenuation of a traditional single-stage isolators under the same operating conditions which begins attenuation at a frequency value of $\lambda = 1.414$. From $\lambda \geq 0.346$, the transmissibility of the optimized two-stage isolator remains significantly lower than that of a single-stage isolator at all proceeding frequencies.

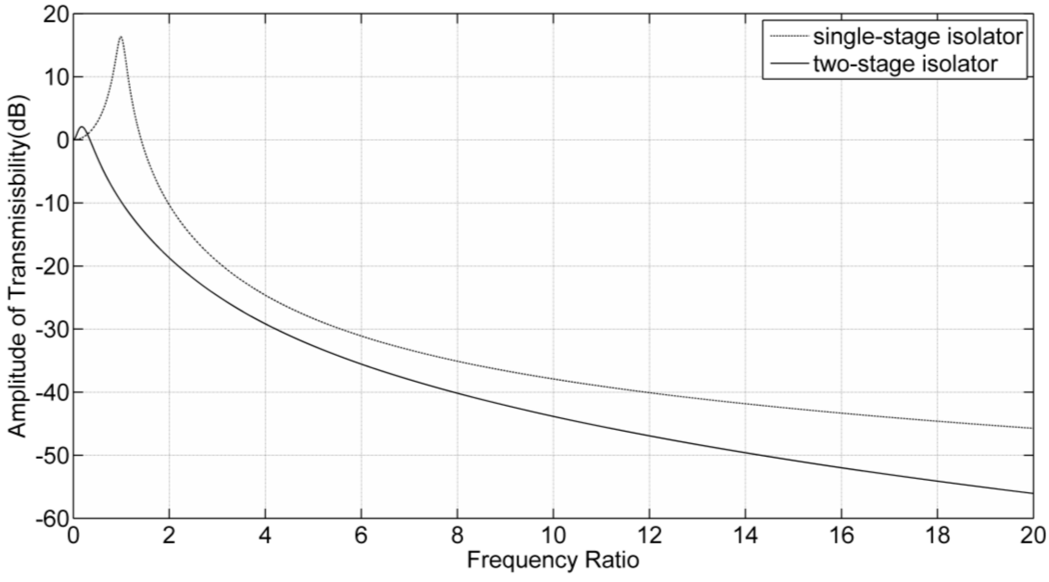

Figure 78 *- Transmissibility of a two-stage isolator at optimized parameters of $\mu = 0.05$, $\alpha = 1.9998$, $\xi = 0.1$ and $v = 1$ against the transmissibility of a single-stage isolator at $\xi = 0.1$*

Effect of Configurational Parameters on the Performance of a Two-stage Isolator:

The numerical parameter study conducted shows that the parameters of a two-stage isolator, μ, α, ξ and v, govern the performance of the isolator. A variation in any of these four parameters will lead to different transmissibility or performance of the proposed two-stage isolator. A minor mass ratio μ benefits the performance of a linear two-stage isolator. By setting $\alpha = 2$, $\xi = 0.03$ and $v = 1$ as shown in Figure 7, the transmissibility of two-stage isolator at mass ratio $\mu = 0.05$ and $\mu = 0.9$ respectively, is investigated in contrast with the transmissibility of a single-stage isolator at a damping ratio of $\xi = 0.03$.

Figure 79 clearly shows that the first peak in transmissibility of the two-stage isolator with a mass ratio $\mu = 0.9$ is nearly the same height of the peak of the single-stage isolator. If $\mu > 0.9$, the first peak will be higher than that of the single-stage isolator. With the focus of the isolator being on reducing transmissibility at lower and higher frequencies, the value of μ should always be adjusted in the design of a two-stage isolator.

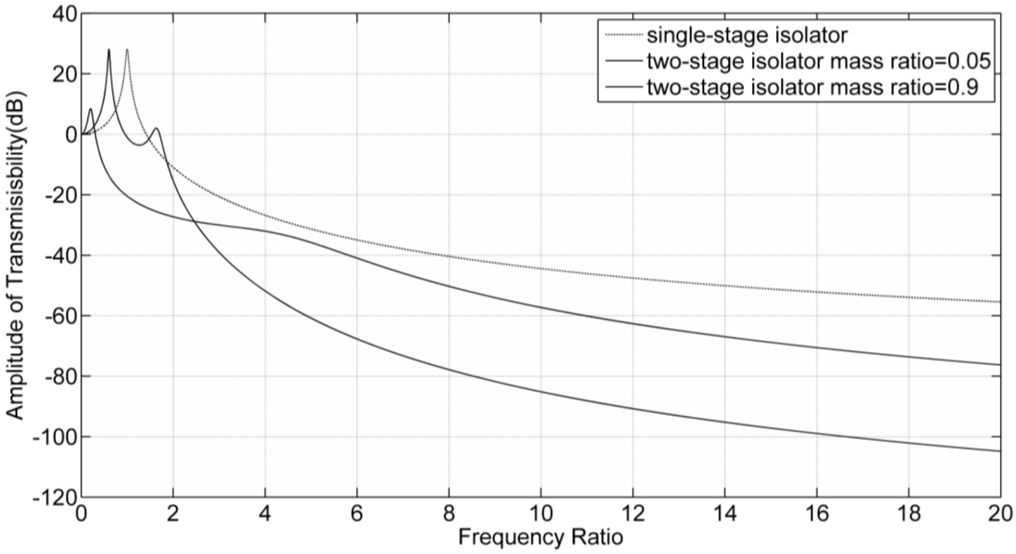

Figure 79 - *Transmissibility of two-stage isolator at $\alpha = 2$, $\xi = 0.03$, $v = 1$ and mass ratio $\mu = 0.05$ and $\mu = 0.9$ respectively in contrast with the transmissibility of a single-stage isolator at damping ratio $\xi = 0.03$*

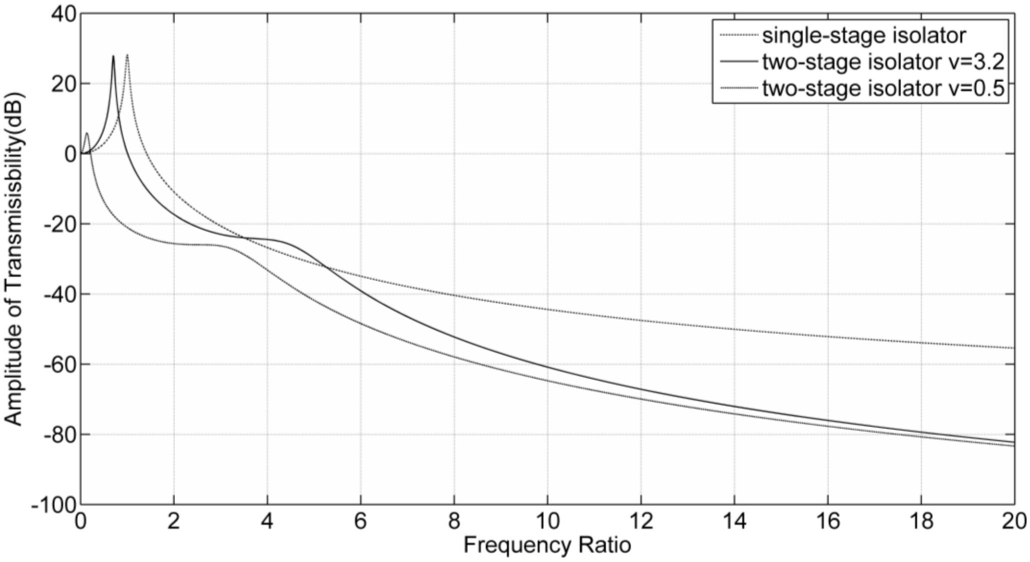

Figure 80 - *Transmissibility of a two-stage isolator at $v = 0.5$ and $v = 3.2$ respectively while $\mu = 0.1$, $\alpha = 2$ and $\xi = 0.03$, against the transmissibility of a single-stage isolator with damping ratio $\xi = 0.03$*

The parameter v affects the performance of a two-stage isolator significantly. The value of v governs the position of the peak or peaks of the transmissibility. With a smaller the value of v, the first peak moves closer to $\lambda = 0$. The second peak of transmissibility occurs at $\lambda \geq v$. Setting $\mu = 0.1$, $\alpha = 2$ and $\xi = 0.03$,we observe in Figure 80, the transmissibility of a two-stage isolator at $v = 0.5$ and $v = 3.2$ respectively, against the transmissibility of a single-stage isolator with damping ratio $\xi = 0.03$. The results clearly shows that the performance of the two-stage is optimal isolator at $v = 0.5$, as the transmissibility is significantly lower than the transmissibility of the other two at almost all frequencies (from

$\lambda \geq 0.21$). If the parameter v is increased to 3.2, the first peak of transmissibility of the two-stage isolator becomes as high as that of a single-stage isolator. Therefore, in the design of a two-stage linear passive isolator, the value of v should be as small as feasible.

The effect of damping ratio ξ on the performance of a two-stage isolator is investigated in the study of the proposed two-stage isolator and depicted in Figure 81 which presents the transmissibility of two-stage isolators with damping ratio $\xi = 0.03$ and $\xi = 0.1$ respectively while the other parameters are kept constant at $\mu = 0.1$, $\alpha = 2$ and $v = 1$. In contrast, the transmissibility of a single-stage isolator with a damping ratio of $\xi = 0.03$ is presented in the same figure. Figure 81 shows that with a higher damping of $\xi = 0.1$, the second peak of transmissibility of a two-stage isolator disappears. However, for the two-stage isolator with a high damping of $\xi = 0.1$, the isolator can only outperform the isolator with lower damping of $\xi = 0.03$ in a very narrow lower frequency range, $\lambda \leq 0.396$. Out of this range, The two-stage isolator with lower damping of $\xi = 0.03$ performs overall much better.

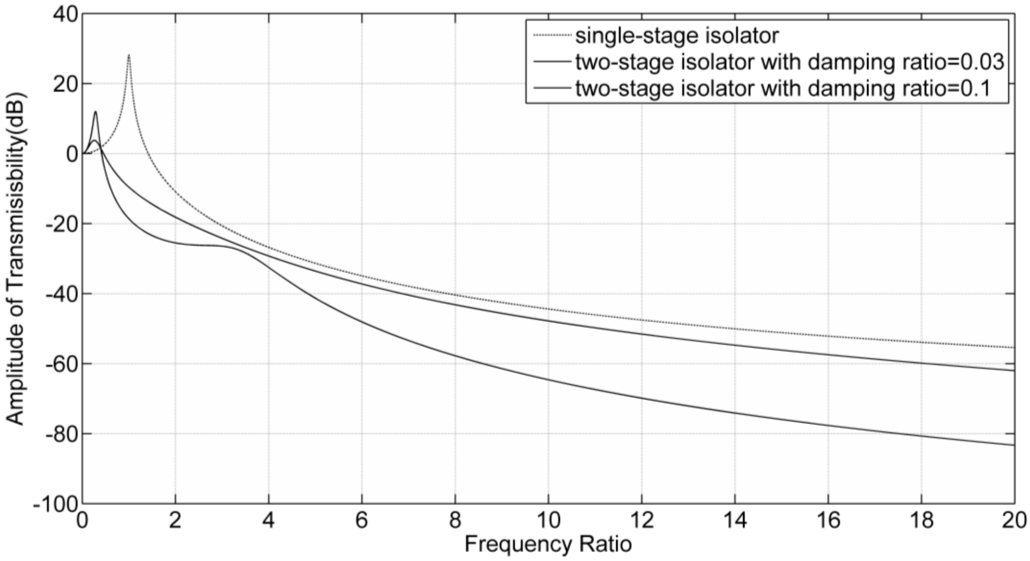

Figure 81 *- Transmissibility of two-stage isolators with damping ratio* $\xi = 0.03$ *and* $\xi = 0.1$ *respectively while* $\mu = 0.1$ *,* $\alpha = 2$ *and* $v = 1$ *in contrast with the transmissibility of a single-stage isolator with same damping ratio* $\xi = 0.03$

By conducting the parameter study using the same procedure as for the damping ratio ξ, we observe that the parameter α also has an effect on the performance of a two-stage isolator. As shown in Figure 82, higher values of α, such as $\alpha = 2$, can reduce the transmissibility in a narrow lower frequency range ($\lambda \leq 0.396$) which sacrifice the performance within the lower frequency range. With $\alpha = 0$, meaning that the system has no damping as $c_2 = 0$, the first peak of transmissibility of the two stage-isolator becomes very high, much higher than that of a single-stage isolator at the same damping ratio. However, out of this narrow lower frequency range, i.e., $\lambda \geq 0.396$, we observe that the transmissibility of the single-stage isolator becomes significantly lower than that of the transmissibility of a two-stage isolator with $\alpha = 2$ and transmissibility of a single-stage isolator with the same damping ratio of $\xi = 0.03$.

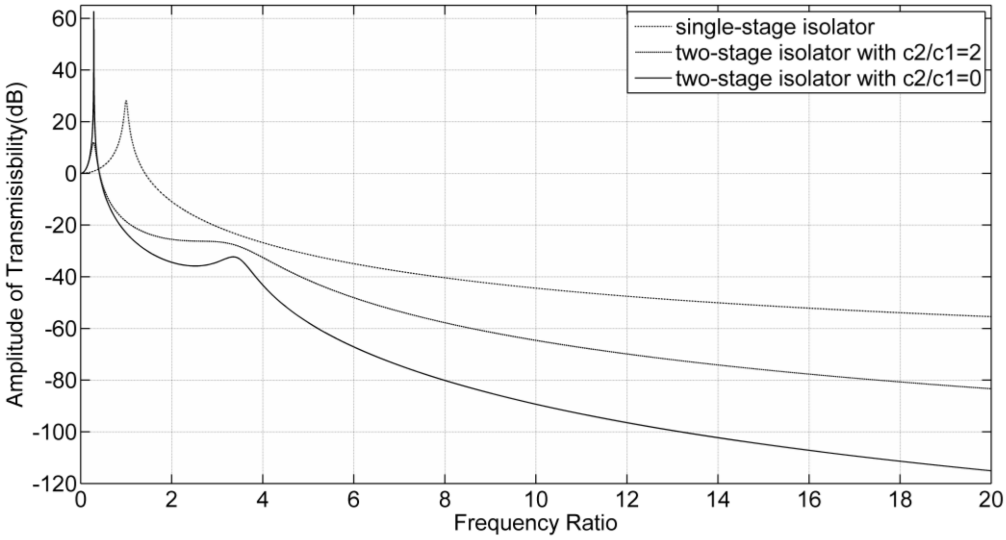

Figure 82 *- Transmissibility of a two-stage isolator with $\alpha = 2$ and $\alpha = 0$ respectively while $\mu = 0.1$, $\xi = 0.03$ and $v = 1$ in contrast with the transmissibility of a single-stage isolator with damping ratio $\xi = 0.03$*

4.3.2 Numerical Optimisation and Analysis

The numerical simulation of the proposed two-stage isolator was performed to verify the results obtained above and enlighten the thought process behind the design of a linear passive two-stage isolator. A 4th order Runge-Kutta method (RK4) was employed in numerical simulation. The parameters of the isolator to be simulated numerically were set to: $M = 100kg$; however, the isolator stiffness k_1 and k_2 have to be first designed. The stiffness element k_2 has to meet the requirement of the structural static load bearing capacity and/or limit on maximum static displacement. The structural design carried out produced a static load requirement of $k_2 = 10000N/m$. By setting $v = 1$ and the mass ratio to μ =*0.05*, which equivalently requires a damping mass of $m = \mu M = 5kg$ which in turn produces $\omega_2^2 = 2000$. Then setting, $\omega_1^2 = \omega_2^2 = 2000$, we then determine the primary stiffness element to be $k_1 = 2000 \times M = 2000 \times 100 = 200000N/m$. It should be noted that, in this instance, k_2 is much smaller than k_1, which is contrary to the traditional design rule of $k_2 \geq k_1$ in the design of a two-stage isolator, where both k_1 and k_2 are normally designed according to the static load bearing requirement and/or the limiting maximum static displacement using the equivalent single-stage isolator design concept. By setting the damping ratio to $\xi = 0.1$ snd $\alpha = 1.9998$, we then determine $c_1 = 2\xi\sqrt{k_1 M} = 894.4272$ which then means that $c_2 = \alpha \times c_1 = 2 \times 894.4272 = 1788.7$. Meaning that the two-stage isolator designed is identical to the two-stage isolator with optimized parameters presented in *3.1* and the transmissibility presented in Figure 78.

Assuming that the harmonic load acting on M is $F_e = 100\cos\omega t$ (N) which results in the force transmitted to the base to be equal to: $F_T = k_2 x_2 + c_2 \dot{x}_2$.

The parameters x_1 , x_2, $\dot{x}_1$ and $\dot{x}_2$ are determined numerically, thus allowing F_T and the transmissibility of the isolator $T_r = \frac{F_T}{F_e}$ to be determined. The loading frequency is assumed to be ω=7.8262, while $\omega_1 = 44.7214$, therefore, $\lambda = \frac{\omega}{\omega_1} = 0.175$. The transmissibility of the designed isolator is read from Figure 6 as $\lambda = 0.175$ as $T_r = 2.085$ dB, or $T_r = 1.2318$.

Using the above parameters and assumptions numerical simulations were performed on the two-stage isolator designed and Figure 83 presents the simulated force transmitted to the base, F_T, while harmonic load acting on M is $F_e = 100\cos 7.8262\mathrm{t}$ (N). In Figure 11, it can be found that the peak value of F_T is 123.18N. The peak value of F_e is 100N.Therefore, the transmissibility at $\lambda = 0.175$ is $T_r = \frac{123.18}{100} = 1.2318$, which is exactly the same as the transmissibility at $\lambda = 0.175$ determined from Figure 6.

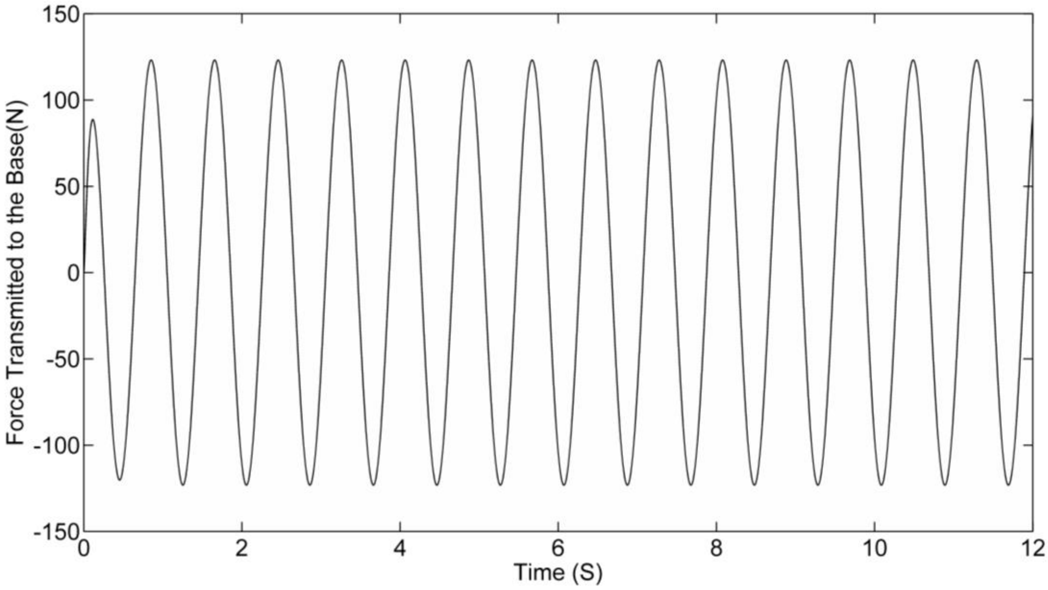

Figure 83 *- Force transmitted to the base produced by numerical simulation*

Extensive simulation on the force transmitted to the base at various values of λ and with different values of parameters of the isolator, such as varying μ, v and so forth, were performed. The transmissibility calculated from the ratio of the peak force transmitted to the base (after the system stabilizes) to the peak of the loading force always gives the same transmissibility value obtained from the transmissibility function at the corresponding λ, although the simulation results will not be presented here due to spatial limitations.

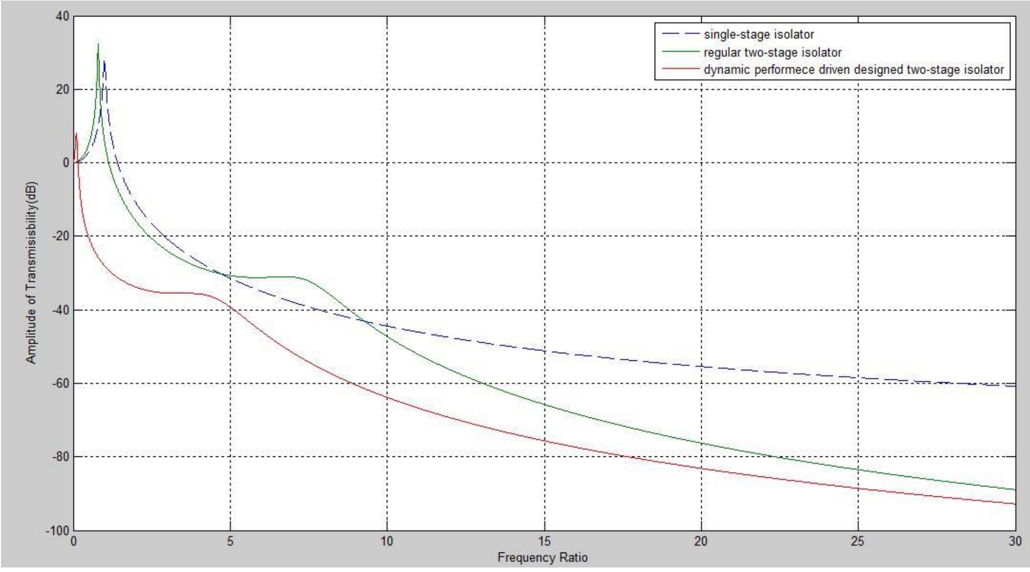

Figure 84 *- Transmissibility of a regular two-stage isolator, a two-stage isolator designed with dynamic performance driven approach in contrast with the transmissibility of a single-stage isolator with the same damping ratio of 0.03.*

In order to design the proposed passive linear two-stage isolator, the stiffness k_2, instead of k_1, has to be determined first according to the requirement on static load bearing capacity and/or limiting maximum static displacement. The Minimax optimization presented in *2.2* can be employed to aid the design. However, the quality of parameters produced by the Minimax process depend on the upper and lower bound limits. More importantly, the frequency range of the dynamic loading or displacement excitation should guide the design and parameter selection for the isolator. According to the result of numerical investigation, the suggested range of mass ratio μ is: 0.01—0.2. A higher mass ratio can improve the isolation performance at higher frequencies, but it will compromise the isolation at lower frequencies.

Generally, a small but feasible v value is preferred in the design of the proposed two-stage isolator. The proposed range of v is from: 0.2-1.5. The use of high damping parameters only enhances the performance by reducing the transmissibility at a very narrow lower frequency range but, it seriously compromises the performance at higher frequencies beyond that of the lower frequency range. The proposed range of α is from: 0.5-2 whereas the proposed range for damping ratio ξ is: 0.02-0.12. After the initial design of the two-stage isolator is completed, numerical simulations can be performed to check if the isolator performs satisfactorily.

The limit on maximum static displacement should be checked using the system's stiffness produced by k_1 connecting k_2 in series. Figure 84 presents the transmissibility of a regular two-stage isolator, a two-stage isolator designed with the dynamic performance driven optimal design approach, in contrast with the transmissibility of a single-stage isolator with the same damping ratio of 0.03.

4.3.3 Simulation under sinusoidal, random and white-noise loading

The numerical simulation of the proposed two-stage isolator was performed to verify the results obtained above and enlighten the thought process behind the design of a linear passive two-stage isolator. A computer model simulation was employed in numerical simulation using the MATLAB Simulink Platform. The parameters of the isolator to be simulated numerically were set to: $M = 100kg;$ however, the isolator stiffness k_1 and k_2 have to be first designed. The stiffness element k_2 has to meet the requirement of the structural static load bearing capacity and/or limit on maximum static displacement. The structural design carried out produced a static load requirement of $k_2 = 10000N/m$. By setting $v = 1$ and the mass ratio to $\mu = 0.05$, which equivalently requires a damping mass of $m = \mu M = 5kg$ which in turn produces $\omega_2^2 = 2000$. Then setting, $\omega_1^2 = \omega_2^2 = 2000$, we then determine the primary stiffness element to be $k_1 = 2000 \times M = 2000 \times 100 = 200000N/m$. It should be noted that, in this instance, k_2 is much smaller than k_1, which is contrary to the traditional design rule of $k_2 \geq k_1$ in the design of a two-stage isolator, where both k_1 and k_2 are normally designed according to the static load bearing requirement and/or the limiting maximum static displacement using the equivalent single-stage isolator design concept. By setting the damping ratio to $\xi = 0.1$ snd $\alpha = 1.9998$, we then determine $c_1 = 2\xi\sqrt{k_1 M} = 894.4272$ which then means that $c_2 = \alpha \times c_1 = 2 \times 894.4272 = 1788.7$. Meaning that the two-stage isolator designed is identical to the two-stage isolator with optimized parameters presented in *3.1* and the transmissibility presented in Figure 6.

Assuming that the harmonic load acting on M is $F_e = 100\cos\omega t$ (N) which results in the force transmitted to the base to be equal to: $F_T = k_2 x_2 + c_2 \dot{x}_2$.

The results obtained from the Simulink analysis were compared against a traditional isolator system in order to draw a concise comparison of the effect of the inclusion of the additional damping mass and the system's configuration as to ascertain the level of improvement of the proposed configuration. Three key performance areas were identified in order to provide a comprehensive comparison of advantages of the proposed system as compared to the traditional single stage isolator. For the purpose and integrity of the analysis, key parameters of the primary system were kept constant whereas the proposed system's parameters were optimised according to the optimisation techniques derived and discussed in the preceding sections, namely, these parameters are:

$M = 100kg;\ k_1 = 200\ 000\ N/m$

Taking $\xi = 0.1$, then, $c = 2\xi\sqrt{k_1 M} = 2 \times 0.1 \times \sqrt{200000 \times 100} = 894.43$

For the purposes of seismic analysis, the uniform random and white-noise loading were analysed as seismic loading inputs whereas the loading on the primary system was modelled as:

$$M\ddot{x} + c\dot{x} + k_1 x = -M\ddot{x}_g$$

The gravitation acceleration due to gravity was assumed to be constant at a value of:

$$g = 9.8\ m/s^2$$

For the traditional isolator, the force transmitted to the base is : $F_T = k_1 x_1 + c\dot{x}_1$.

4.3.3.1 Sinusoidal Loading

Suppose that a harmonic load is acting on M is $F_e = 100\sin\omega t$ (N).

Where the loading frequency $\omega = \omega_1 = 7.8262$

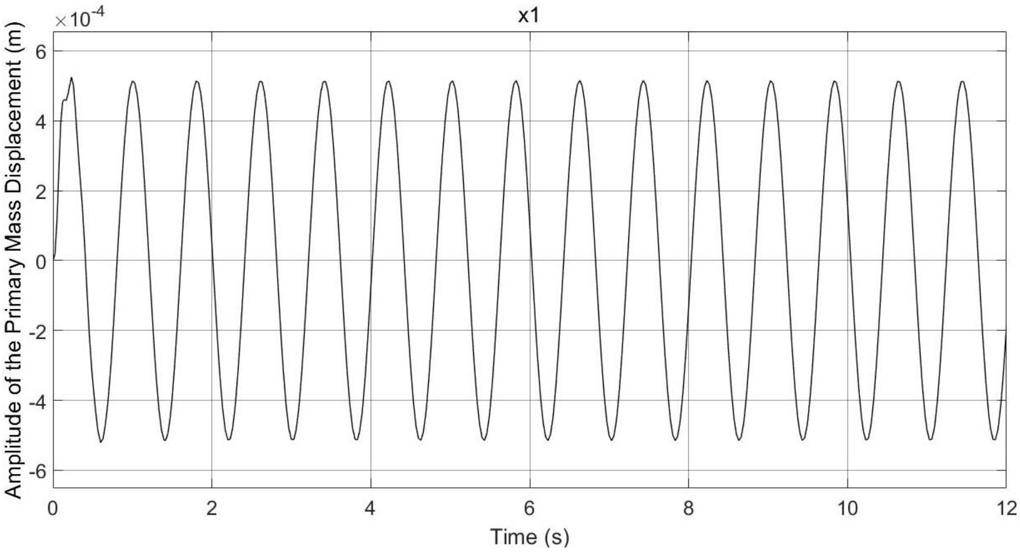

Figure 85 *- Simulated Primary Mass Displacement of the Primary System with the Traditional Single Stage Isolator under Sinusoidal Loading*

Figure 85 shows the simulated displacement response of the traditional isolator shown in Figure 73. The displacement of the primary mass shows a slight increase in amplitude as the system initialises, the displacement shows a stable period in oscillations due to the imposed sinusoidal loading, the plot indicates that the system requires a short time lapse in order to stabilise into a steady state condition with the imposed loading, the system is observed to stabilise at a time lapse of 0.595 seconds with a steady-state displacement of 5.112×10^{-4}. A peak amplitude of 5.2379×10^{-4} metres is observed at a time lapse of 0.219 seconds.

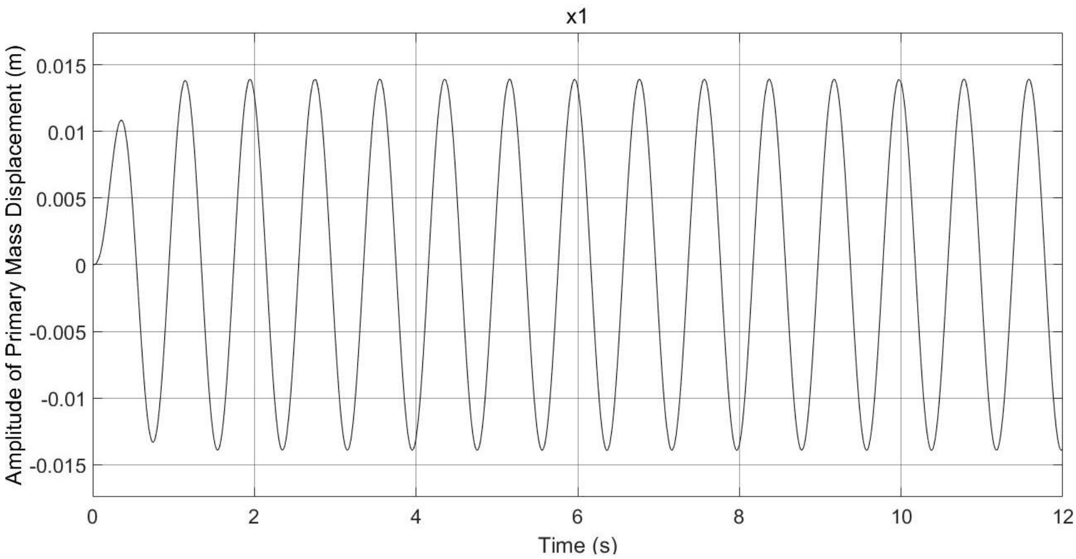

Figure 86 *- Simulated Primary Mass Displacement of the Primary System with the Two-Stage Vibration Isolator under Sinusoidal Loading*

Figure 86 shows the performance of the two-stage vibrational isolator shown in Figure 74. The system with the two-stage vibrational isolator displays significant an increase in the maximum peak displacement of the primary mass as opposed to the response of the traditional isolator shown in Figure 85 whereas in Figure 86 we observe a maximum displacement of 0.0138 metres which is a 96.20% increase in primary mass displacement. Furthermore, the system stabilises at a longer timeframe than the traditional isolator at a time lapse of 1.1409 seconds.

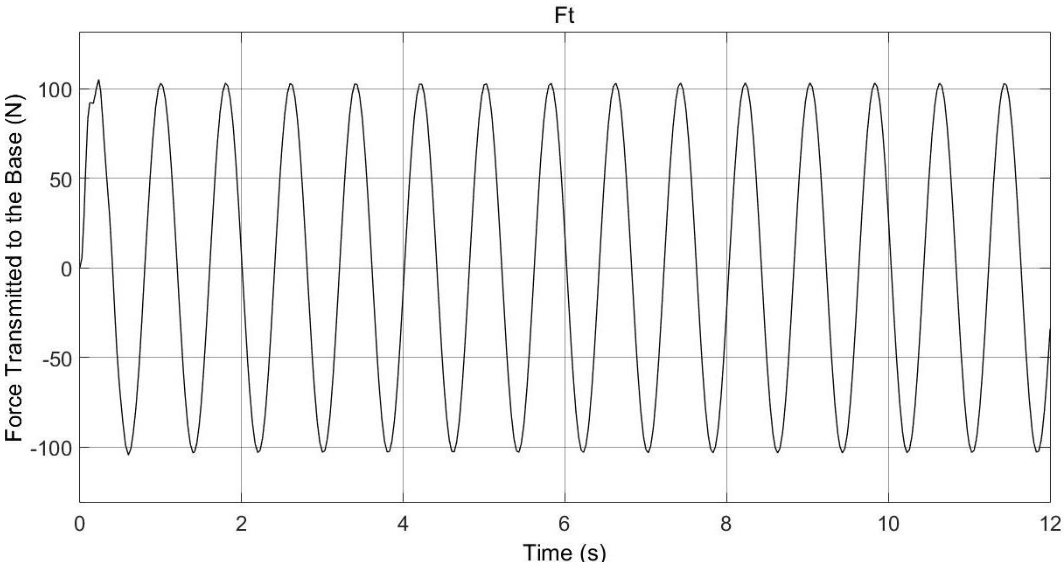

Figure 87 *- Simulated Loads Transmitted to the Base of the Primary System of the Traditional Single Stage Isolator under Sinusoidal Loading*

Figure 87 shows the simulated loads transferred to the base of a system with a traditional isolator shown in Figure 73. The loads transferred to the base of the primary system shows a slight increase in amplitude as the system initialises and stabilises at a time lapse of 0.602 seconds achieving a steady-state load transfer of 103.586N. The peak load transfer is recorded at a time lapse of 0.232 seconds at a maximum load transfer of 105.132N.

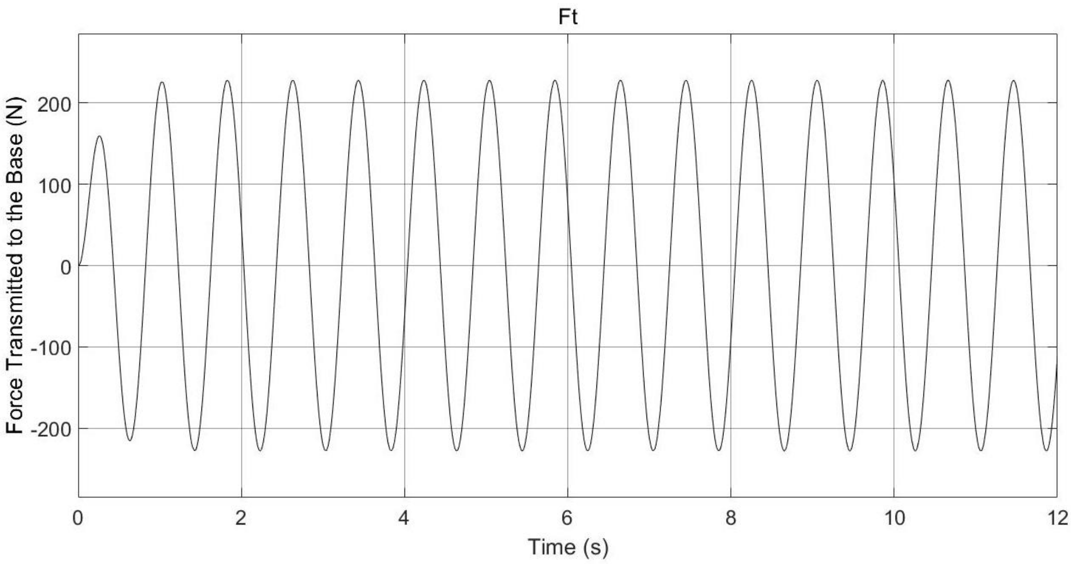

Figure 88 *- Simulated Loads Transmitted to the Base of the Primary System of the Traditional Single Stage Isolator under Sinusoidal Loading*

Figure 88 shows the simulated loads transferred to the base of a system with a two-stage vibrational isolator. The system with the two-stage vibrational isolator displays a significant increase in the maximum peak loads transferred to the base of the primary mass as opposed to the traditional isolator shown in Figure 87 whereas in Figure 88 we observe a maximum load transferred to the base of the primary system of 226.959N which is a 53.68% increase in load transferred to the base of the primary system with a traditional isolator. The peak load transmission occurs at the steady-state response of the loads transmitted

The traditional single-stage vibration isolator displays an enhance performance, significantly better than the proposed isolator which may be due the loading frequency may be too low in order to enable the two-stage isolator to provide enhanced isolation thus resulting in the inertial forces of the secondary damping mass to be transmitted to the base. A sensitivity analysis is required to establish an optimal frequency range that will enable the two-stage vibration isolator to provide satisfactory vibration isolation.

4.3.3.2 Random Loading

Suppose that a random uniform load is acting on M

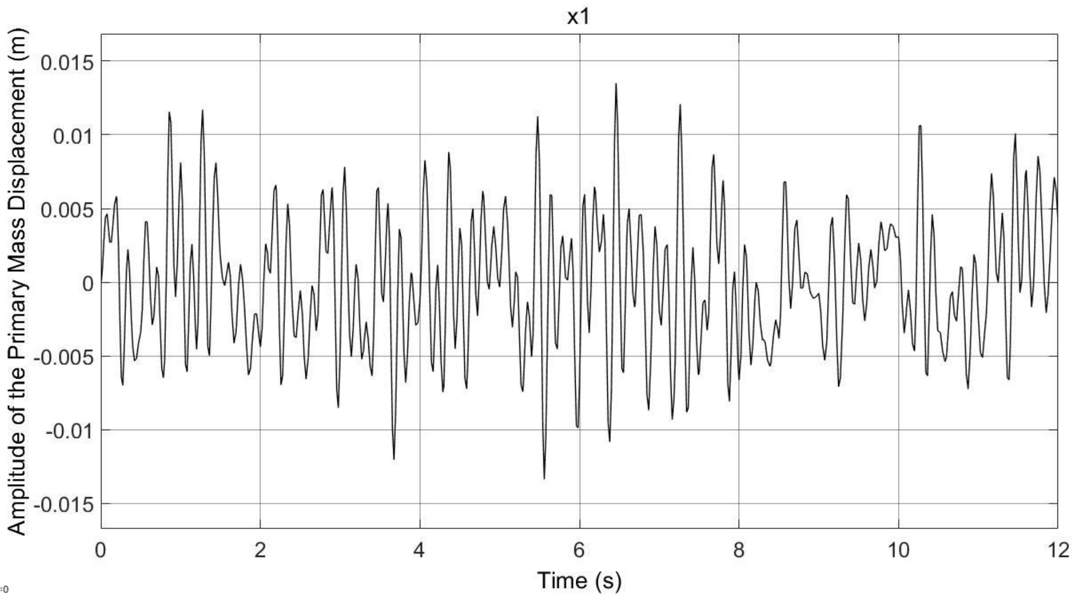

Figure 89 *- Simulated Primary Mass Displacement of the Primary System with the Traditional Single Stage Isolator under Random Loading*

Figure 89 shows the simulated displacement response of the primary system with the traditional single-stage vibrational isolator under random loading. The displacement of the primary mass shows a varied response throughout the time lapse, the peak displacement recorded occurs at a time lapse of 6.459 seconds at a peak value of 0.0136 metres.

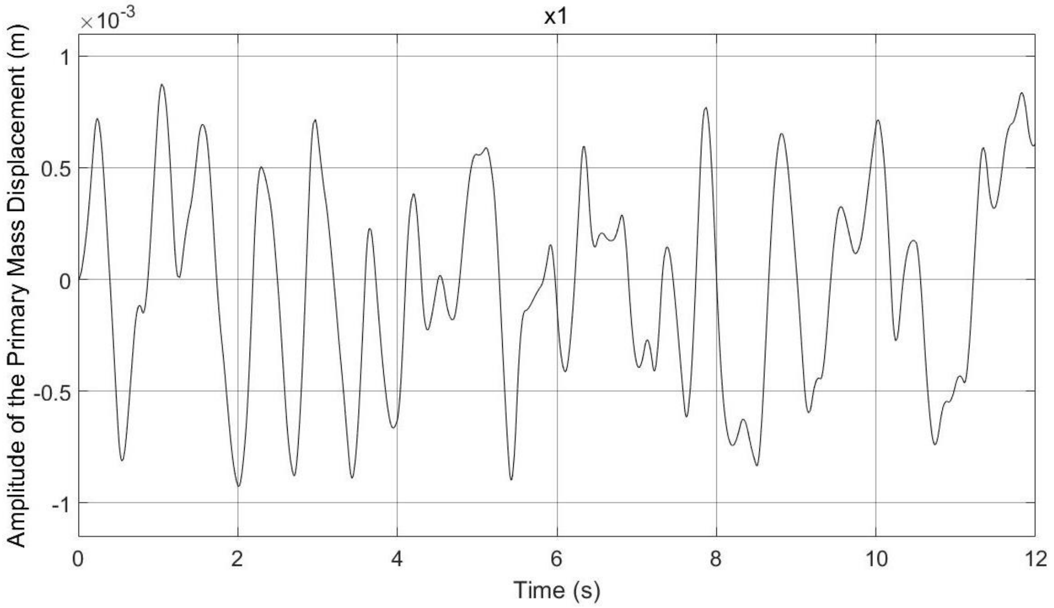

Figure 90 *- Simulated Primary Mass Displacement of the Primary System with the Two- Stage Isolator under Random Loading*

Figure 90 shows the displacement response of a system with a two-stage vibrational isolator under random loading. A varied sequence of loading is observed from the recorded response. The peak displacement recorded at 9.177×10^{-4} metres at a time lapse of 2.014 seconds, which is a 93.25% reduction as compared to the peak displacement recorded in Figure 89.

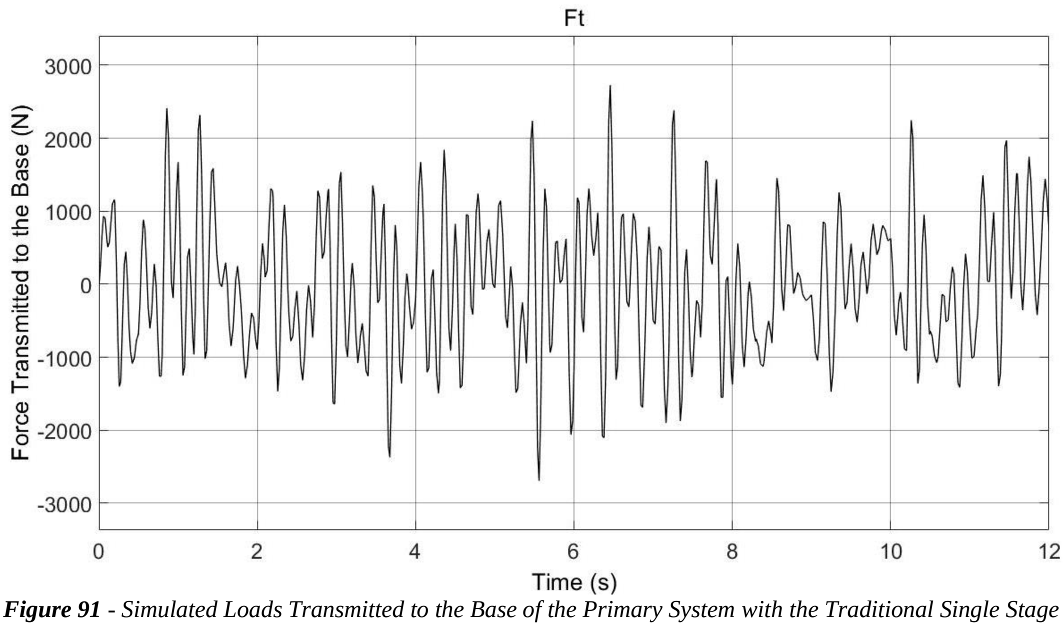

Figure 91 *- Simulated Loads Transmitted to the Base of the Primary System with the Traditional Single Stage Isolator under Random Loading*

Figure 91 shows the simulated loads transferred to the base of a system with a traditional isolator under random loading. The loads transferred to the base of the primary mass shows a varied response as time lapses with a peak load transfer of 2740.6N at a time lapse of 6.454 seconds.

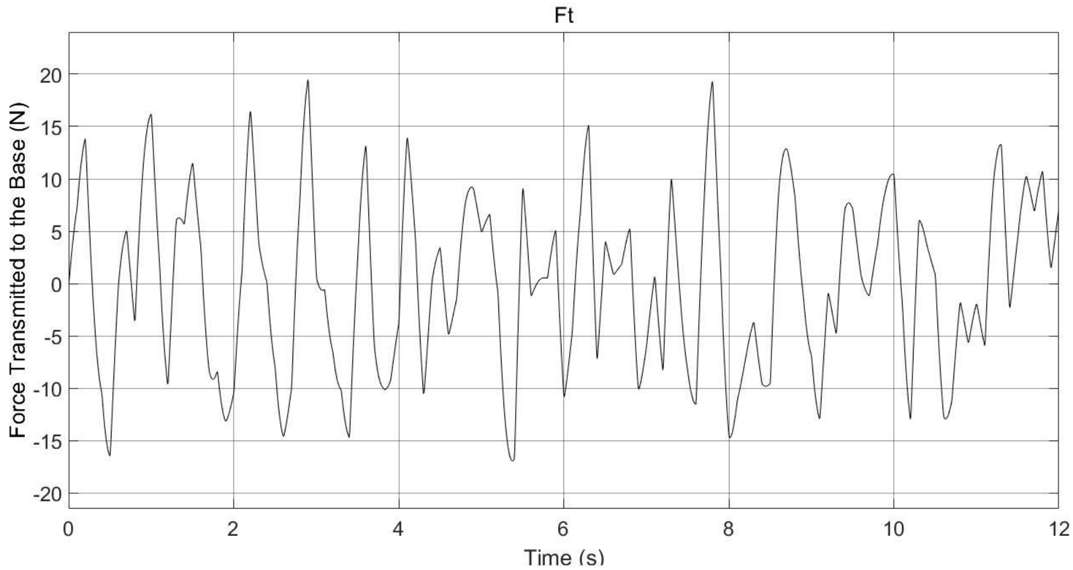

Figure 92 *- Simulated Loads Transmitted to the Base of the Primary System with the Two-Stage Isolator under Random Loading*

Figure 92 shows the simulated loads transferred to the base of a system with a two-stage vibrational isolator. The system with the two-stage vibrational isolator displays a significant decrease in the maximum peak loads transferred to the base of the primary mass as opposed to the traditional isolator shown in Figure 91 whereas in Figure 92 we observe a maximum load transferred to the base of the primary system of 19.5N which is a 99.29% reduction in load transferred to the base of the primary system with a traditional isolator.

4.3.3.3 White-Noise Loading

Suppose that a seismic (white-noise band) load is acting on M

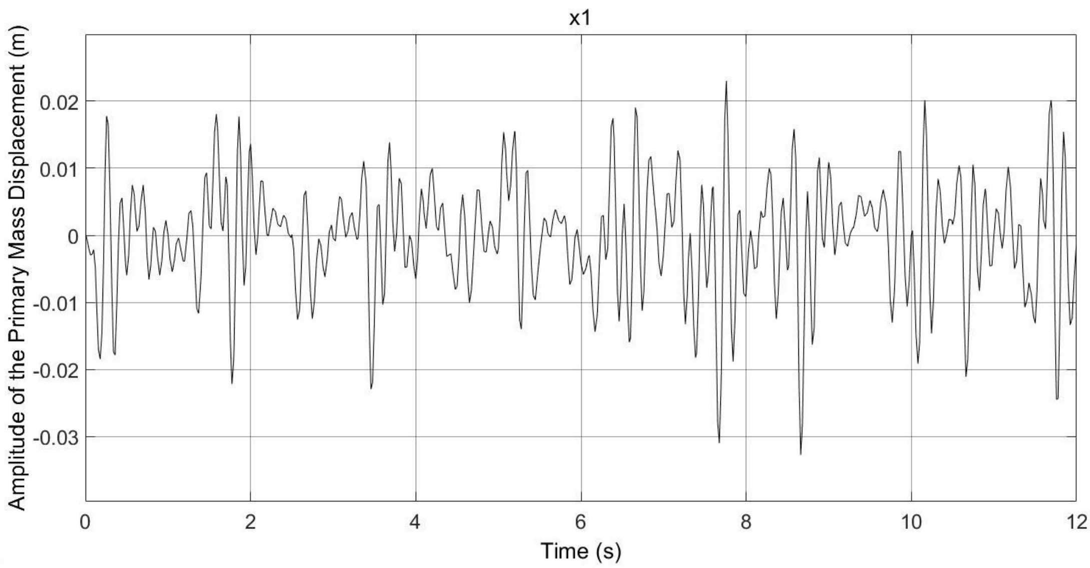

Figure 93 *- Simulated Primary Mass Displacement of the Primary System with the Traditional Single Stage Isolator under White Noise Frequency Band Loading*

Figure 93 shows the simulated displacement response of the primary system with the traditional single-stage vibrational isolator under white-noise frequency band loading. The displacement of the primary mass shows a varied response throughout the time lapse, the peak displacement recorded occurs at a time lapse of 8.6652 seconds at a peak value of 0.033 metres.

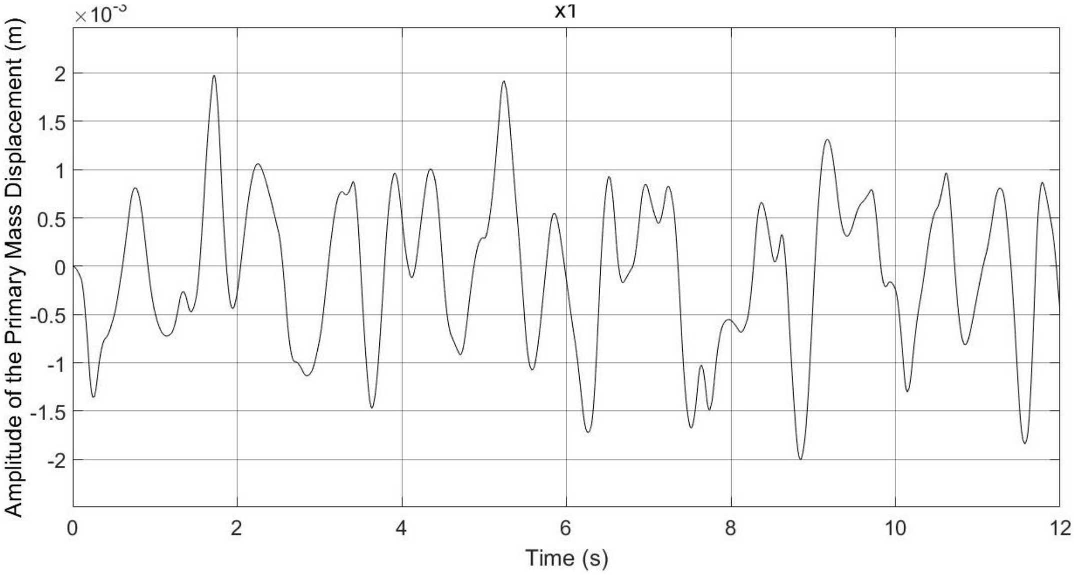

Figure 94 *- Simulated Primary Mass Displacement of the Primary System with the Two- Stage Isolator under White-Noise Frequency Band Loading*

Figure 94 shows the displacement response of a system with a two-stage vibrational isolator under random loading. A varied sequence of loading is observed from the recorded response. The peak displacement recorded at 0.002 metres at a time lapse of 8.851 seconds, which is a 93.25% reduction as compared to the peak displacement recorded in Figure 93.

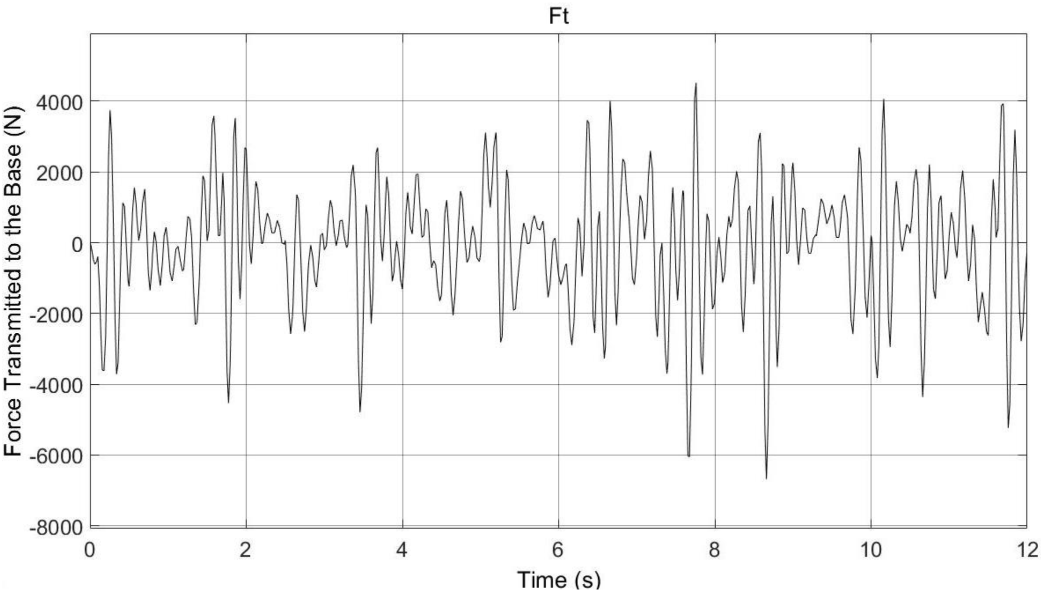

Figure 95 *- Simulated Loads Transmitted to the Base of the Primary System with the Traditional Single Stage Isolator under White Noise Frequency Band Loading*

Figure 95 shows the simulated loads transferred to the base of a system with a traditional isolator. The loads transferred to the base of the primary mass shows a varied response as time lapses with a peak load transfer of 6667.2N at a time lapse of 8.667 seconds.

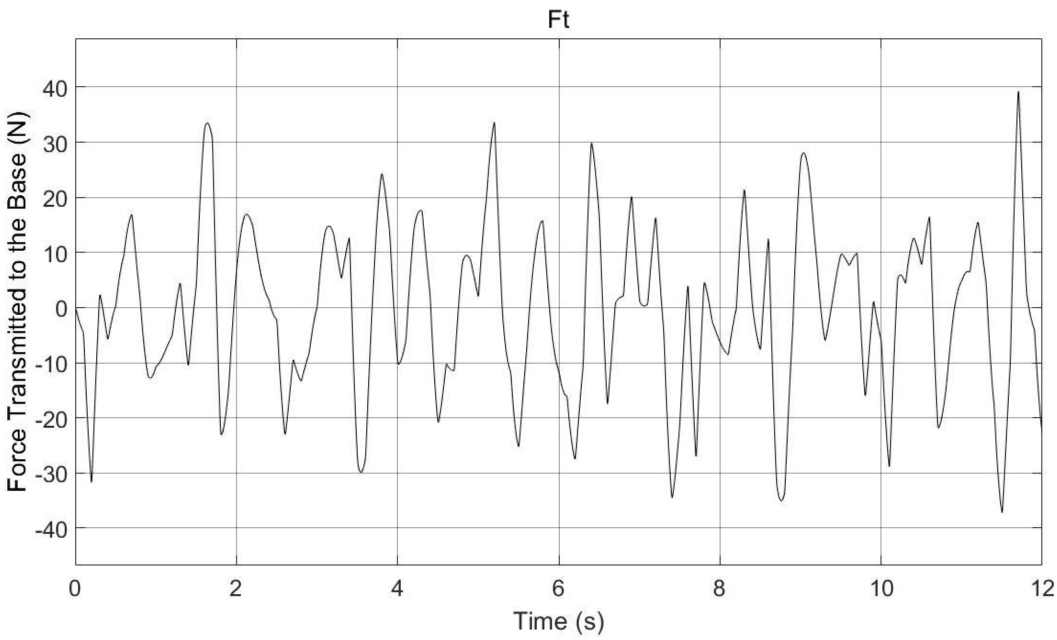

Figure 96 *- Simulated Loads Transmitted to the Base of the Primary System with the Two-Stage Isolator under White Noise Frequency Band Loading*

Figure 96 shows the simulated loads transferred to the base of a system with a two-stage vibrational isolator. The system with the two-stage vibrational isolator displays a significant decrease in the maximum peak loads transferred to the base of the primary mass as opposed to the traditional isolator shown in Figure 95 whereas in Figure 96 we observe a maximum load transferred to the base of the primary system of 39.330N at a time lapse of 11.699 seconds which is a 99.41% reduction in load transferred to the base of the primary system with a traditional isolator.

4.4 Conclusion

A passive linear two-stage vibration isolator and its design was re-examined. The force and displacement transmissibility, a common measure of the performance of an isolator, were derived based on a two-degree-of-freedom model of the proposed isolator. It is proven that the two-stage isolator examined is a linear isolator. A Minimax optimization on the transmissibility of the isolator was developed and thoroughly studied.

The numerical studies revealed that the performance of a passive linear two-stage isolator depends on the configuration parameters of the isolator. By optimization and design using an unorthodox set of design rules for passive two-stage isolator, such as $k_2 > k_1$ or even $k_2 = k_1$, a new linear passive two-stage isolator can be produced. Instead of using the traditional passive two-stage isolator which just reduces the transmissibility at higher frequencies while either having no effect or even increasing the transmissibility at lower frequencies, the proposed linear passive two-stage isolator, however, without employing high damping elements ($\alpha = 2\ and\ \xi = 0.03$), can significantly reduce the transmissibility at almost any frequencies, both high or low, even outperforming many previously proposed nonlinear two-stage isolators.

The inherent conflict requirements on a linear isolator: high static stiffness to bear high static load or limit on static displacement and to achieve low or even zero dynamic stiffness to reduce the fundamental natural frequency so that the frequency range over which attenuation occurs ($T_r < 1$) can be increased, is thus completely eliminated. Now, the stiffness of the passive linear two-stage isolator, k_2, can be simply designed according to the requirement of static load bearing capacity only while the frequency range over which attenuation occurs can be extended to $\omega > 0.175\omega_1$, instead of $\omega > \sqrt{2}\omega_1$,which is achieved with dynamic performance driven optimal design without the need of varying the stiffness element k_2.

The Minimax optimization and numerical simulation presented can be used to aid the design of the proposed linear passive two-stage isolator. The design procedures and the proposed parameter values ranges can be used in the design and parameters optimization. Parameter optimization under different type of loading needs to be further investigated. Prototype developing and experimental investigation of the proposed two-stage isolator must be performed to produce a detailed design guideline for its application in practice.

Simulations conducted on the two-stage vibrational isolator displayed significant vibration isolations for systems with a large range of frequency loading on the primary system. The proposed isolator displayed a poor performance under a low-frequency sinusoidal load hence this must be stipulated as an operation criterion for the practical application of the vibration isolator. An extensive sensitivity analysis is required to determine the optimal loading frequency that this isolator can offer satisfactory vibration isolation performance.

The proposed two-stage isolator discussed and analysed in this chapter also provides enhanced performance when compared to the traditional vibration isolator which is supported by extensive theoretical and practical simulations conducted which indicate that proposed linear isolator is not subject to limitation criteria on the fundamental natural frequency of the primary observed for a traditional isolator. However, extensive practical analysis and testing is required to develop implementation codes of practice of the proposed two-stage vibrational isolator.

CHAPTER FIVE – GENERAL DISCUSSIONS AND CONCLUSION

5.1 General discussion and comparison of proposed vibration isolators

In this thesis, three varied vibration isolation systems are proposed whereas the aim is to develop a practical passive vibration system that can be seamlessly implemented in practice which is not subject to the observed restricted performance of a traditional vibrational isolator where the vibration can only be attenuated at frequencies above the square root of two times the fundamental natural frequency of the system, i.e., $T_r < 1$ only happens as $\lambda > \sqrt{2}$ or $\omega > \sqrt{2}\omega_1$.

It should be highlighted that the configurations of the proposed systems limit the general comparisons that can be made of the proposed systems as their configurations influence the performance against the same boundary conditions, i.e., parameter selection. The recorded performance depicted in the preceding chapters effectively indicates that all the proposed system produce fundamentally different optimal parameter requirements hence a direct comparison is impractical. Therefore, in this section, the general observed performance against the traditional linear vibration isolator is discussed.

The skyhook and groundhook vibration isolation systems are limited in their application due to the requirement of an inertial reference point hence as per [21], a framework consisting of a damping mass is required to provide rigidity and simulate the effect of the inertial reference frame in order to be able to be able to provide satisfactory vibration isolation performance. Extensive simulations is undertaken against a traditional isolator whereas the performance against deterministic and random loading is studied and discussed in order to provide a wholistic performance evaluation of the proposed isolator. The proposed vibration isolator integrated with a skyhook damper displayed enhance vibration isolation across all frequency bands as well as different types of loading thus rendering it efficient for implementation across multiple engineering industries where vibration isolation is essential

The proposed isolator integrated with a negative stiffness element also displayed enhanced vibration isolation across a wide loading frequency range with the difference in performance attributed to the positioning of the negative stiffness element. Configuration I provided greater load transmission isolation under sinusoidal loading, but significant time delays were observed with regard to the stabilisation of the system under the sinusoidal load. Configuration II provided greater vibration isolation for both the primary mass displacement and the load transmission to the base of the primary system under random and white-noise frequency band loading. Configuration II also displayed significantly shorter stabilisation periods for the system to reach a steady state thus overall, configuration II provides better vibration isolation. However, both configurations provided enhanced performance when compared to the traditional linear vibration isolation under the sensitivity analyses done in assessing the transmissibility response of the systems as well as numerical simulation under deterministic and random loading

Lastly, the proposed two-stage vibrational isolator produced enhanced transmissibility response as compared to that of the traditional linear vibration absorber under the same governing parameters, i.e., the same base conditions. However, the proposed isolator displayed a poor performance under a low-frequency sinusoidal load. This performance thus provides more clarity on the inherent limitations of the practical applications of the proposed two-stage isolator. This must then be stipulated as an operation criterion for the practical application of the vibration isolator as, contrarily, the isolator displayed significant vibration isolations random loads with a large frequency loading band imposed on the primary system. An extensive sensitivity analysis is required to determine the optimal loading frequency that this isolator can offer satisfactory vibration isolation performance.

As stated in Chapter 1, the aim of this research is to explore the performance of passive linear vibration absorbers performance when integrated with a variety of Dynamic Vibration Absorbers (DVAs) in order to increase the efficiency of energy dissipation without compromising on the practical applicability of the proposed solutions. This thus has been successively achieved based on the performance recorded, analysed and discussed in Chapters 2 to 4. The proposed passive linear vibrational isolators are applicable to a wide range of practical application within multiple industries based on the operational and functional requirements of the primary system. The proposed isolators displayed significant resilience to varying base conditions and varied dynamic load types thus indicating great resistance to the critical flaw of linear vibration absorbers of detuning as the systems proposed are designed to provide wholistic vibration isolation across a broad range of frequencies and load types. The information contained within, provides a baseline for further practical implementation of the proposed passive linear vibration isolators.

5.2 Research improvement and additional parameters to be investigated

Research improvement is primarily dependent on the execution of practical and field testing in order to developed detailed design and construction codes of practice, but, most critically, to verify the accuracy of base assumptions made during the theoretical analysis of the proposed systems. This enables the industry to access real-time data that can be feedback into ongoing research in order to refine the nature and basis of the general assumptions made in applied physics required to simplify complex equations and theories into reasonably practicable solutions to be implemented in real-time.

The three systems proposed in this thesis are extensively studied theoretically but due to the spatial limitations imposed during the declaration of a National State of Emergency in the Republic of South Africa (ZA), the planned construction and practical testing to verify assumptions and optimisation processes utilised was effectively decommissioned from the scope of this thesis, thus the data produced and published within is fundamentally theoretical. Extensive laboratory and field testing is required before the work contained in this thesis is declared a viable and feasible solution to be used in practice.

Extensive study is also required for the development of viable metamaterials that can be implemented as damping components in the practical application of the proposed systems contained in this thesis in order to replace the existing viscous damping elements currently found in practice. This is essential to the minimisation of the dimensions of vibration isolators especially in civil engineering applications which will allow for the simplified implementation of passive vibration isolation systems in structure prone to dynamic and seismic activities thus increasing the current factors of safety implemented to preserve life in the event of cataclysmic event. This is of especial concern to priority structures such as power plants, dams, bridges and all high occupancy buildings in an area prone to seismic or dynamic loading.

The extensive studies will subsequently assist as well in the development of current optimisation techniques as with more data, more accurate procedures and techniques can be implemented industry wide to aid in the design and construction vibration isolation systems. This is of especial benefit as in the research community, a variety of theories and techniques have been proposed by scholars around the globe but we still lack sufficient data to implement the plethora of solutions that have been postulated which in essence, demeans the key purpose of undertaking research which is, to develop solutions for implementation, solutions are not meant to reside in a book but are required to improve the quality of life of all who share space with us on this planet.

5.3 Research Declaration

The author declared no potential conflicts of interest with respect to the research, authorship, and/or publication of this thesis.

The author(s) received no external financial support for the research, authorship, and/or publication of this thesis.

REFERENCES

[1] Soong TT, Constantinuo MC (1994). Passive and Active Structural Vibration Control In Civil Engineering. New York: Springer.
[2] F, Orban (2011). Damping of Materials and Members in Structures. Journal of Physics: Conference Series (pp. Conference Series 268 1 - 15). Pecs, Hungary: IOP Publishing.
[3] Heuer R, Adam C (2004). Passive Control of Structural Elements Considering Nonlinear Response. Third European Conference on Structural Control. Vienna: European Conference on Structural Control.
[4] Jain S,Chakraborty S (2022). Detuning Effect of Multiple Tuned Mass Damper Systems in Vibration Control of Rail Bridge Girder. 7th International Conference on Civil Structural and Transportation Engineering (pp. Paper 213 1 - 4). Niagara Falls, Canada: International Conference on Civil Structural and Transportation Engineering.
[5] Menkveld K, Pence WO (2001). Tacoma Narrows Bridge. The Physics Teacher, American Association of Physics Teachers, 1-19.
[6] Inala R, Mohanty SC (2012). A Review on Free, Forced Vibration Analysis and Dynamic Stability of Ordinary and Functionally Grade Material Plates. Caspian Journal of Applied Sciences Research, 57-70.
[7] Karnovsky IA, & Lebed E (2016). Theory of Vibration Protection. Coquitlam, BC, Canada: Springer.
[8] Griffin S, Gussy J, Lane S.A, Henderson B.K and Sciulli D (2002), Virtual Skyhook Vibration Isolation System, *Journal of Vibration and Acoustics*, Vol. 124, 63-67

[9] Antoniadis I, Chronopoulos D, Spitas V and Koulocheris D (2015), Hyper-damping properties of a stiff and stable linear oscillator with a negative stiffness element, *Journal of Sound and Vibration*, Vol. 346, 37-52

[10] Li K (2012), A Passive Vibration Isolator Integrated a Skyhook Damper or Groundhook Damper, *Journal of Vibration Testing and System Dynamics*, Journal homepage: https://lhscientificpublishing.com/Journals/JVTSD-Default.aspx

[11] Den Hartog JP (1956) Mechanical Vibrations (4th edition), McGraw Hill, New York.

[12] J. Ormondroyd, J.P. Den Hartog, The theory of the dynamic vibration absorber, J. Appl. Mech. 50 (1928) 9–22.

[13] Ren, M. Z., 2001. A Variant Design of the Dynamic Vibration Absorber. Journal of Sound and Vibration, 245(4), pp. 762-770.

[14] Peng Haibo, S. Y. Y. S., 2015. Parameters optimisation of a new type of dynamic vibration absorber with negative stiffness. Chinese Journal of Theoretical and Applied Mechanics, 47(2), pp. 320-327

[15] Ioannis A Antoniadis, S. A. K. K. G., 2016. KDamping : A Stiffness Based Vibration Absorption Concept. Journal of Vibration and Control

[16] Rao, S.S. (2011), *Mechanical Vibrations*, 5th Edition, Pearson Education.

[17] Carrella, A., Brennan, M. J., Waters, T. P. and Lopes, V. (2012), Force and displacement transmissibility of a nonlinear isolator with high-static-low-dynamic-stiffness, *International Journal of Mechanical Sciences*, 55, 22–29

[18] Shaw, A. D., Neild, S. A., Wagg, D. J., Weaver P. M. and Carrella, A.(2013), A nonlinear spring mechanism incorporating a bistable composite plate for vibration isolation, *Journal of Sound and Vibration*,332, 6265–6275

[19] Liu, C. and Yu, K.(2018), A high-static–low-dynamic-stiffness vibration isolator with the auxiliary system, *Nonlinear Dyn*, 94:1549–1567

[20] Cheng, C., Li, S. and Wang, Y.(2017), Force and displacement transmissibility of a quasi-zero stiffness vibration isolator with geometric nonlinear damping, *Nonlinear Dyn*, 87: 2267–2279

[21] Yan, B., Ma, H., Jian, B. *et al.*(2019), Nonlinear dynamics analysis of a bi-state nonlinear vibration isolator with symmetric permanent magnets. *Nonlinear Dyn*, 97: 2499–2519

[22] Li, Q., Zhu, Y., Xu, D., Hu, J., Min, W. and L. Pang (2013), A negative stiffness vibration isolator using magnetic spring combined with rubber membrane, *Journal of Mechanical Science and Technology*, 27 (3): 813-824

[23] Yan, L., Xuan, S. and Gong, X. (2018), Shock isolation performance of a geometric anti-spring isolator, *Journal of Sound and Vibration* 413: 120-143

[24] Wen, H., Guo, J., Li, Y., Lin, Y. and Zhang, K. (2018), The transmissibility of a vibration isolation system with ball-screw inerter based on complex mass, *Journal of Low Frequency Noise, Vibration and Active Control*, 37(4): 1097–1108

[25] Ledezma-Ramírez, D. F., Tapia-González, P. E., Ferguson, N., Brennan, M. and Tang, B.(2019), Recent Advances in Shock Vibration Isolation: An Overview and Future Possibilities, *Appl. Mech. Rev., 71(6): 060802 (23 pages)*

[26] Chen, J. L. and Georgakis, C. T. (2015), Spherical tuned liquid damper for vibration control of in wind turbines, *Journal of Vibration and Control*, 21(10): 1875-1885

[27] Choi, E., Choi, G., Kim, H-T. and Youn, H. (2015), Smart damper using the combination of magnetic friction and pre-compressed rubber springs, *Journal of Sound and Vibration*, 351: 68–89

[28] Griffin, S., Gussy, J., Lane, S. A., Henderson, B. K. and Sciulli, D.(2002), Virtual skyhook vibration isolation system, *Journal of Vibration and Acoustics*, 2002, 124(1): 63-67

[29] Nie, J., Yang, Y., Jiang, T. and Zhang, H. (2019), Passive skyhook suspension deduction for improvement of ride comfort in an off-road vehicle, *IEEEAccess*， Vol 7:150710-150719

[30] Caterino, N., Spizaoco, M., Occhiazzi, A. and Bonati, A. (2018), Experimental assessment of a skyhook semiactive strategy for seismic vibration control of a steel structure, *Shock and Vibration*, Article ID 6460259, 12 pages

[31] Ding, R., Wang, R., Meng, X. and Chen, L. (2019), A modified energy-saving skyhook for active suspension based on a hybrid electromagnetic actuator, Journal *of Vibration and Control*, 25(2): 286–297

[32] Kou, F., Jing, Q., Chen, C., and Wu, J. (2020), Endocrine composite skyhook-groundhook control of electromagnetic linear hybrid active suspension, *Shock and Vibration*, Article ID 3402168, 17 pages

[26] Chen JL and Georgakis CT (2015), Spherical tuned liquid damper for vibration 502 control in wind turbines, Journal of Vibration and Control, 21(10) 1875–1885 503

[27] Choi, E, Choi, G, Kim, H-T and Youn, H (2015), Smart damper using the 504 combinations of magnetic friction and pre-compressed rubber springs, Journal 505 of Sound and Vibration 351: 68–89 506

[28] Antoniadis, I, Chronopoulos, D, Spitas V and Koulocheris, D (2015), Hyper-damping properties of a stiff and stable linear oscillator with a negative stiffness element, Journal of Sound and Vibration 346: 37–52 509

[29] Shen, Y, Wang, X, Yang, S and Xing, H (2016), Parameters Optimization for a Kind of Dynamic Vibration Absorber with Negative Stiffness, Mathematical Problems in Engineering, 4:1-10 512

[30] Shen, Y, Peng, H, Li, X and Yang, S (2017) Analytically optimal parameters of dynamic vibration absorber with negative stiffness, Mechanical Systems and Signal Processing 85: 193–203 515

[31] Zhou, S, Jean-Mistral, C and Chesne, S (2019), Closed-form solutions to optimal parameters of dynamic vibration absorbers with negative stiffness under harmonic and transient excitation, International Journal of Mechanical Sciences 157–158: 528–541 519

[32] Rao, SS (2003), Mechanical Vibrations. 4th Edition. Pearson Education 520

[33] Carrella, A, Brennan, MJ, Waters TP and Lopes Jr. V (2012), Force and displacement transmissibility of a nonlinear isolator with high-static-low-dynamic-stiffness, International Journal of Mechanical Sciences 55: 22–29 523

[34] Shaw, AD, Neild, SA, Wagg, DJ, Weaver, PM and Carrella, A(2013), A nonlinear spring mechanism incorporating a bistable composite plate for vibration isolation, Journal of Sound and Vibration 332: 6265–6275 526

[35] Liu, C and Yu, K (2018), A high-static–low-dynamic-stiffness vibration isolator with the auxiliary system, Nonlinear Dyn. , 94:1549–1567 528

[36] Cheng, C, Li, S and Wang, Y (2017), Force and displacement transmissibility of a quasi-zero stiffness vibration isolator with geometric nonlinear damping, Nonlinear Dyn. 87: 2267–2279 531

[37] Li, Q, Zhu, Y, Xu, D, Hu, J, Min, W and Pang, L (2013), A negative stiffness vibration isolator using magnetic spring combined with rubber membrane, 533Journal of Mechanical Science and Technology 27 (3): 813~824 534

[38] Yan, L, Xuan, S and Gong, X (2018), Shock isolation performance of a geometric anti-spring isolator, Journal of Sound and Vibration, 413: 120-143 536

[39] Wen, H, Guo, J, Li, Y, Lin, Y and Zhang, K (2018), The transmissibility of a vibration isolation system with ball-screw inerter based on complex mass, Journal of Low Frequency Noise, Vibration and Active Control, 37(4): 1097– 1108 540

[40] Ledezma-Ramírez, DF, Tapia-González, PE, Ferguson, N, Brennan,M and Bin Tang(2019), Recent Advances in Shock Vibration Isolation: An Overview and Future Possibilities, Appl. Mech. Rev. Nov., 71(6): 060802 (23 pages)

[41] Li K., Gohnert M. (2010), Lever mechanism for vibration isolation, Appl. Tech. Innovat. 1 (1): 21–28, doi: 10.15208/ati.

[42] Özyar O and Yılmaz C (2021), A self-tuning adaptive-passive lever-type vibration isolation system, Journal of Sound and Vibration, 505 1-19

[43] Zhou W., Qiu N.,Wang L. , Gao B. and Liu D.(2018) , Dynamic analysis of a planar multi-stage centrifugal pump rotor system based on a novel coupled model, Journal of Sound and Vibration, 434, 237-260

[44] Lu, Z., Brennan, M. J., Yang, T., Li, X., and Liu, Z., (2013), An Investigation of a Two-Stage Nonlinear Vibration Isolation System, *J. Sound Vib.*, 322(4–5), pp. 1456–1464

[45] 20 Wu Z., Jing X., Sun B. and Li F.(2016), A 6DOF passive vibration isolator using X-shape supporting structures, Journal of Sound and Vibration, 380, 90-111

[46] Ibrahim, R. A. (2008), Recent advances in nonlinear passive vibration isolators, *Journal Sound and Vibration*, 314, 371–452.

[47] Ledezma, R.D.F.; Tapia, G.P.E.; Ferguson, N.; Bennan, M.; Tang, B. (2019), Recent advances in shock vibration isolation: An overview and future possibilities. *Appl. Mech. Rev*., 71, 060802.

[48] Shaw, A. D., Neild, S. A., Wagg, D. J., Weaver P. M. and Carrella, A. (2013), A nonlinear spring mechanism incorporating a bistable composite plate for vibration isolation, *Journal of Sound and Vibration*,332, 6265–6275

[49] Liu, C. and Yu, K. (2018), A high-static–low-dynamic-stiffness vibration isolator with the auxiliary system, *Nonlinear Dyn*, 94:1549–1567

[50] Valeev, A.; Tokarev, A.; Zotov, A. (2019), Material with quasi-zero stiffness for vibration isolation in civil and industrial structures and buildings. Int. IOP Conf. Ser: Earth Environ. Sci. 272, 032048.

[51] Sorokin, V.N.; Kalashnikov, B.A.; Efimov, I. Y. (2019), Dynamics of anti-vibration mount with quasi-zero stiffness., *Int. J. Mod. Phys. Conf. Ser.*, 1210, 012135.

[52] Cheng, C., Li, S. and Wang, Y. (2017), Force and displacement transmissibility of a quasi-zero stiffness vibration isolator with geometric nonlinear damping, *Nonlinear Dyn*, 87: 2267–2279

[53] Yan, B., Ma, H., Jian, B. *et al.* (2019), Nonlinear dynamics analysis of a bi-state nonlinear vibration isolator with symmetric permanent magnets. *Nonlinear Dyn*, 97: 2499–2519

[54] Li, Q., Zhu, Y., Xu, D., Hu, J., Min, W. and L. Pang (2013), A negative stiffness vibration isolator using magnetic spring combined with rubber membrane, *Journal of Mechanical Science and Technology*, 27 (3): 813-824

[55] Yan, L., Xuan, S. and Gong, X. (2018), Shock isolation performance of a geometric anti-spring isolator, *Journal of Sound and Vibration* 413: 120-143

[56] Wen, H., Guo, J., Li, Y., Lin, Y. and Zhang, K. (2018), The transmissibility of a vibration isolation system with ball-screw inerter based on complex mass, *Journal of Low Frequency Noise, Vibration and Active Control*, 37(4): 1097–1108

[57] Soliman, J. I. and Ismailzadeh, E. (1974), Optimization of unidirectional viscous damped vibration isolation system, *Journal of Sound and Vibration*, 36, 527-539

[58] Lu, Z., Brennan, M. J., Yang, T., Li, X., and Liu, Z., (2013), An Investigation of a Two-Stage Nonlinear Vibration Isolation System, *J. Sound Vib.,* 322(4–5), pp. 1456–1464

[59] Lu, Z., Yang, T., Brennan, M. J., Li, X., and Liu, Z. (2014), On the performance of a two-stage vibration isolation system which has geometrical nonlinear stiffness, *Journal of Vibration and Acoustics*, 136/064501: 1-5

[60] Xia, Z., Wang, X., Hou, J. and Wen, S. (2016), Non-linear dynamic analysis of a double-layer semi-active vibration isolation systems using revised Binham model, *Journal of Low Frequency Noise, Vibration and Active Control*, 35(1) 17-24

[61] Wang, X.; Zhou, J.; Xu, D.; Ouyang, H.; Duan, Y. (2017), Force transmissibility of a two-stage vibration isolation system with quasi-zero stiffness., *Nonlinear Dyn*., 87, 633–646.

[62] Yang, J., Jiang, J. Z., Zhu, X. and Chen, H. (2017), Performance of dual-stage inerter-based vibration isolator, *Procedia Engineering*, 199:1822-1827

[63] Ledezma-Ramirez, D. F., Tapia-Gonzalez, P. E., and Castillo-Morales, M. (2019), Theoretical analysis of two stage shock isolation mount with switchable stiffness control, *INGENIERÍA MECÁNICA TECNOLOGÍA Y DESARROLLO,* 6(4):141-150

[64] Chen, X., Qi, H. and Zhang, H. (2001), Optimal design of a two-stage mounting isolation system by maximum entropy approach, *Journal of Sound and Vibration*, 243(4) 591-599

[65] Lu, Z., He, L. and Shuai, C. (2016), Optimization of natural frequencies of large-scale two-stage raft system, *Journal of Physics: Conference Series* 744 /012180: 1-8.

[66] S, Nagarajaiah, L, Chen, & M, Wang (2022). Adaptive Stiffness Structures with Dampers: Seismic and Wind Response Reduction Using Passive Negative Stiffness and Inerter Systems. Journal of Structural Engineering, 04022179 1 - 21.

[67] H, Li., Y, Li., & J, Li. (2019). Negative Stiffness Devices for Vibration Isolation Application: A review. Advances in Structural Engineering, 1-47.